8th Annual Meeting

AMERICAN SOCIETY

OF

BIOMECHANICS

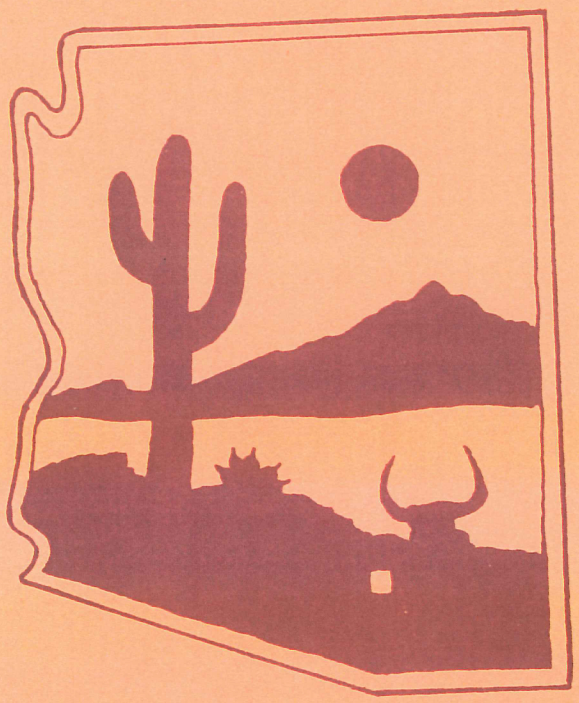

October 3-5, 1984

University of Arizona

Tucson, Arizona

AMERICAN SOCIETY OF BIOMECHANICS

8th Annual Meeting

October 3-5, 1984

University of Arizona

Tucson, Arizona

TABLE OF CONTENTS

SCHEDULE

Wednesday, October 3, 1984*

1300-1700 Registration — Plaza Hotel main lobby
Laboratory tours

1800-2000 Welcoming reception
Plaza Hotel Conference Center (Salons B & C)

2000-2200 Executive Committee Meeting
Plaza Hotel Conference Center(Board Room)

Thursday, October 4, 1984*

0600-0700 6-mile group run or lap swim - meet in Plaza Hotel lobby

0730-1130 Registration - Conference Center lobby

0750-0800 Introduction, Welcome, Announcements (Conference Center, Salon C)

0800-0900 Sport Biomechanics — Elite Athlete Symposium (Salon C)
C. Dillman, The Elite Athlete Program
J.G. Hay, Biomechanics of the Horizontal Jump
C. Kyle, Cycling Aerodynamics

0900-0915 Break

0915-1015 **Session A** - Sport Biomechanics (Salon C)
Session B - Calcified Tissue Properties (Salon A)

1015-1030 Coffee Break

1030-1130 **Session C** - Fluid Mechanics (Salon C)
Session D - Calcified Tissue Properties (Salon A)

1130-1200 Society Business Meeting (Salon C)

1200-1300 Lunch - Plaza Hotel

1300-1415 **Session E** - Spine Mechanics (Salon A)
Session F - Biology (Salon C)

1415-1425 Break

1425-1500 Keynote Lecture
D. Speer, Growth Plate Injuries (Salon C)

1500-2200 Tour of and cookout at the Desert Museum
Buses depart from the front of the Plaza Hotel at 1520

Friday, October 5, 1984*

0600-0700 6-mile group run or lap swim - meet in Plaza Hotel lobby

0730-0800 Authors set up poster presentations (Salon A)

0800-0905 Biology — Locomotion Symposium (Salon C)

G.E. Goslow, Vertebrate Locomotion
P. Webb, Fish Locomotion
A.T.W. Cheung, Locomotion of Micro-organisms

0905-0915 Break

0915-1030 **Session G** - Soft Tissue Mechanics (Salon C)

Session H - Gait (Salon B)

1030-1045 Coffee Break

1030-1200 **Poster Session** (Salon A)

1200-1300 Lunch
Executive Committee Meeting (Board Room)

1300-1345 Borelli Lecture

T. Brown, Some Aspects of the Biomechanics of Femoral Head Osteonecrosis (Salon C)

1345-1400 Break

1400-1530 **Session I** - Ergonomics (Salon C)

Session J - Joint Function (Salon A)

1530-1545 Coffee Break

1545-1715 **Session K** - Skeletal Muscle Mechanics (Salon C)

Session L - Locomotion (Salon A)

1715 Close of Conference

* Room numbers refer to meeting rooms of the Plaza Hotel Conference Center.

CONFERENCE PROGRAM

Thursday, October 4

0750-0800

Opening, Welcome and Announcements

0800-0900

SPORT BIOMECHANICS — Elite Athlete Symposium
Chairperson: D.I. Miller

0800 C. DILLMAN
The Elite Athlete Program

0810 J.G. HAY
Biomechanics of the horizontal jump

0830 C. KYLE
Cycling aerodynamics

0850 Discussion

0915-1015

Session A - SPORT BIOMECHANICS
Chairperson: C.A. Putnam

0915 K.N. AN, B.F. MORREY, & E.Y. CHAO
Individual muscle and joint forces across the elbow in sports.
Mayo Clinic.

0930 W. BODA & L. ABRAHAM
The relationship between arm motion at entry and rip entries in diving.
Dept. Physical & Health Education, University of Texas, Austin.

0945 D.J. KRIELLAARS
Dynamics of an upper extremity striking skill.
School of Physical Education, Dalhousie University.

1000 M. HUBBARD & M.L. HULL
Javelin throw optimization using computer simulation and trajectory instrumentation.
Dept. Mechanical Engineering, University of California, Davis.

Session B - CALCIFIED TISSUE MECHANICS
Chairperson: R.B. Martin

0915 A.A. BIEWENER, S. SWARTZ, & M. LEE
Mechanical loading and skeletal remodeling during growth.
University of Chicago.

0930 T.D. BROWN & D.T. SHAW
Instantaneous in vitro contact stress distributions on the femoral condyles.
Dept. Orthopaedic Surgery, University of Pittsburgh.

0945 W.J.M. CZYZ, J.A. FAIRCLOUGH, I.G. MACKIE, & L.D.M NOKES
Tibial vibration transmission - The effects of incremental osteotomy.
Cardiff Royal Infirmary, Great Britain.

1000 J.A. FAIRCLOUGH, W.J.M. CZYZ, I.G. MACKIE, & L.D.M. NOKES
Time domain vibration analysis in the assessment of stability after internal fixation of tibial fractures.
Cardiff Royal Infirmary, Great Britain.

1030-1130

Session C - FLUID MECHANICS
Chairperson: M. Hubbard

1030 T.D. BROWN, R.H. GABEL, D.R. PEDERSEN, L.D. BELL, & W.F. BLAIR
Some characteristics of laminar flow velocity spectra detected by a 20 MHz pulsed ultrasound Doppler.
Depts. Orthopaedic Surgery and Biomedical Engineering, University of Iowa.

1045 A.T.W. CHEUNG, M.E. MILLER, E.M. WALSH, & R.M. DONOVAN
In vivo studies on leukoemboli formation - an intravital microscopic analysis.
School of Medicine and California Primate Research Center, University of California, Davis.

1100 R.M. DONOVAN, A.T.W. CHEUNG, M.E. MILLER, & E. GOLDSTEIN
A computer-assisted method for measuring cell movement.
School of Medicine and California Primate Research Center, University of California, Davis.

1115 T.W. SECOMB & J.F. GROSS
Red blood cell mechanics and blood flow in narrow capillaries.
Dept. Physiology, University of Arizona.

Session D - CALCIFIED TISSUE MECHANICS
Chairperson: T. Brown

1030 J.B. KOENEMAN
An improved 2-D finite element model of the proximal femur.
Harrington Arthritis Research Center, Phoenix.

1045 R.B. MARTIN
Computer modeling of temporal effects in bone remodeling physiology.
West Virginia University.

1100 T.E. ORR & D.R. CARTER
Stress analysis of porous ingrowth joint arthroplasty in the proximal humerus.
VA Medical Center, Palo Alto and Mechanical Engineering Department, Stanford University.

1115 R. SUMNER
Material and geometric properties of the human femur during growth.
Dept. Anthropology, University of Arizona

1300-1415

Session E - SPINE MECHANICS
Chairperson: A.H. Soni

1300 M.R. GUDAVALLI & A.H. SONI
Flexibility properties of normal and injured lumbar spine.
Mechanical and Aerospace Engineering, Oklahoma State University.

1315 T. JAKOBS, J.A.A. MILLER, & A.B. SCHULTZ
Lateral movement of the upper body in response to static lateral moments.
Dept. Mechanical Engineering, University of Michigan.

1330 J.M. LIPKA & H.S. RANU
Comparison of an in vivo spondylolysis fracture to those obtained in vitro.
Dept. Biomedical Engineering, Louisiana Technical University.

1345 J.A.A. MILLER, H. STEEN, L.B. SKOGLUND, & A.B. SCHULTZ
Paravertebral muscle recruitment patterns in the thoracic and lumbar spine.
Sophies Mindes Orthopaedic Hospital, University of Oslo, Norway and Dept. Mechanical Engineering, University of Michigan.

1400 B.R. SIMON, J.S.-S. WU, J.H. EVANS, & L.E. KAZARIAN
Poroelastic structural models for human spinal motion segments.
Aerospace and Mechanical Engineering, University of Arizona, Strathclyde University, Glasgow, Scotland, and Wright-Patterson Air Force Base, Dayton.

Session F - BIOLOGY
Chairperson: A.T.W. Cheung

1300 D.B. BURR & M.B. SCHAFFLER
Structural-mechanical indicators of limb specialization in primates.
Dept. Anatomy and Orthopedic Surgery, West Virginia University.

1315 J.H. HEBRANK & S.A. WAINWRIGHT
Elastic recoil in the marlin backbone.
Duke University

1330 N.H. MENDELSON
Growth dynamics of bacterial macrofiber fragments.
Dept. Microbiology and Immunology, University of Arizona

1345 M.E. MORBECK
Biomechanics and human evolution.
Dept. Anthropology, University of Arizona.

1400 M.B. SCHAFFLER & D.B. BURR
Bone microstructure: a study in comparative locomotion.
Dept. Anatomy and Orthopedic Research Lab, West Virginia University.

1425-1500

KEYNOTE LECTURE

1425 D. SPEER
Growth plate injuries

1455 Discussion

Friday, October 5

0800-0905

BIOLOGY — LOCOMOTION SYMPOSIUM
Chairperson: R.A. SATTERLIE

0800 G.E. GOSLOW
Vertebrate locomotion.

0820 P. WEBB
Fish locomotion.

0840 A.T.W. CHEUNG
Locomotion of micro-organisms

0915-1030

Session G - SOFT TISSUE MECHANICS
Chairperson: G. Pijanowski

0915 D.I. BYLSKI, T.J. KRIEWALL, N. AKKAS, & J.W. MELVIN
Mechanical behavior of fetal dura mater in axisymmetric biaxial tension.
University of Michigan, Surgical Products Division, 3M Company, and Middle East Technical University, Ankara, Turkey.

0930 R.N. HINRICHS, P.H. WERNER, J.E. RINK, T.W. JACKMAN, & R.A. JOSEPHS
Impact forces upon landing from a height in children.
Dept. Physical Education, University of of South Carolina.

0945 G.J. PIJANOWSKI, R.V. ALLHANDS, & S.A. KINCAID
Use of force plate data to screen young pigs for osteochondrosis.
Dept. Veterinary Biosciences and Bioengineering Program, University of Illinois, and Dept. Anatomy, Purdue University.

1000 H.S. RANU
Modeling of the human skin with particular reference to radiotherapy effects.
Dept. Biomedical Engineering, Louisiana Technical University.

1015 G.A. VALIANT & P.R. CAVANAGH
An in vivo determination of the mechanical characteristics of the human heel pad.
Nike Sport Research Laboratory and Pennsylvania State University.

Session H - GAIT
Chairperson: A.E. Atwater

0915 S. Yu. ALESHINSKY
Total, external, and internal work for human movement.
Pennsylvania State University.

0930 P.E. MARTIN
Mechanical work done on the lower extremities during the recovery phase of loaded running.
Dept. Health & Physical Education, Arizona State University.

0945 D.I. MILLER & C.F. MUNRO
Joint torque patterns of below-knee amputees during running stance.
Faculty of Physical Education, University of Western Ontario and Dept. Kinesiology, University of Washington.

1000 C.A. PUTNAM
Segment interaction in treadmill running at four different speeds.
School of Physical Education, Dalhousie University

1015 K.R. WILLIAMS & J.L. ZIFF
Changes in rearfoot motion associated with systematic variations in running style.
University of California, Davis.

1030-1115

POSTER SESSION I

A.T. BAHILL
Baseball players cannot keep their eyes on the ball.
Systems and Industrial Engineering, University of Arizona.

J. DANOFF, W. SCHNEIDERWIND, B. MOY, B. THORNTON, L. GERBER, A. RICH, & J. LEDERMANN
Variable force coil spring hand splint.
Dept. Rehabilitation Medicine, NIH.

J. DANOFF, T. WAGGONER, & G. HUNT
Assessment of footpad dependability.
Dept. Rehabilitation Medicine, NIH.

D.R. PEDERSEN, T.D. BROWN, & R.J. SINGERMAN
Quantitation of Fuji prescale film pressures using digital image scanning.
Depts. Orthopaedic Surgery and Biomedical Engineering, University of Iowa.

M.S. PINZUR, P. DIMONTE-LEVINE, R. SHERMAN, J. TRIMBLE, & K. HAAG
Temporal gait analysis by inter-ankle distance monitoring.
Hines VA Hospital and Dept. Orthopaedics and Rehabilitation, Loyola University.

J. RICHARDS
An application of photoelastic techniques to the measurement of tibial stiffness.
Institute of Science and Technology, University of Wales, Cardiff, United Kingdom.

G.L. SCHEIRMAN & P.J. CHEETHAM
Temporal and kinematic characteristics of skilled tracking movements.
Dept. Biomechanics and Computer Services, United States Olympic Center.

D.S. SCHNUR & J.L. LEWIS
Structural modeling and design of knee orthoses.
Harrington Arthritis Research Center, Phoenix and Northwestern University.

1115-1200

POSTER SESSION II

M. SHARAN, M.P. SINGH, & A. AMINATAEI
Two layer model for the oxygenation of blood in pulmonary capillaries.
Centre for Atmospheric and Fluids Sciences, Indian Institute of Technology, New Delhi, India.

J.H. STAGALL & L.D. ABRAHAM
Effects of arm action on the height attained in a maximal vertical jump.
Dept. Physical and Health Education, University of Texas, Austin.

E.K. STAUFFER, R.S. POZOS, & R.F. PIERCE
Spectral analysis of tremor patterns associated with stuttering speech.
Depts. Physiology and Communicative Disorders, University of Minnesota.

J.J. TRIANO
Accurate determination of motion from plane films.
University of Illinois and National College.

B. TURAN, A. VILMAZ, & H.S. RANU
Spin lattice relaxation time of human blood: an NMR study.
University of Ankara and University of Dicle, Turkey and Dept. Biomedical Engineering, Louisiana Technical University.

J. M. WINTERS & L. STARK
Analysis of fundamental human movement patterns by using in-depth antagonistic muscle models: examples of knee and elbow movements.
Dept. Engineering Science, University of California, Berkeley.

Y.G. ZORBAS & I.O. MATVEYEV
Effect of hypokinesia on man's desirability in performing physical activities.
Instituto di Medicina dello Sport, CONI, Rome, Italy.

1300-1345

BORELLI LECTURE

1300 J.G. HAY, Introduction

1305 T. BROWN
Some aspects of the biomechanics of femoral head osteonecrosis.

1340 Discussion

1400-1530

Session I - ERGONOMICS
Chairperson: T. Armstrong

1400 M. ADRIAN & G. SMITH
The kinematics and kinetics of swinging two types of railroad hammers.
University of Illinois.

1415 R.O. ANDRES, D.S. BLOSWICK, & D.B. CHAFFIN
A biodynamic model for investigating industrial push/pull tasks.
Center for Ergonomics, University of Michigan.

1430 K.L. KREUTZBERG & R.O. ANDRES
Field study methods for applying a biodynamic model to investigate push/pull tasks.
Center for Ergonomics, University of Michigan.

1445 T.J. ARMSTRONG, M. ROBERTSON, B. BUCHHOLZ, B.S. JOSEPH, C. WOOLLEY, & B. SILVERSTEIN
A system for analysis of postures and forces in manual work.
Center for Ergonomics, University of Michigan.

1500 M. KRAG, L. GILBERTSON, & M.H. POPE
A test of the hypothesis of abdominal pressure as a disc load-reducing mechanism: a study using quantitative electromyography.
Dept. Orthopaedic Surgery, University of Vermont.

1515 K.S. LEE, L. HALL, & F. CHEN
Musculoskeletal stress evaluation of microscopist using electromyography.
Dept. Industrial and Systems Engineering, Ohio University.

SESSION J - MECHANICS OF JOINT FUNCTION
Chairperson: J.G. Andrews

1400 K. FUKUDA, K.N. AN, E.V. CRAIG, R.H. COFIELD, & E.Y.S. CHAO
Ligamentous restraints to acromioclavicular joint motion: A biomechanical study.
Mayo Clinic and Dept. Orthopedics, University of Minnesota.

1415 S.A. GOLDSTEIN, T.L. GREENE, D.S. LOUIS, W.S. WARD, & L.S. MATTHEWS
A biomechanical evaluation of the function of the digital pulleys.
University of Michigan Medical Center.

1430 C. JOHNSON & M.L. HULL
Torsional load-deformation characteristics of the human leg in vivo.
Dept. Mechanical Engineering, University of California, Davis.

1445 M.W. MARZKE & R.F. MARZKE
The function of the third metacarpal styloid process: a force analysis employing magnetic resonance imaging.
Depts. Anthropology and Physics, Arizona State University.

1500 D.J. RAPPERPORT & D.R. CARTER
Contact finite element stress analysis of the hip joint and acetabular region.
Dept. Mechanical Engineering, Stanford University and Veterans Administration, Palo Alto.

1515 J.R. TOLBERT, W.F. BLAIR, J.G. ANDREWS, & R.D. CROWNINSHIELD
The kinetics of normal and prosthetic wrists.
Depts. Mechanical Engineering and Orthopaedics, University of Iowa.

1545-1715

Session K - SKELETAL MUSCLE MECHANICS
Chairperson: K. An

1545 J.G. ANDREWS
Strength curves for multiple-joint single degree of freedom exercises.
Dept. Mechanical Engineering, University of Iowa.

1600 P.E. CRAGO & S.V. ZACHARKIW
Fatigue-induced changes in stiffness of the flexor pollicus longus in human subjects with intact reflexes.
Depts. Biomedical Engineering and Orthopaedic Surgery, Case Western Reserve University.

1615 S.L. LEHMAN
Control of human wrist movements during adaptation to inertial loads.
Rehabilitation Institute, Chicago.

1630 S.-P. MA & G.I. ZAHALAK
The mechanical response of the active human triceps brachii to very rapid lengthening and shortening.
Dept. Mechanical Engineering, Washington University.

1645 M.H. MOEINZADEH, L.D. METZ, L.R. WHITE, & J.L. GROPPEL
Biomechanical force analysis of the leg motion for the standard and supine recumbent bicycle pedaling.
Depts. General Engineering and Physical Education, University of Illinois.

1700 J.M. WINTERS & L. STARK
Interaction between ongoing eccentric/concentric movement and fast movements for the limb.
Dept. Engineering Science, University of California, Berkeley.

Session L - LOCOMOTION AND PROPULSIVE MOVEMENTS
Chairperson: K. Williams

1545 J. DAPENA
Systematic error in 3D coordinates within a large object-space when using DLT and NLT methods of 3D cinematography.
Dept. Physical Education, Indiana University.

1600 M. HUBBARD, E.G. PATERSON, & A.E. ORCUTT
Theoretical prediction of energetically optimal step length-velocity programming in biped locomotion.
Dept. Mechanical Engineering, University of California, Davis.

1615 B.J. JAEGER, S.A. OLIVARES, & M.C. WETZEL
Control of human electromyographic activity during different walking velocities.
Dept. Psychology, University of Arizona.

1630 L.W. LAMOREUX
A computerized system for real-time visualization of ground reaction forces in walking.
Shriners Hospital for Crippled Children, San Francisco.

The University of Arizona College of Medicine's Continuing Medical Education activities are accredited by the ACCME. This program meets the criteria for 17 credit hours in Category I of the Physician's Recognition Award of the American Medical Association.

INDEX OF PARTICIPANTS

Abstracts are arranged in the order in which they appear in the program.

Individual Muscle and Joint Forces Across the Elbow in Sports

K. N. An, B. F. Morrey and E. Y. Chao

Biomechanics Laboratory
Mayo Clinic, Rochester, MN 55905

Sports biomechanics has received much attention and great progress occurred in the area of kinematic analysis. By combining kinematic data with information on segmental mass moments of inertia, the resultant intersegmental joint forces and moments can be calculated. Further decomposition of these resultant loads into individual muscle and joint forces is significant in several respects. Insight into the contractile activity of individual muscles during various phases of sports is provided and can be used to design athletic training procedures. Forces encountered in the surrounding ligaments and at the articular surfaces can be obtained. This information is important to the understanding of the mechanisms and management of sports injuries.

To proceed beyond the resultant intersegmental joint forces and moments to individual muscle forces, an analytic model to describe the muscular structures around the joint is required. Development of a model requires anatomic study of human specimens to identify parameters such as the lines of action, moment arms, physiological cross-sectional areas and tendon excursions at various joint configurations. In attempting to solve the problem for muscle forces, a frequently encountered difficulty is that the problem formulated is an indeterminate one in which the number of unknown variables exceeds the number of available equations; thus no unique solution can be obtained. Many approaches, including reduction and optimization methods, have been developed to resolve this indeterminate problem. By using the optimizing method, not only can a unique solution be obtained but also a possible associated rationale for solution. Both linear and nonlinear objective functions have been adopted for use with the optimization method; however, each has a drawback in that either the solution does not match what is expected experimentally, or the method for solution is not efficient. A new optimization approach, based on minimizing the upper bound of muscle stress, has been introduced to obtain a unique solution. Muscle force results obtained with this method compare favorably with experimental results, as well as with results obtained by other optimization techniques.

Individual muscle and joint forces at the elbow joint under various isometric loading conditions have been studied extensively [1]. Combining these data with resultant intersegmental joint moment and force data makes it possible to estimate individual muscle and joint forces for sport activities such as throwing, running, weight lifting and gymnastics. By using the data of intersegmental moments and joint angles at the elbow during running [2], the results of major elbow muscle forces are calculated (Figure 1).

[1] K.N. An, B.M. Kwak, E.Y. Chao, B.F. Morrey: Determination of Muscle and Joint Forces Across Human Elbow. pp. 70-71, Advances in Bioengineering, ASME, 1983.

[2] R.N. Hinrichs: A Three-dimensional Analysis of the Net Moment at the Shoulder and Elbow Joint in Running and their Relationship to Upper Extremtiy EMG Activity. IX International Congress of Biomechanics, 1983, P. 61.

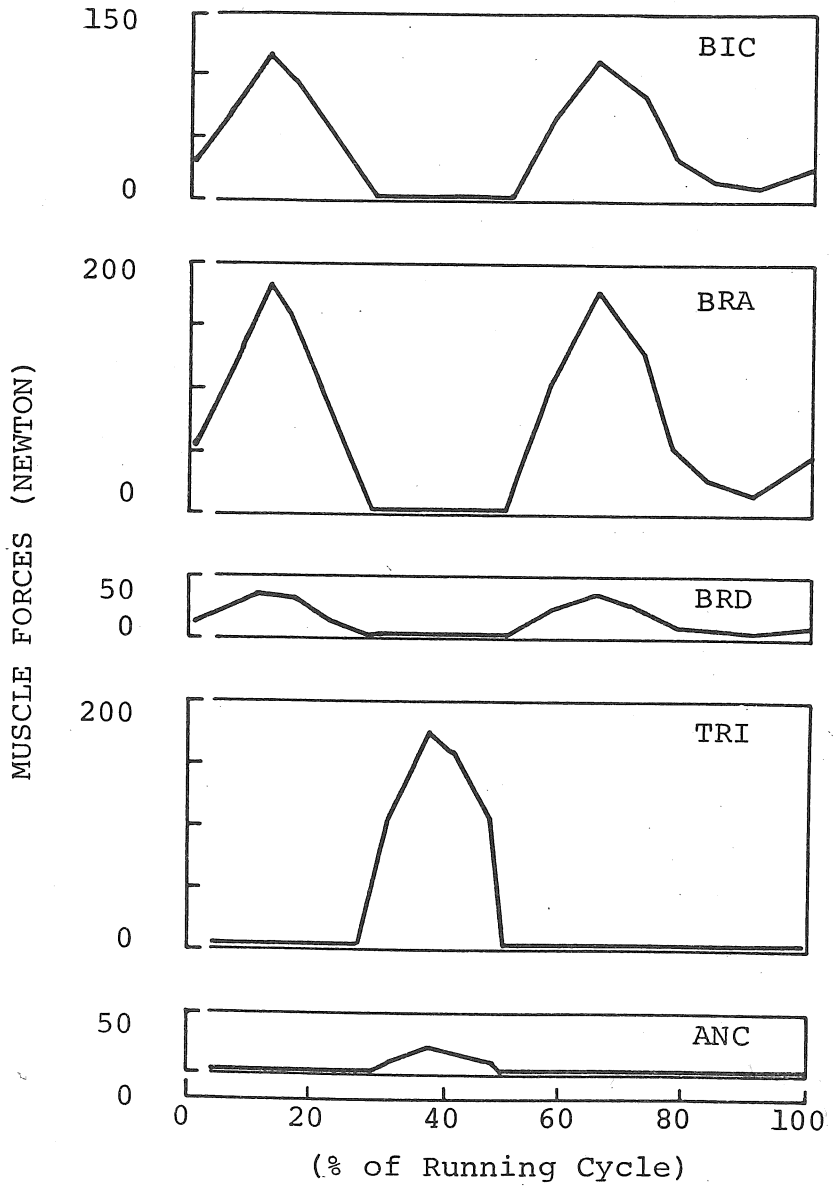

Fig. 1 - Forces in the major muscles across the elbow joint during running: Biceps (BIC); Brachialis (BRA); Brachioradialis (BRD); Triceps (TRI); Anconeus (ANC).

Acknowledgement

This study is supported in part by NIH grant AM 26287. Data of net moment at the elbow joint during running for calculation are kindly provided by Dr. R. N. Hinrichs.

THE RELATIONSHIP BETWEEN ARM MOTION AT ENTRY AND RIP ENTRIES IN DIVING

W. Boda and L. Abraham, Dept. of Physical & Health Education, The University of Texas at Austin, Austin, TX 78712.

An important aspect of ideal form in competitive diving is the rip entry, which is named for its characteristic sound and which results in little or no splash. Characteristics of rip entries produced under controlled conditions have been described in detail by Brown et al. (1984). One suggestion from that work was that the direction of arm movement immediately prior to entry was related to rip entry production. The purpose of this study was to extend that work by examining relationships between rip and non-rip entries and the sagittal-plane arm motion required by typical competitive dives.

Two elite competitive divers able to rip entries consistently were filmed during typical 10 meter platform workouts while performing both forward and backward spinning dives. A 16 mm cine camera (Locam) was used, set at 50 frames/sec, and positioned one meter above water level to provide a side view of the diver entering the water (perpendicular to the plane of rotation). Data from the film for seventeen dives -- eight backward- and nine forward-spinning -- was digitized using a Numonics 1224 graphics calculator and a PDP11/03 laboratory computer. Six points on the near side of the diver's body were used to represent the position of the body in each frame: wrist, elbow, shoulder, hip, knee, and ankle. In order to examine arm movement immediately prior to entry, the shoulder joint angle and the arm angular velocity were calculated for four frames prior to impact.

Eight of the dives (four forward and four backward) were judged to be rip entries, based on the sound produced and the splash thrown. Analysis of the data showed that all of the rip entries were produced with shoulder joint angles at impact between 157 and 179 degrees, while the shoulder joint angles for all of the non-rip entries were outside this range. In addition, the angular velocity of the arms at impact appeared to be related to entry type. Seven of the rip entries were produced with arm angular velocities less than 100 degrees/sec, compared to only two of nine non-rips. Direction of whole body rotation did not appear to be related to these interactions between entry type and arm action. These data support the suggestion that arm motion at entry is related to the production of a rip entry in typical competitive dives from the 10 meter platform.

Brown, J.G., Abraham, L.D., & Bertin, J.J. Descriptive analysis of the rip entry in competitive diving. Res. Quart. for Exerc. & Sport, 1984, 55, in press.

Dynamics of an Upper Extremity Striking Skill

D.J. Kriellaars School of Physical Education
Dalhousie University, Nova Scotia, Canada

Rapid swinging motions, such as throwing, kicking and hitting represent a large proportion of sports skills. One objective of these skills is to maximize angular speed distally. The kinematics of these skills have been examined and a similar pattern exists. Generally, extremities have been modeled as two segment systems, proximal & distal. Initially, the proximal segment angularly accelerates in the hitting direction and then near mid-movement, begins and continues to decelerate until impact or release. The angle between proximal and distal segments decreases for the first half of the motion followed by a phase where this angle opens rapidly, increasing in speed for the remainder of the movement.

For rapid swinging skills the nature by which this kinematic pattern is achieved is not well established. Two high speed cine film trials were collected on six athletic subjects performing a planar upper extremity striking skill from an overhead position. Simultaneous EMG was recorded from representative agonists and antagonists. Three load conditions were used, no load, medium load (m=.45 kg) and heavy load (m=.91 kg). The standard inverse dynamical approach and Newtonian equations of motion were utilized on a two segment model of the upper extremity to derive segment kinetics. The kinetic parameter-time functions were averaged across subjects for each load condition. As well as the resultant joint moment, an interactive moment was calculated representing the rotational effects of joint reaction forces that develope during multisegmental motion.

For all load conditions, the shoulder joint moment indicated that the net muscular activity was agonistic throughout the course of the motion. This was supported by the EMG records which showed agonist activity to be near maximum voluntary contraction (MVC) and no antagonist activity throughout the movement. This accounted for the proximal segments initial angular acceleration in the hitting direction. The fact that the proximal segment angularly decelerated during the latter half of the motion was therefore attributed to the interactive moment.

For the first 60 % of motion (independent of load) the angle between the proximal and distal segment (elbow angle) decreased. The elbow joint moment, however, was in the direction of extension corresponding with the triceps EMG. Thus, the monoarticular heads of triceps were eccentrically contracting to limit the extent of elbow flexion. During the final 40 % of movement, the elbow angular speed increased rapidly reaching, on average, 19 rad/s at the target height (independent of load). The triceps EMG was active at MVC levels but the elbow joint moment diminished, as predicted by the torque/velocity relationship. The interactive moment was a substantial contributor to angular acceleration of the distal segment in the hitting direction during the final 40 % of movement and the primary contributor in the heavy load condition.

These results are in accordance with those found for kicking skills and demonstrate that during the motion of multi-segmental systems the moments about a joint not only arise from muscular and gravitational forces but also from reaction forces that arise during system motion. Further, the moment of the intersegmental reaction forces have been shown to contribute to segmental motion during phases where muscular action was previously thought to be the primary effector.

JAVELIN THROW OPTIMIZATION USING COMPUTER SIMULATION AND TRAJECTORY INSTRUMENTATION

M. Hubbard and M. L. Hull
Department of Mechanical Engineering
University of California, Davis

In the javelin, as in all other throwing events, the range depends uniquely on the state (position, velocity, attitude, angular velocity) of the instrument at the instant of release by the thrower. Because clearly defined gravitational and aerodynamic forces act during the flight phase, numerical integration of the differential equations of motion can illuminate the mapping of initial conditions into range [1,2]. In addition, numerical optimization techniques can then be used to find the particular set of initial conditions which maximize the range [3]. Beyond the theoretically optimal set of initial conditions, such simulation and optimization studies can yield valuable insight about the sensitivity of the trajectories to perturbations in the initial conditions from the optimal.

Clearly, the ultimate goal of such research must be communication of the results to the athletes so that their throwing techniques can be modified to make actual throws be as close as possible to the theoretically optimal release conditions [4]. This, in turn, requires more or less immediate feedback to the thrower regarding performance, since even if the optimal initial conditions are known they are of little use if the athlete does not know what his or her actual throw initial conditions are and thus does not know how they should be changed to more closely approximate the optimal ones. Therefore, it is important to devise an instrumentation scheme which can accurately measure the conditions at release. This information must be accessible to the athlete within a relatively short time period (of the order of seconds or minutes rather than hours or days) so that succeeding throws in a training session may be modified using the information about previous throws.

The design of an onboard instrumentation scheme is extremely challenging. Since the total javelin weight is only 0.8 Kg, in order to maintain the total weight at this figure, the upper bound on the instrumentation system weight budget is roughly 0.2 - 0.3 Kg. This weight restriction virtually eliminates most standard inertial attitude instrumentation (e.g. gyros) from consideration. Extremely lightweight accelerometers are available, however. It has been shown that a set of linear accelerometers may be used to deduce angular accelerations, velocities, and attitudes, but such calculations involve numerical instabilities [5]. Thus, one is led to seek an independent source of attitude information.

The instrumentation scheme presently under development relies on a measurement of the earth's electrostatic field for attitude information and on a set of lightweight accelerometers for linear accelerations. Both kinds of information are telemetered to a collecting station more or less instantaneously using standard telemetry technology [6]. In what follows, we briefly discuss the electrostatic attitude and accelerometer portions of the instrumentation system.

In 1750, Benjamin Franklin discovered that lightning transfers large amounts of negative charge to the earth [7]. This charge results in a potential difference between the earth's surface and the upper atmosphere (altitudes > 5×10^4 m) of roughly 3.5×10^5 Volts, and in a set of very smooth horizontal equipotential surfaces between the upper atmosphere (the positive plate of the capacitor) and the earth (the negative plate) [8].

Although the potential gradient varies with altitude, it is constant to within a few percent in the first 50 or so meters at roughly 300 V/m. The attitude information of the javelin relies on the tapping of these equipotential surfaces using sensors similar to those discussed in [9]. The altitude difference between two separated voltage nodes on the javelin then equals their measured potential difference divided by the earth's potential gradient. This altitude difference can then be processed to yield javelin pitch attitude.

Space limitations prevent a complete discussion of the algorithms involved in processing the accelerometer and electrostatic field attitude data to obtain a complete description of the dynamic javelin state. The scheme uses ideas from [5] and [10], incorporating the electrostatic field attitude information to stabilize the numerical instabilities inherent in processing accelerometer data above.

The particular data processing scheme appears to hold promise, not only in the particular javelin application discussed here, but also in the instrumentation of other biomechanical motions.

References

1. Hubbard, M. and H. J. Rust, "Javelin Dynamics with Measured Lift, Drag, and Pitching Moment," J. appl. Mech., to appear, 1984.

2. Hubbard, M. and H. J. Rust, "Simulation of Javelin Flight Using Experimental Aerodynamic Data," J. Biomechanics, to appear, 1984.

3. Hubbard, M., "Optimal Javelin Trajectories," J. Biomechanics, to appear, 1984.

4. Hubbard, M., "Javelin Trajectory Simulation and Its Use in Coaching," presented at the Second International Symposium on Biomechanics in Sports, Colorado Springs, CO, January 1984.

5. Padgaonkar, A. J., Krieger, K. W. and King, A. I., "Measurement of Angular Acceleration of a Rigid Body Using Linear Accelerometers," J. appl. Mech., 42, 552-556, Sept. 1975; also discussion, J. appl. Mech., 43, 377-378, 1976.

6. Hull, M. L. and Mote, C. D., Jr., "PCM Telemetry in Ski Injury Research: Part 1 - Instrumentation," Journal of Biotelemetry, 1(4), 1974, pp. 182-191.

7. Franklin, B., Phil. Trans. Roy. Soc., 47, 289, 1752.

8. Chalmers, J. A., Atmospheric Electricity, Pergamon Press, 1967.

9. Hill, M. L., "Introducing the Electrostatic Autopilot," Astronautics & Aeronautics, 22-31, Nov. 1972.

10. Mitai, N. K. and King, A. I., "Computation of Rigid-Body Rotation in Three-Dimensional Space from Body-Fixed Linear Acceleration Measurements," J. appl. Mech., 46, 925-930, 1979.

MECHANICAL LOADING AND SKELETAL REMODELING DURING GROWTH. A.A. Biewener, S. Swartz, and M. Lee, University of Chicago, Chicago, IL.

Whereas the biochemical and hormonal factors governing bone growth have been studied in great detail, the importance of mechanical loading as a factor modifying skeletal remodeling during growth is relatively unknown. Studies that have been conducted present a conflicting view of the effects of exercise on developing bone. Differences in data reported for bone mass, length, % mineralization, and chemical composition may in large part due to differences in exercise protocol, as well as differences in the growth rates and ages of the species studied. The present study has been designed to factor out the importance of specific differences in strain history (eg. strain magnitude, strain rate, # loading cycles) on the remodeling response of chick tibiae during growth from 4 - 17 wks of age.

The animals were trained and run on a treadmill at 30% of their top speed (constant stride frequency over this age range) for 15 min at five days/wk. In vivo strain recordings were made using both single element and rosette gauges at six sites on the chick tibia (right tibia: proximal/medial, P/M, cranial midshaft, Cr/M, caudal midshaft, Cd/M, medial midshaft, M/M; left tibia: cranial distal, Cr/D, and caudal distal, Cd/D). Separate recordings were made at 5, 11 & 17 wks age. Periodic flourescent bone labels were also administered to the animals to correlate loading measurements and age with changes in bone structure.

Strain levels were found to vary significantly with gauge location. For instance at 5 wks, running at 0.96 m/s, the following strain levels (in microstrain) were recorded: -710 ± 63 (SD), P/M; $+330 \pm 87$, Cr/M; -1550 ± 120, Cd/M; -930 ± 89, M/M; -1025 ± 114, Cr/D; $+130 \pm 42$, Cd/D (n=15 strides). The distribution of loading was similar over a range of speed,

but as the animals changed speed from a walk to a run (65% of top speed) strain magnitude increased markedly (eg. 54% at Cd/M). These strains show the chick tibia to be loaded primarily in bending (but in opposite directions at the midshaft and distal levels). The orientation of maximum principal strains at the midshaft (37° proximo-lateral, Cd/M; 40° proximo-medial, Cr/M), however, indicate significant torsional loading as well. Strain levels, and the orientation of principal strains at the P/M, Cr/M, and Cd/M sites, recorded at each age were generally consistent. The variance in strain magnitude normalized to the levels recorded at wk 5 ranged from 18 $\pm$ 5% at Cd/M to 63 $\pm$ 21% at Cd/D (n=9). Some of this variability was due to differences between individuals, in addition to differences in age. This suggests that the bone cell population regulates and integrates its remodeling activity so as to maintain similar patterns of strain during growth, a period when the bone's mass and length increase 10- and 2-fold, respectively. Ongoing experiments in which the loading regime of the bone is varied with regard to the above defined loading parameters, will allow a comparative evaluation of the importance of differences in strain history on the size, mass, shape, % mineralization, and details of tissue histology of this bone model. (Supported by The Whitaker Foundation & Biomedical Research Support Fund, Univ. of Chicago).

Instantaneous In Vitro Contact Stress Distributions on the Femoral Condyles

Thomas D. Brown and Daniel T. Shaw, Department of Orthopaedic Surgery, University of Pittsburgh, Pittsburgh, Pa. 15261

Although the magnitude and direction of resultant contact forces at the knee have been well characterized, little is known about the manner in which such loads are distributed across the articular surfaces. Several recent studies of contact stress distribution across the tibiofemoral articulation have explored the mechanics of static contact using viscoplastic indentation sheets or Fuji Prescale film, and have considered the effects of meniscectomy upon intra-articular pressures [1,2]. Statically-measured pressure distributions may not be fully representative of the pressures prevailing under transient physiological loading, however, due to the biphasic, time-dependent behavior of articular cartilage. This study discusses tibiofemoral contact stress distributions measured instantaneously, using arrays of miniature piezoresistive transducers.

Contact stress distributions were measured in vitro on the femoral condyles of 11 fresh normal knee specimens obtained at routine autopsy. Arrays of 24 thin pressure sensors [3] were mounted in recesses milled in the superficial cartilage layers of the femoral condyles. Calibrated outputs from the sensors were recorded, digitized, and input to a contouring algorithm which assembled a continuous spatial map of the instantaneous pressure distribution. Knees were fixed at 0, 10, 20, and 30 degrees of flexion and were subjected to cyclic ($\simeq$1 Hz) compressive loads from 0 to 2200 N. Similar recordings were made from fully extended knees after performance of medial and then lateral meniscectomies. Numerical integration of the plotted pressure distributions yielded resultant force overestimations averaging 17.7%, and having an average angular deviation of 8.92 degrees from the direction of applied load.

The dynamic spatial pressure patterns were complex and highly variable. A representative distribution is shown for a fully extended knee, prior to meniscectomy, in Figure 1. Each condyle usually showed a single, centrally located peak pressure, with a smooth decay toward the contact periphery, and generally with an anteriorly-to-posteriorly elongated topography. As load increased the general topographical features were preserved, but with additional contact area recruitment (Fig 2) and with increases in the peak local pressure (Fig 3). With flexion from 0 to 30 degrees, the pressure patch shifted posteriorly, and there were substantial changes in topographical details. However, neither the contact area nor the peak or spatial mean contact stresses demonstrated statistically significant changes in this flexion range. The contact area and peak pressure parameters agreed reasonably well with previous static measurements for the intact knee, but the present results were much less sensitive to the performance of meniscectomy than were previous static measurements. A possible explanation for this meniscectomy disparity is that static loading tends toward contact pressure equilibration, and hence emphasizes the load-bearing contributions of peripheral regions.

REFERENCES: [1] Ahmed & Burke, J. Biomech. Engr. 105:216-225, 1983.
[2] Fukubayashi & Kurosawa, Acta. Orthop. Scand. 51:871-879, 1980.
[3] Brown & Shaw, J. Biomech. 15:329-333, 1982.

Financial assistance was provided by NIH Grant AM26010.

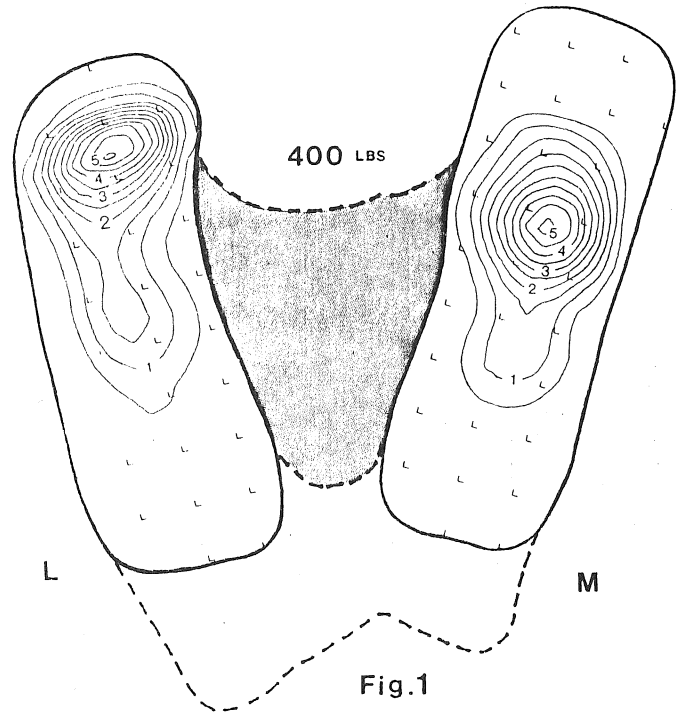

Fig.1

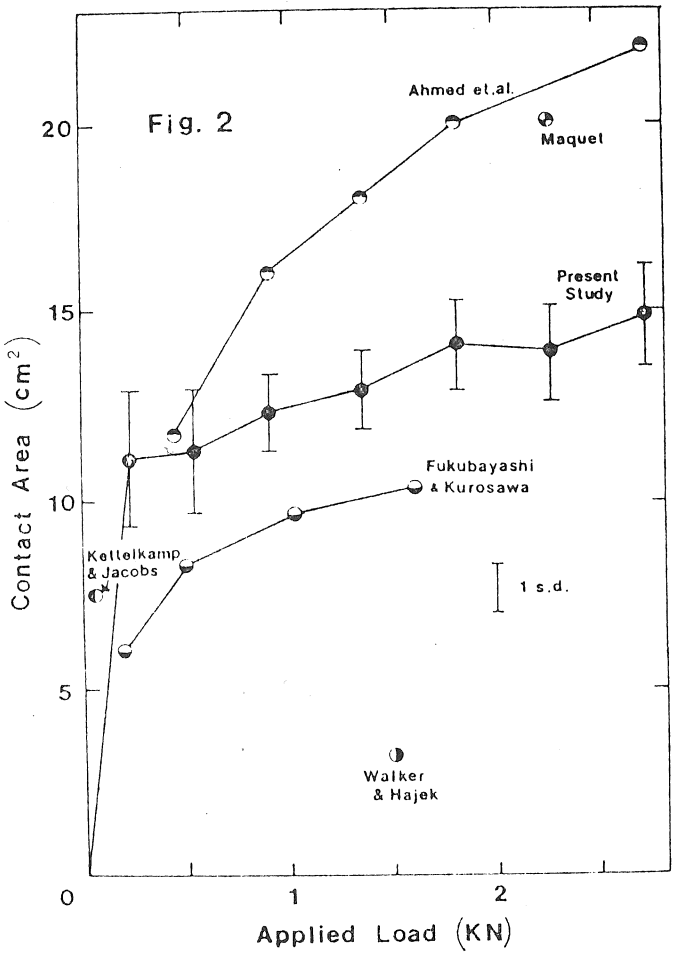

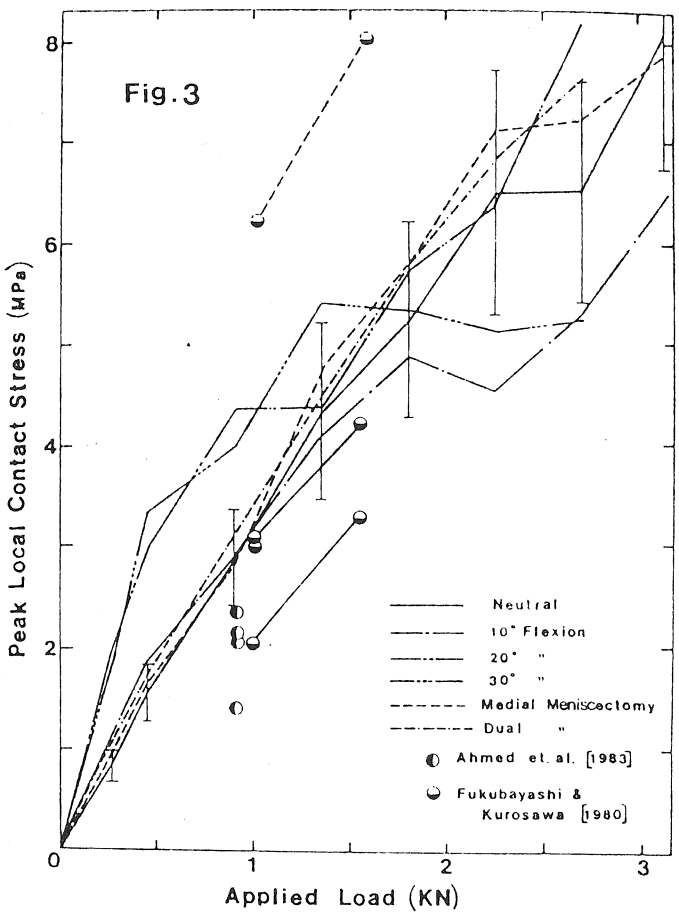

Figure 1. Pressure contours (multiples) of 100 PSI) for a natural knee in full extension loaded to 400 pounds.

Figure 2. Series average values for growth of contact area with applied load.

Figure 3. Series average values for peak local contact stress as a function of applied load.

TIBIAL VIBRATION TRANSMISSION - THE EFFECTS OF INCREMENTAL OSTEOTOMY.

W.J. Mintowt Czyz, FRCS
J.A. Fairclough, FRCS
I.G. Mackie, FRCS
L.D.M. Nokes, M.Sc.,Ph.D.

The human tibia will transmit vibration along its length in response to an impulse at one end. Accelerometers positioned proximally and distally detect the vibration and can measure its magnitude. The ratio of the distal to the proximal measurements yields a measure of the attenuation of the vibration as it passes along the bone. This "attenuation factor" (AF) has been shown to change predictably during fracture union and has been used as a measure of bone healing.

This cadaver study was performed to investigate the changes in vibration attenuation consequent upon the making of an osteotomy in stages through the tibia with the intention of discovering what was the influence of the residual intact bone in allowing vibration transmission to occur.

Five tibiae were studied. Incremental osteotomies were made with a gigli saw in five stages through each bone and the attenuation factor measured at each stage. The depth of the cut was used as an assessment of the residual intact bone.

Standard transmission theory suggests that energy transmission along an object is proportional to its cross sectional area. The results of this study show that the attenuation factor is proportional to the calculated residual area of intact bone, making the assumption that the tibia at the point of division has a triangular cross-section with a triangular section to its medullary cavity.

The results imply that measurement of the attenuation factor might be a useful technique for the assessment of the mechanical integrity of bone and support the finding that in life attenuation factor changes in parallel with fracture healing.

TIME DOMAINE VIBRATION ANALYSIS IN THE ASSESSMENT OF STABILITY AFTER INTERNAL FIXATION OF TIBIAL FRACTURES.

J.A. Fairclough, FRCS
W.J. Mintowt-Czyz, FRCS
I.G. Mackie, FRCS
L.D.M. Nokes, M.Sc.,Ph.D.

The human tibia will transmit vibration along its length in response to an impulse at one end. Accelerometers positioned proximally and distally detect the vibration and can measure its magnitude. The ratio of the distal to the proximal measurements yields a measure (AF, the attenuation factor) of the attenuation of the vibration as it passes along the bone. Transmission of vibration does not occur across an interuption but can be restored if the interuption is bridged. We have used osteotomies in cadaver tibiae to simulate fractures, and have then fixed them with different plates put on in various fashions with the object of finding out if the level of vibration transmission can reflect the stability of the internal fixation. The models studied were:

(i) unfixed osteotomy

(ii) optimum fixation with 4.5mm AO plate and compression.

(iii) AO plate (4.5mm) fixation with a gap

(iv) compression fixation with a 1/3 tubular AO plate

The results show that the unfixed osteotomy does not transmit vibration significantly, but that an optimum compression fixation with an adequate implant restores vibration transmission to normal. The gap fixed single plate model transmits vibration only slightly better than the unfixed osteotomy, but in contrast, the inadequate 1/3 tubular implant fixed in compression increases transmission three-fold.

The inference is drawn that if an osteotomy is fixed with an adequte implant using optimum technique then the stability obtained is mirrored in the vibration analysis. However, if either the implant or the technique are inadequate the loss of stability will be reflected by the change in vibration attenuation. The technique of vibration analysis described is easily applied to the living fracture victim and offers the opportunity for the post operative objective measurement of implant stability with the intention of detecting inadequate fixation and avoiding the hazards of implant failure.

Some Characteristics of Laminar Flow Velocity Spectra Detected by a 20 MHz Pulsed Ultrasound Doppler

Thomas D. Brown, Ronald H. Gabel, Douglas R. Pedersen, Lawrence D. Bell, and William F. Blair, Departments of Orthopaedic Surgery and Biomedical Engineering, University of Iowa, Iowa City IA 52242

Recently reported laboratory studies have shown that 20 MHz pulsed ultrasonic Doppler velocimetry (PUDVM) is a sensitive method for measuring velocities and for calculating volumetric flow rate in small vessels following a number of microsurgical or pharmacological manipulations. Detection of Doppler frequency shifts in this class of instruments has previously relied upon zero-crossing detector (ZCD) circuitry, but such phasic output can be influenced by several factors not directly related to local particle velocity in the insonated field. To make possible more accurate quantitation of the details of the flow field in vessels with lumen diameters in the range of 1 mm, we have now implemented spectral analysis of the Doppler signal. This paper reports details of the data capture and processing techniques, and discusses major phenomena observed in the Doppler spectra from a series of benchtop Poiseuille flows, for which the true velocity distribution is known analytically.

Outputs from quadrature phase detectors in the existing PUDVM circuit were sampled at 12.8 KHz by an A/D convertor and were then stored in RAM of a MINC (PDP 11/23) laboratory computer. As the location of the PUDVM sample volume was incrementally advanced (under MINC control) across the flow stream, data were digitized for individual 20 msec collection intervals. Subsequently, these local scans were transformed to the frqeuency domain by the MINC implementing a fast Fourier transform (FFT) software routine. In addition to the conventional phasic (ZCD) velocity, three spectral indices characterizing the sampled local flow were identified: the mean velocity (V_M), maximum significant velocity (V_{MS}), and the velocity of dominant spectral energy (V_{DE}). To aid interpretation of the effects of finite sample volume size upon these spectral indices, an off-line geometrical analysis program was written to construct hypothetical velocity spectra based upon searches of (analytically-determined) velocity contents of cells in a finely-subdivided mesh network.

For 0.2 mm wide sample volumes sited at centerstream, the contents of the velocity spectrum showed substantially more broadening (Fig. 1) than could be accounted for by ostensible sample volume geometry or by numerical roundoff for digital FFT arithmetic. In the raw spectrum, V_M falls well below the analytical centerstream velocity, although it substantially exceeds the phasic velocity. By contrast, V_{MS}, if defined in terms of a zero noise threshold, was always greater than centerstream analytical velocity. Excellent analytical velocity agreement was achieved with V_{DE} and with V_{MS} when a noise threshold τ_e corresponding to 95% of backscattered energy was imposed. Operated in this manner, the system output was linear and accurate for velocities up to the apparatus design limit of 60 cm/sec (Fig. 2), above which aliasing effects became significant for the FFT sampling rates employed.

Analyzed performance varibles included the effects of physical probe proximity vs. electronic ranging, and the spectral broadening associated with increases in the width and in the breadth of the sample volume. Spectrum reproducibility was evaluated following axial probe rotations and following complete apparatus breakdown and reassembly, as well as for variations in the reflective particle types and concentrations.

Financial assistance was provided by P.H.S. Grant HL31362 and by a grant from the Orthopaedic Research and Education Foundation.

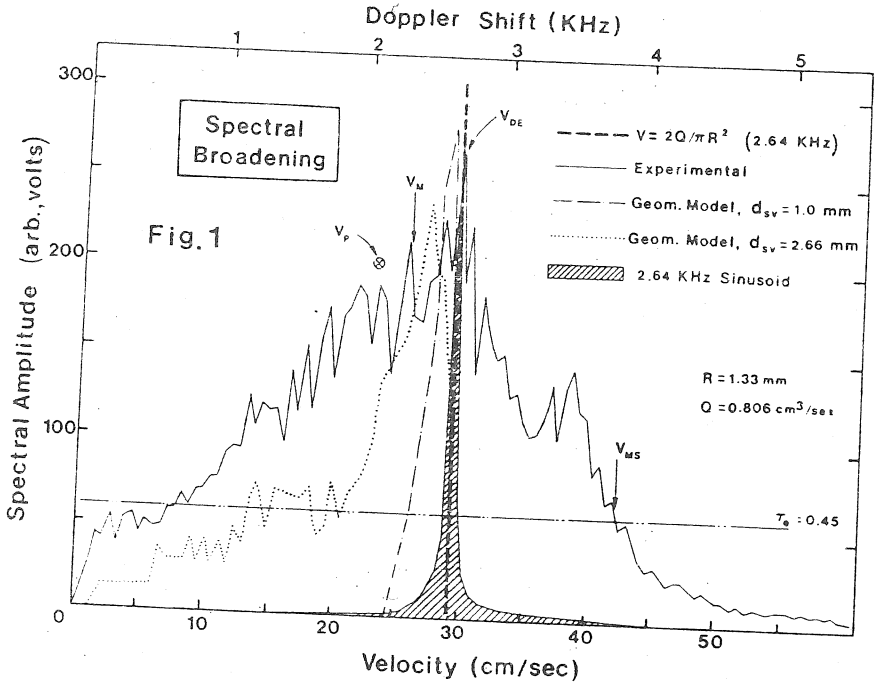

Broadening of experimentally observed velocity spectrum compared to centerstream Poiseuille flow velocity. The geometrical search model shows that much of the lower frequency energy can be accounted for by sample volume diameter increases of from 1 mm (actual crystal diameter) to 2.66 mm (full vessel diameter). The shaded region indicates the spectrum computed for a 2.64 KHz sinusoid delivered by a function generator.

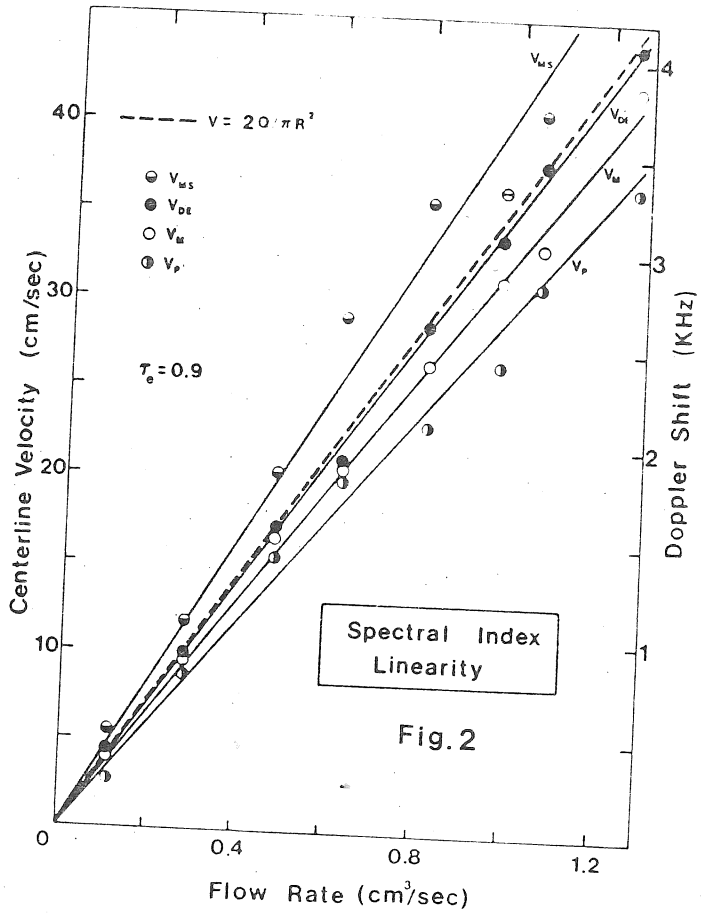

Linearity of the spectral indices was consistent in the velocity range of interest for small vessels. The V_{DE} index showed excellent correlation with the analytical centerstream velocity.

IN VIVO STUDIES ON LEUKOEMBOLI FORMATION--AN INTRAVITAL MICROSCOPIC ANALYSIS

Anthony T.W. Cheung, Michael E. Miller, Erin M. Walsh and Richard M. Donovan
School of Medicine and California Primate Research Center
University of California at Davis

It is acknowledged that interactions between plasma complement and leukocytes play an important role in the inflammatory host defense mechanism. This broad role includes the opsonization of microbial invaders for phagocytosis and the attraction of leukocytes to the inflammatory site (chemotaxis) under controlled conditions. However, under uncontrolled conditions (as in the case when the complement-leukocyte interaction is inappropriate or prolonged), potential harm can be inflicted. Such uncontrolled interactions have long been felt to contribute to the damages in rheumatoid arthritis and glomerulonephritis (Hammerschmidt and Jacob 1978). Postulations of the significance of plasma complement-leukocyte interactions in the genesis of a variety of immune injuries have been proposed, but the in vivo role of complement-leukocyte interaction and the phenomenon of leukoemboli formation have not been fully analyzed or quantified.

Early investigations on in vivo complement-leukocyte interaction were initiated at the Bioengineering Laboratory of the California Institute of Technology (Wayland 1982). Pilot research on leukoemboli formation originates from Wayland's laboratory, with the collaborative usage of his prototype intravital microscope (Cheung and Miller 1982; Hammerschmidt and Jacob 1978; Wayland 1982).

A specially-equipped intravital microscope has been constructed for in vivo microcirculatory use. The microscope was specifically designed to be used in the documentation and quantification of in vivo movement and aggregation characteristics of leukocytes in the mesenteric microvasculature of laboratory rats.

Briefly, Sprague-Dawley white rats were set up for intravital manipulation and microvascular documentation. FITC-labeled leukocytes previously prepared before experimentation were intravenously injected into the rats. With epi-monochromatic irradiation set at line 488, the FITC-labeled leukocytes were activated to fluoresce and their flow and movement

characteristics were videotaped with a SIT camera. The rate of movement, optical density, size of each fluorescent cell and interaction with the vessel wall were determined and quantified later by manual analysis and by computer-assisted micro-image-processing. Synthetic chemotactic peptides (FMLP) and endotoxin-activated plasma (mostly C5a complex) were injected into separate animals and the effect of the injections on the functional and behavioral characteristics of the leukocytes and the resulting leukoemboli formation were videotaped and analyzed.

Manual analysis was conducted by the commonly used tracing technique. Computer-assisted analysis and quantification was carried out by a developed in-house micro-image-processing procedure. Briefly, videotapes on in vivo fluorescent cell movement and aggregation were digitized at a resolution of 240 x 320 x 8 bits using a Datacube analog to digital converter, interfaced with a LSI 11/23 computer operating under RT-11/TSX. The digitized data were then used for computation (of cell or aggregate perimeter, surface area, optical density, position, speed/direction of movement, adhesion characteristics to vessel wall and other morphometric and pathological characteristics) with the utilization of computer programs written in FORTRAN and ASSEMBLY language.

The result obtained from this computer-assisted intravital microscopic approach will provide a quantitative and in-depth characterization of complement-leukocyte interaction and will generate a better understanding of the in vivo leukoemboli formation phenomenon arising as a result of complement action. The data generated can provide a better rationale in the treatment and probably prevention of this harmful pathological condition.

References:

Cheung ATW and Miller ME (1982). In vivo movement of polymorphonuclear leukocytes: an intravital-microscopic analysis. Proc. 5th UCD Biomed. Engr. Sym. pp. 59-62.

Hammerschmidt DE and Jacob HS (1978). Complement-granulocyte interaction, pp. 117-122. In Landel (ed), Harold Wayland Symposium, Satellite Session of 2nd World Congress and 25th Anniversary Meeting of the Microcirculatory Society of U.S.

Wayland H (1982). A physicist looks at the microcirculation. (E. Landis Award Lecture). Microvas. Res. 23:139-171.

A COMPUTER-ASSISTED METHOD FOR MEASURING CELL MOVEMENT

Richard M. Donovan, Anthony T.W. Cheung,
Michael E. Miller and Elliot Goldstein
School of Medicine and California Primate Research Center
University of California at Davis

Most studies of cell movement have used indirect methods (such as neutrophil migration into filters or through agar) or visual assays (such as manual tracings of time-lapsed movies and videotapes of ciliary, amoeboid or tracer movement). Although indirect methods can give an overall account of cell movement, they can only serve to investigate movement characteristics of a biased sample of only the fastest and most mobile cells. Visual assays can give a more comprehensive and time-dependent view of cell movement, however data acquisition/analysis tends to be slow, tedious and subjective.

We have developed a computer-assisted method to quantify movement and morphometric characteristics of individual moving cells. This computer-assisted system consists basically of a video-recorder (JVC CR-60604) on line with a Digital LSI 11/23 computer interfaced with a Datacube frame-grabber/digitizer. Video signals from the video-recorder are digitized at a resolution of 240 x 320 pixels (picture elements) and 256 gray levels. The system is equipped with a

Winchester disc, two terminals, a printer, a plotter and a video-monitor.

Videotapes of cell movement (taped under phase contrast microscopy) can be digitized by the LSI 11/23 computer operating under RT-11/TSX. The digitized data can then be used for computation of cell perimeter, area, optical density, position, speed and direction of movement with the utilization of micro-image-processing programs written in FORTRAN and ASSEMBLY language. Our system can simultaneously trace up to 50 cells at time intervals as short as 10 seconds and can determine instantaneously and accurately the speed, direction as well as morphometric characteristics related to movement.

The reliability, compatibility and reproducibility of measurements and quantifications made with our computer-assisted system was tested by comparison with established (tracing) measurements on neutrophil chemotaxis. A correlation coefficient of 0.99 was obtained between the two methods. However, the computer-assisted method is much faster, accurate, less tedious and more objective than the manual method.

Red blood cell mechanics and blood flow in narrow capillaries

T.W. Secomb and J.F. Gross
Department of Physiology, University of Arizona, Tucson AZ 85724

Introduction

The rheological properties of blood in microvessels are largely determined by the mechanical properties of the individual red blood cells. When blood flows along narrow capillaries (3-6 microns in diameter) the red cells travel in single file, each almost filling the lumen. Reynolds lubrication theory may then be used to calculate the flow in the narrow gap between the cells and the vessel wall. Early models using this approach (1,3) lacked a realistic treatment of the mechanical properties of the red cells. These are now fairly well established (6). The cytoplasm is an incompressible Newtonian fluid, surrounded by a thin membrane, whose elastic response depends on the types of deformation it undergoes: dilation, in-plane shear or bending. The elastic modulus of dilation (about 5×10^{2} dyn/cm) greatly exceeds the shear modulus (about 5×10^{-3} dyn/cm), while the bending modulus (about 10^{-12} dyn cm) is so small that bending stresses are important only in regions of high curvature or when in-plane forces are small.

Here we report a series of models for red cell motion in narrow capillaries. Lubrication theory is used and the approximation of axisymmetric geometry is made, as in earlier models. In the simplest model, the shear and bending resistance of the membrane are neglected, and the membrane stress is then isotropic tension. Inclusion of shear and bending resistance results in models applicable at lower flow rates. The results are compared with published measurements of apparent blood viscosity in microvessels.

Methods

With the assumptions described, the equations governing both the fluid flow in the gap and the mechanical equilibrium of the membrane may be written as a system of nonlinear ordinary differential equations. The independent variable is arc length, measured from the axis. The boundary conditions, including fixed

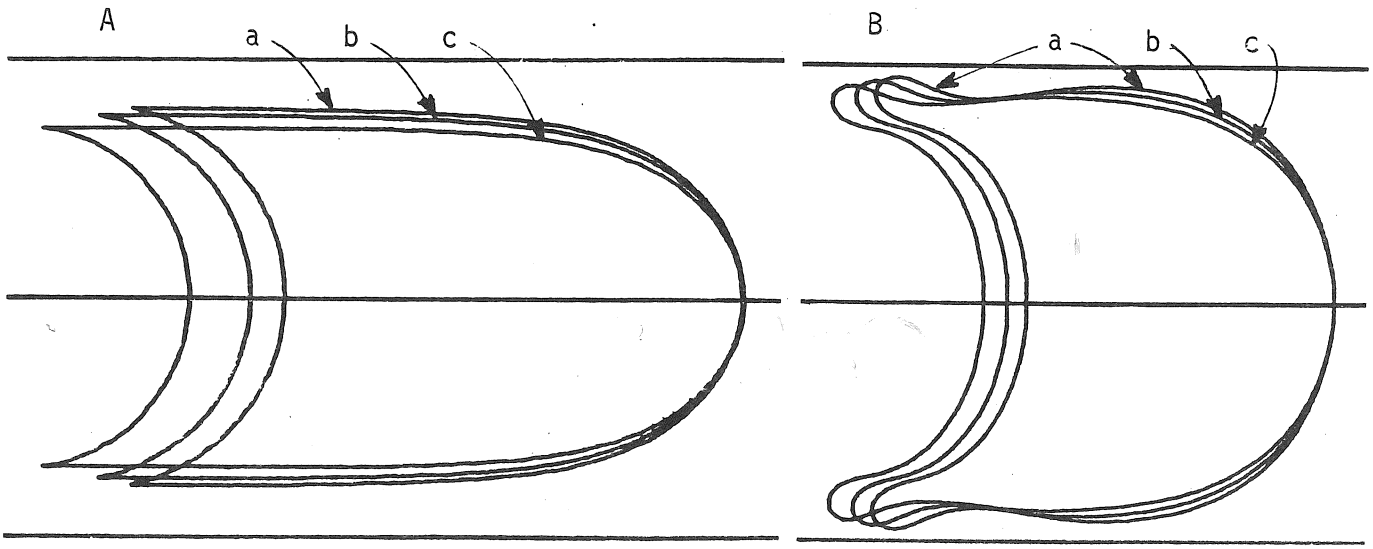

Figure 1. Computed shapes of axisymmetric red blood cells passing along a vessel of diameter 6 μm. Cell volume is 90 μm^3, surface area is 135 μm^2. Motion of cell is from left to right. A. Results of model including shear elasticity: (a) u_o = 0.125 cm/s; (b) u_o = 0.25 cm/s; (c) $u_o \to \infty$, which corresponds to the isotropic surface tension model. B. Results of model including both shear and bending elasticity: (a) u_o = 0.005 cm/s; (b) u_o = 0.01 cm/s; (c) u_o = 0.02 cm/s.

surface area and volume, lead to a two-point boundary value problem which is solved numerically. In those calculations which neglect bending resistance, a cusp is formed at the trailing edge of the cell (Fig. 1), and the rear concavity is approximated with a spherical segment.

Results

The simplest model, assuming isotropic membrane tension, is described in (5). It predicts an apparent viscosity independent of flow rate, and is appropriate at moderate to high flow rates (above 1 mm/s). At lower flow rates the inclusion of shear and bending resistance leads to an increase in apparent viscosity, because the cell tends to broaden and more nearly fill the lumen (Fig. 1). Figure 2 shows results from the three models for a wide range of flow velocities in 6 micron tubes. The results are seen to agree fairly well with available experimental data (2,4).

This work was supported by NIH Grant HL 17421.

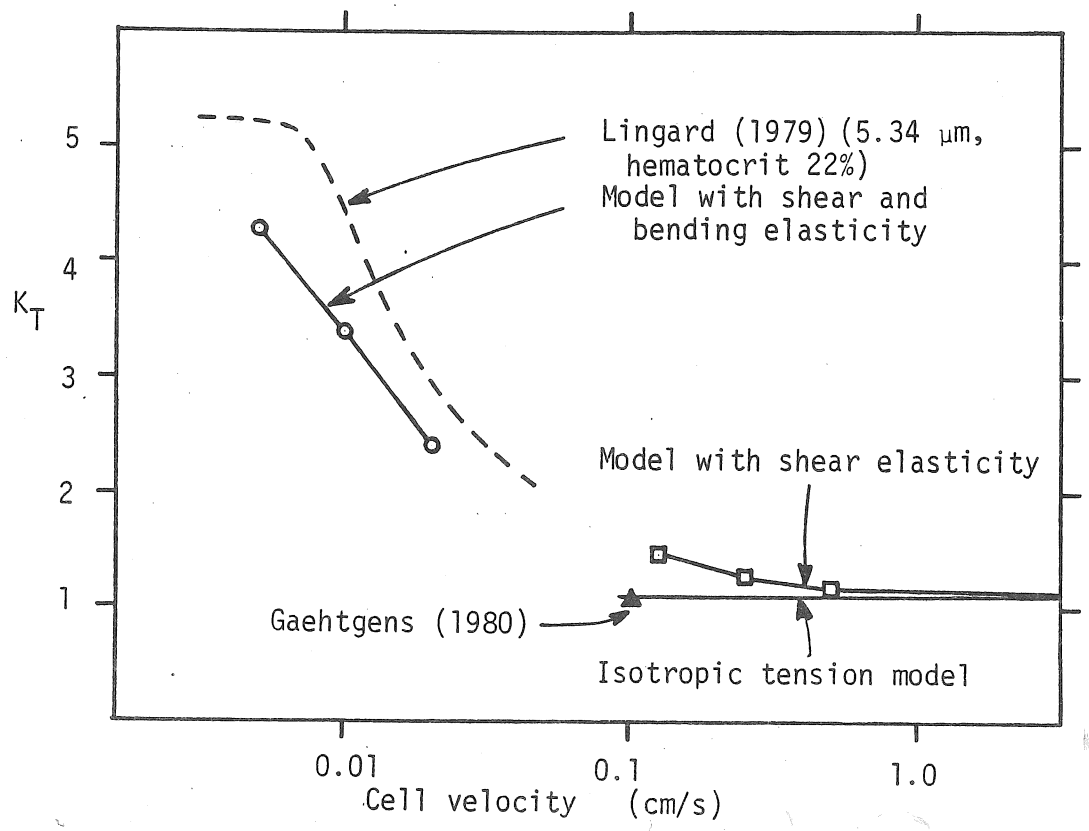

Figure 2. Variation of apparent viscosity with cell velocity in a vessel with diameter 6 μm. Predictions from theoretical models are compared with published experimental data. The relative apparent viscosity η_{rel} is related to the parameter K_T through the equation $\eta_{rel} = 1 + H_T K_T$ where H_T is the tube hematocrit.

References

(1) Barnard, A.C.L., Lopez, L. and Hellums, J.D. (1968) Microvasc. Res. 1, 23-34.
(2) Gaehtgens, P. (1980) Biorheology 17, 183-189.
(3) Lighthill, M.J. (1968) J. Fluid Mech. 34, 113-143.
(4) Lingard, P. (1979) Microvasc. Res. 17, 272-289.
(5) Secomb, T.W. and Gross, J.F. (1983) Int. J. Microcirc. Clin. Exp. 2, 229-240.
(6) Skalak, R. (1976) In "Microcirculation, Vol. I" ed. J. Grayson and W. Zingg, pp. 53-70. New York: Plenum.

AN IMPROVED 2-D FINITE ELEMENT MODEL OF THE PROXIMAL FEMUR

J. B. Koeneman, Ph.D.
Harrington Arthritis Research Center, Phoenix, AZ.

Three dimensional finite element analysis of the proximal femur is very time consuming and expensive. Thus, many 2-D finite element analyses have been done of the proximal femur. Three methods have been used to model the 3-D aspects of the problem: a) a frontal plane slice with no connection between the lateral and medial bone strips and using actual material properties of the constituents, b) a composite materials calculation to determine "effective" elastic properties of each region, and c) side plates which connect the lateral and medial bone slices. The first case does not represent the overall stiffness of the structure nor does it model the interaction of the various regions. The second case represents the overall stiffness but not the interaction. The third case represents both the overall stiffness and interaction of the regions, however, it over-estimates the stiffness of the connection between the lateral and medial bone strips. The purpose of this work was to develop a side plate which modeled the overall stiffness of the proximal femur and also the interaction of the slices in a more realistic manner.

Method. The cross section of the proximal femoral cortex can be represented as circular or elliptical. Figure 1 compares a cross section of a femur to the side plate model.

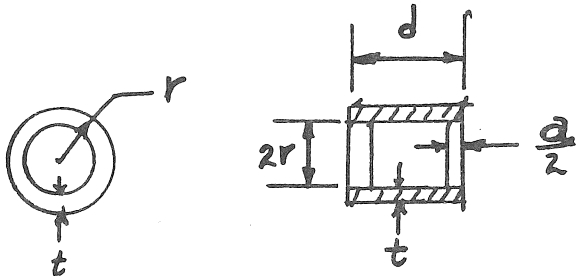

Actual Bone Side Plate Model

Fig. I Comparison of Actual Bone & Side Plate Model Cross Sections

The approach was to try to obtain dimensions and material properties of the side plates so that the axial, bending and transverse stiffnesses of the model and the actual section were the same. This was not possible if the side plate was isotropic. Even if an orthotropic side plate was used, the equality of the axial, bending and transverse stiffnesses could not be satisfied exactly. However, using orthotropic material properties, dimensions could be determined which made the stiffnesses of the model within ten percent of the actual section.

Results. A proximal femur with a prosthesis was modeled as shown in Figure 2. Side plate properties were calculated depending on the cross sectional geometry of the bone at that level. The thicknesses of the model were reasonable so that the interfacial stresses were not greatly distorted. The overall deflections calculated compared well with 3-D finite element calculations. The calculated forces between the bone, cement and prosthesis compared much better to the 3-D calculations than did calculations with 2-D methods (a) and (b).

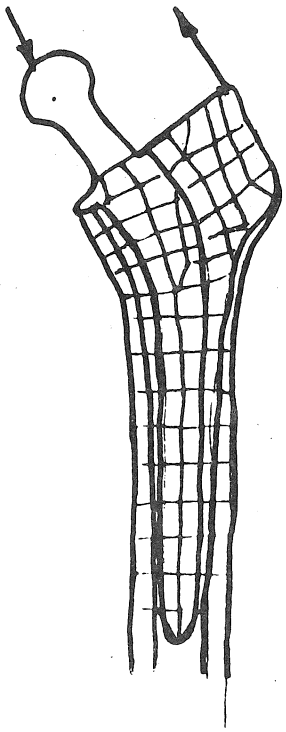

Fig. 2 Two Dimensional Finite Element Model

It is recommended that these anisotropic 2-D side plates be used in studies involving many calculations such as sensitivity studies of numerous parameters.

COMPUTER MODELING OF TEMPORAL EFFECTS IN BONE REMODELING PHYSIOLOGY

R. Bruce Martin, Orthopedic Research Laboratory,
West Virginia University, Morgantown, WV 26506

An important aspect of bone remodeling is the lag between osteoblastic and osteoclastic activity that occurs in both osteonal and surface remodeling. Response lags in feedback control systems are capable of introducing oscillating responses. Experimental data indicating such behavior in bone have been published by Jaworski and Uhthoff (JBJS,60-B,420,1978;JBJS,62-B,104,1980) for the case of canine disuse osteoporosis. Similar responses have been observed by other investigators, including our own laboratory in the case of bone loss caused by estrogen deficiency. A clear understanding of these phenomena is of great importance in skeletal research because the observed response in various experiments may depend upon the time between the onset of the treatment and the observation. The complexity of such phenomena is increased by the fact that the skeleton is affected by a number of stimuli and two major homeostatic mechanisms (calcemic and mechanical) which frequently are at odds with one another.

In order to better understand the temporal aspects of bone remodeling, analytical models are being developed on a digital computer which correspond closely to the actual bone physiology. The models' variables are histologically measurable and relate cell function to such mechanically important attributes as cross-sectional moment of inertia (via endosteal and periosteal radii) and elastic modulus (via porosity). Figure 1 presents a simplified flow chart of a model used to study disuse atrophy in cortical bone. BMU activation on various bone envelopes is assumed to be a sigmoid function of surface strain; the model assumes that 800 microstrain results in normal bone turnover and that strains above or below this level increase BMU activation. The constants in this relationship are determined by the physiologic range of values for strain and activation. Overstrain is assumed to inhibit osteoclastic function and enhance osteoblastic function, and understrain is assumed to have the opposite effect; again, the constants of proportionality are determined by the range of strains and cell responses that are observable.

Figure 2 compares the response of such a model to the experimental results of Jaworski and Uhthoff. The analysis to date demonstrate that a feedback signal proportional to strain on various bone surfaces is capable of producing the general exponential decline in bone mass observed in young Beagles, and the rate at which bone is lost is consistent with the model's rate of loss. If the amount of feedback is increased, the model predicts an oscillation in bone mass having the same period as the experimental data, but a waveform that is quite different. The model is currently being expanded to include other homeostatic mechanisms in an attempt to duplicate the experimental data.

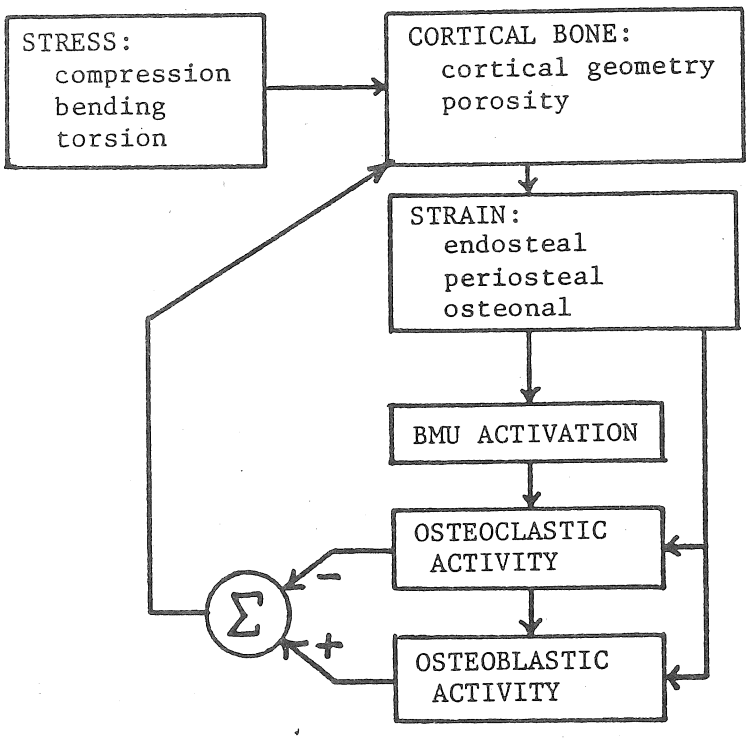

Figure 1

Figure 2A

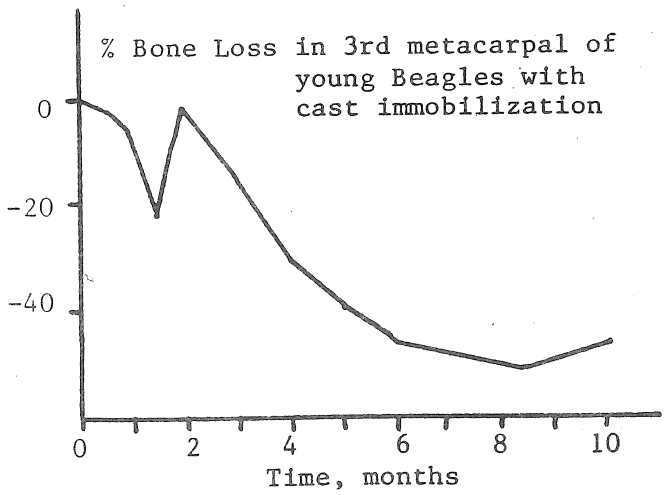

Figure 2B

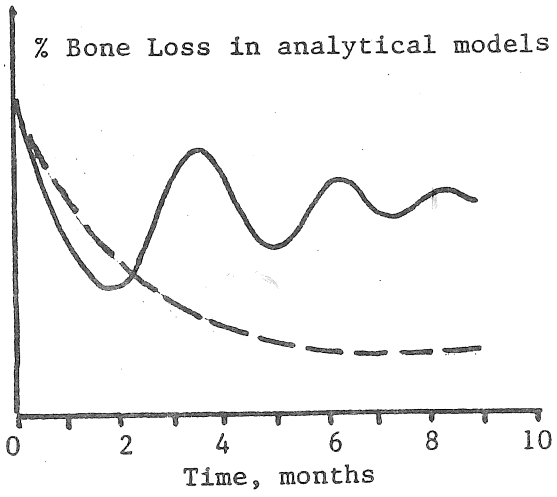

Stress Analysis of Porous Ingrowth Joint Arthroplasty in the Proximal Humerus

T.E. Orr and D.R. Carter

Rehabilitation Research and Development Center, VA Medical Center, Palo Alto, CA and
Design Division, Mechanical Engineering Department, Stanford University, Stanford, CA

INTRODUCTION: The successful ingrowth of bone into the surface of an implant will result in a firm fixation and a continuous, intimate interface which is efficient in stress transfer. However, the stress fields in the surrounding bone tissue can be radically changed from those in the normal skeleton. This has resulted in extreme bone remodelling and eventual implant failure in experimental animal models [1,5]. Carter et al. [2] conducted finite element analyses on canine femoral head surface replacements which incorporated bony ingrowth. Their results agreed with the animal studies, and indicated that with the implantation of shell-type surface replacements, forces were transmitted more distally at the rim of the shell and at the end of the peg or rod, thereby reducing stresses in the proximal head cancellous bone. Bone remodels to the extent that it can no longer support the implant. The supporting bone fractures and the interface bonding is destroyed. Because of the importance of bone remodelling with the use of porous ingrowth implants, the question of where to apply the porous coating has arisen.

In this study, we determined the stress distributions for the normal humerus, and then compared with those of an implanted shoulder prosthesis. We examined the difference in stresses between a totally coated porous humeral prosthesis and one with coating only on the undersurface of the humeral head of the implant. In analyzing and interpreting the results, special attention was paid to: 1) consistency between the calculated stress fields and the bone trabecular morphology; 2) the changes in stress fields due to various loading conditions; 3) the pattern of bone stress change caused by the implant; 4) the types of stresses created at the porous ingrowth surface (compression, tension, shear) and; 5) the manner in which bone may remodel in response to the stress changes.

MATERIALS AND METHODS: The internal trabecular pattern and geometry were examined and documented with roetgenograms and photographs of slices of a normal cadaver humerus. The bone was modelled as a regionally homogeneous isotropic structure. Material regions were designated in three dimensions, and yield strength, modulus of elasticity, and Poisson's ratio were assigned to each region based on local bone density and literature values.

The finite element models consisted of 2–D planar type elements (constant strain triangles and quadrilaterals) depicting the central coronal section of the humerus. Equivalent thickness models were employed to account for the out–of–plane stiffness. Three models were analyzed: 1) the normal humerus, 2) a fully porous–coated humeral prosthesis, and 3) a partially–coated prosthesis, coated only on the underside of the humeral head replacement. The implant was geometrically modelled as a "generic" stemmed humeral component with a flat head interface oriented at 45° with respect to the stem. This basic geometry approximates that of most commercially available designs. To model the characteristics of a uncemented stemmed prosthesis loose in the intramedullary canal, the stem was removed for the partially–coated prosthesis analyses. This approach assumes that the uncemented stem becomes completely surrounded by a fibrous layer which is inefficient in transferring load to the cancellous bone under normal loading conditions.

The mesh consists of 24 different stiffness regions and contains 1067 nodes and 1012 elements. Three different loading conditions were selected for stress analyses depicting three degrees of abduction of the arm: 90°, 45°and 0° (loading case 1,2, and 3 respectively). Each had a 1000 N joint force over the humeral head and a 450 N muscle force at the superior facet of the greater tuberosity. The distributed loads were transformed into nodal point loading for the analyses. Boundary conditions consisted of lateral and medial rigid support of the distal cortical bone.

RESULTS: In the normal humeral head, the joint resultant compressive forces were transmitted through the cancellous bone to the inferior wall of the humerus. Tensile stresses were created along the superior–lateral region of the bone. The calculated stress fields correspond with the trabecular bone orientation and density distributions of the cadaver humerus. The different stress distributions of the three loading cases were distinguished by the direction of the stress transmitted to the inferior wall. In addition, the amount of bending at the distal end increased with each sucessive loading case.

When a fully porous–coated prosthesis was implanted, significant forces were transmitted through the

stem of the prosthesis. The stresses in the inferior–medial cancellous bone were greatly reduced. There was little difference in stress distribution among the three loading cases. Loading case 1 resulted in lower stresses at the prosthesis/cortical bone interface on the medial side of the humerus. In the stem and humeral diapyhsis, the stresses were higher as the degree of abduction of the arm decreased due to the increase in the bending moment distally.

When the implant was porous–coated only on the underside of the prosthetic humeral head, higher stresses were developed in the inferior–medial region of the humeral head. These stresses were similar to the stress distribution of the normal humerus. Higher stresses were created in the proximal cancellous bone in loading case 1 than the other two loading cases.

The normal and shear stresses at the prosthesis/bone interface were examined. Because most of the forces in the totally porous–coated prosthesis were transmitted through the stem, both the normal and shear stresses were extremely low at the prosthesis/bone interface for the three loading cases. In the model which had bony–ingrowth only on the underside of the prosthetic head, the shearing stresses at the interface were lower overall with loading case 2 than the other two loading cases. However, all three loading cases had high shear stresses on the lateral–superior side of the prosthesis; loading case 1 had higher stress than the other two cases. The normal stresses were compressive in all three loading cases. Loading case 3 had lower normal stresses than the other two cases.

DISCUSSION: This study compared the stress distribution of a normal humerus, a totally porous–ingrowth stemmed prosthesis, and a prosthesis with bony–ingrowth only on the underside of the prosthetic humeral head. The stress pattern of the normal humerus corresponds with the distribution of density and trabecular orientation observed in the bone tissue of the humeral head. The results indicate that when the humerus is implanted with a totally porous–ingrowth prosthesis, a significant fraction of the forces are transmitted to the stem and severe stress shielding occurred in the proximal humerus.

The comparison of the three loading conditions indicates that one case does not give lower shear stresses than the others. Shear stresses results at the interface at one end of the implant in all cases. For simplification and direct comparison, the three loading cases that were used have the same joint reaction and muscle force. In the physiological situation, these forces would not be the same for the different degrees of abduction of the arm and activity.

As more is being learned about porous–ingrowth technology, one point is very clear: prosthestic design and its influence on bone remodelling is a more important concern with porous–ingrowth devices than with cemented devices. The earliest use of porous–ingrowth prosthesis was with existing prostheses which were modified to incorporate the porous material. It was soon realized that new prostheses must be designed to accommodate the requirements of the bony–ingrowth interfaces. An important design aspect is how much of the bone/prosthesis surface is to be covered by porous–coating. This study emphasizes the observations of other investigators [3,4] who have reduced the amount of porous–coating on the stem of the prosthesis. When the stem is firmly fixed inside the intramedullary canal due to bony–ingrowth along the stem, the forces are transmitted down the stem distally and the stresses are greatly reduced in the proximal cancellous bone of the humeral head. This will probably result in increased bone deposition distally and bone loss proximally. In animal studies, stress shielding in the proximal femoral head [5] and in the distal femur [1] was caused by the implantation of component with stems or pegs. In clinical studies, there is evidence of bone hypertrophy at the distal end of the prosthetic stem and calcar resorption proximally [3]. In the case of the shoulder, we feel that the implementation of uncemented smooth stems will reduce deleterious bone remodelling and creat stresses which are more like those of the normal humerus.

REFERENCES:

1. Bobyn, J.D., et al. *Clin Orthop* 166:301–311, 1982.
2. Carter, D.R., et al. *Trans 30th Ann Meeting Orthop Res Soc* Atlanta, GA, 9:376, 1984.
3. Engh, C.A. *Clin Orthop* 176:52–66, 1983.
4. Galante, J.O. In: *The Hip Society: Proceedings of the Twelfth Open Scientific Meeting of the Hip Society*; St. Louis, MO, C.V. Mosby Co., 1984, pp 181–189.
5. Hedley, A.K., et al. *Clin Orthop* 163:300–311, 1982.

This work was supported in part by DePuy, Inc., Warsaw, IN

Material and Geometric Properties of the Human Femur During Growth. Rick Sumner (Department of Anthropology, University of Arizona, current address: Department of Orthopedic Surgery, Rush-Presbyterian-St. Luke's Medical Center, Chicago, Illinois, 60612).

Changes in geometric and material properties need to be known to adequately describe and understand growth of the human femur from a biomechanical perspective. This paper (1) presents preliminary data on bone geometry and material properties of the human femur during growth and (2) emphasizes the importance of true two-dimensional imaging of long bone cross-sections.

At the tissue level, bending strength is known to increase during growth and is correlated with an increase in the percent ash content of bone (Currey and Butler, 1975). Because of the lower mineral densities, subadult bone is less stiff, but tougher than adult bone (Sloof and Huiskes, 1979). At the macroscopic level, an increase in size is the most obvious change in whole bone geometry during growth. There are also changes in whole bone shape, but true two-dimensional shape changes of shaft cross-sections are not well known.

A large sample of subadult left femora from the Grasshopper Ruin skeletal collection was analyzed with photon absorptiometry (n=86) and a subset of this sample was analyzed with computed tomography (n=12). This prehistoric archaeological site is located in east-central Arizona and was occupied for no longer than 125 years. There is little evidence of variability due to sources other than growth (Sumner, 1984).

Photon absorptiometry was used to assess the bone mineral content (BMC), the subperiosteal mediolateral diameter (WIDTH), and the bone mineral index (BMI), the ratio of BMC to WIDTH, at five sites along the femoral diaphysis. Cross-sectional images were obtained at these same sites with computed tomography. The images were analyzed using an automated outlining algorithm interfaced with the SLICE computer program (Nagurka and Hayes, 1980). The only SLICE variables reported here include the cortical area (AREA) and the torsional moment of inertia (J), which can be considered an average bending strength.

Thephoton absorptiometric and cross-sectional geometric variables were used to calculate the apparent density (APDNS = BMC/AREA) and this variable was used to infer compressive strength (CS) and stiffness (E) (Carter and Hayes, 1976, 1977). These variables were then converted to percent adult values for each age category so that changes in BMC, WIDTH, BMI, APDNS, CS, E, AREA and J could be compared.

Results for the midshaft scan site are shown (Figs. 1 and 2). Photon absorptiometry gives the impression that structural strength, as indicated by WIDTH, is nearer to the adult value at any given age than are material properties, as indicated by BMC or BMI (Fig. 1). However, when the true two-dimensional images are considered, material properties (CS and E) are nearer to their respective adult values at any given age than are AREA or J (Fig. 2). Results for the other scan locations are similar.

This study indicates that (1) adult values for material properties are reached at the midshaft during the second decade of life, (2) adult values for geometric properties are not reached

within the first two decades of life even though growth in length has ceased and (3) information on cortical area is needed because bone growth involves both the subperiosteal and endosteal surfaces. Therefore, simple measures of mineral content (BMC or BMI) can give misleading impressions about the interaction of material and geometric properties during growth.

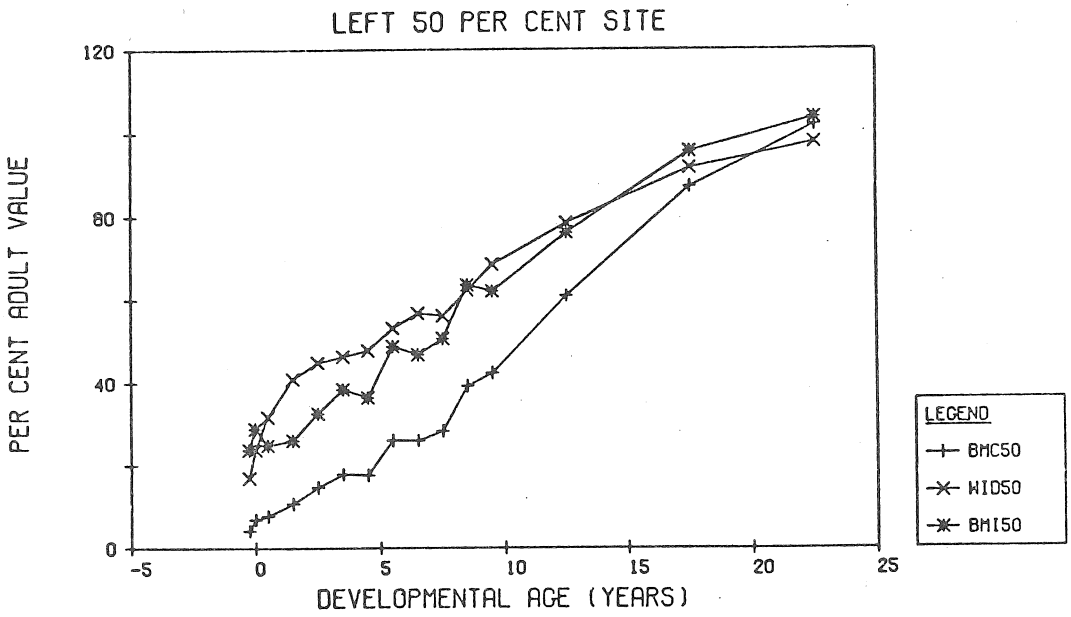

Figure 1. BMC, WIDTH and BMI at the femoral midshaft.

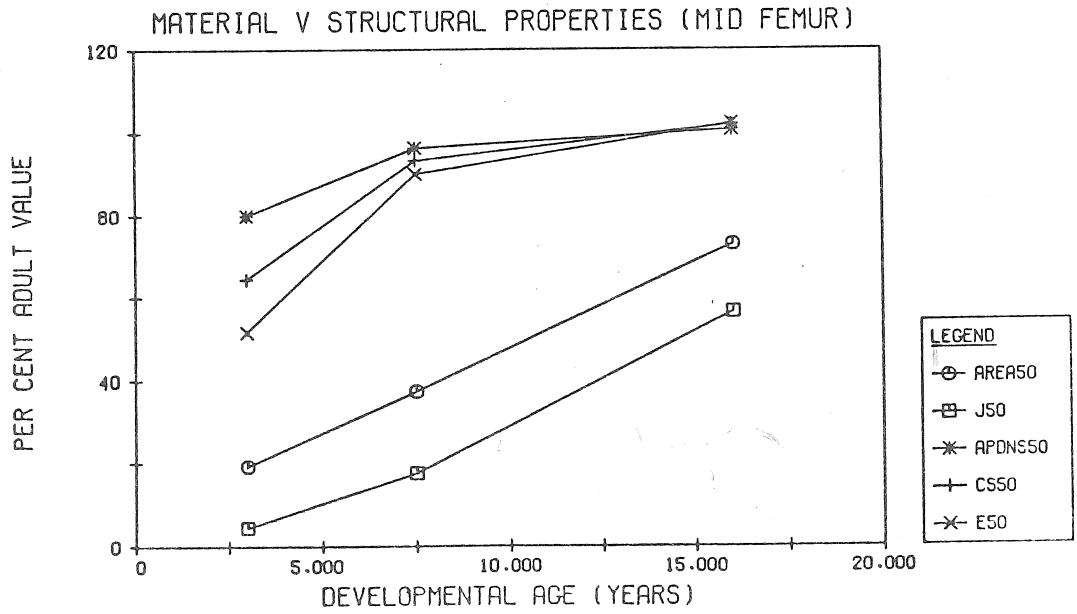

Figure 2. Material and Geometric Properties at the femoral midshaft.

References Cited

Carter, DR, and Hayes, WC (1976) Science 194:1174.
Carter, DR, and Hayes, WC (1977) J. Bone Jt. Surg. 59A:954.
Currey, JD, and Butler, G (1975) J. Bone Jt. Surg. 57A:810.
Nagurka, ML, and Hayes, WC (1980) J. Biomechanics 13:59.
Sloof, TJ, and Huiskes, R (1979) Recontr. Surg. Traumat. 17:16.
Sumner, DR (1984) Ph.D. Dissertation, University of Arizona.

Flexibility Properties of Normal and Injured Lumbar Spine

by

M. R. Gudavalli, Research Associate
and
A. H. Soni
School of Mechanical and Aerospace Engineering
Oklahoma State University
Stillwater, Oklahoma

Introduction

The motion of the human spine is governed by the primary components such as intervertebral discs, ligaments and facet joints. Pathologic motion may result between vertebrae, when one of these components are either damaged or degenerated. This may alter the normal motion characteristics of the spine and inturn lead to clinical instability of spine. Recently, research work is focussed in studying the mobility of the human spine under experimentally simulated injuries to these anatomical components. The objective of this paper is to study the flexibility properties of the lumbar spine segments, while transecting each of the anatomical components from posterior to anterior direction.

Experimental Methods

The experimental set up consists of a spine fixture and a linkage transducer. The spine fixture holds the bottom vertebra of the motion segment and the top vertebra subjected to external loads can execute its normal mode of motion such as: flexion/extension, lateral bending or axial twist. A known amount of compressive preload can also be applied to the pair of vertebrae. The linkage transducer consists of six revolute open-loop kinematic chain and is capable of tracking three-dimensional motion.

Results and Discussion

The lumbar spine motion segment (L_4 - L_5) was tested under incremental moment loads of 15 IN-LB in flexion as well as in Extension. The ligaments are transected in the following sequence

(a) Intact spine
(b) Intraspinous and supraspinous ligaments and facet joints (IS + SS + FJ)
(c) Intertransverse ligaments (ITL)
(d) Ligamentum flavum and posterior longitudinal ligament (YL + PLL)
(e) Posterior half of the intervertebral disc.

Flexibility of the motion segments are plotted as a function of the load steps and can be seen in Figures 1 (a) and (b). Flexibility is defined as displacement for unit load (Deg/In - LB). From the charts, the following observations are noted.

As the load steps are increased there is a decrease in the flexibility. This can be attributed to the nonlinear load deflection characteristics of the spine and to the stiffening effect of the tissue under load.

As the ligaments are transected there is a definite increase in the flexibility in flexion. The increase in the flexibility in flexion is significant when the

yellow ligament and posterior longitudinal ligament are transected. The motion segment was not stable in flexion when the intervertebral disc is transected. Thus we can conclude that the flexion motion is controlled mainly by the intervertebral disc, yellow ligament and posterior longitudinal ligament. In contrast there is no significant change in the flexibility in extension even when the ligaments are transected. This can be attributed to the fact that the spinous processes limit the extension motion.

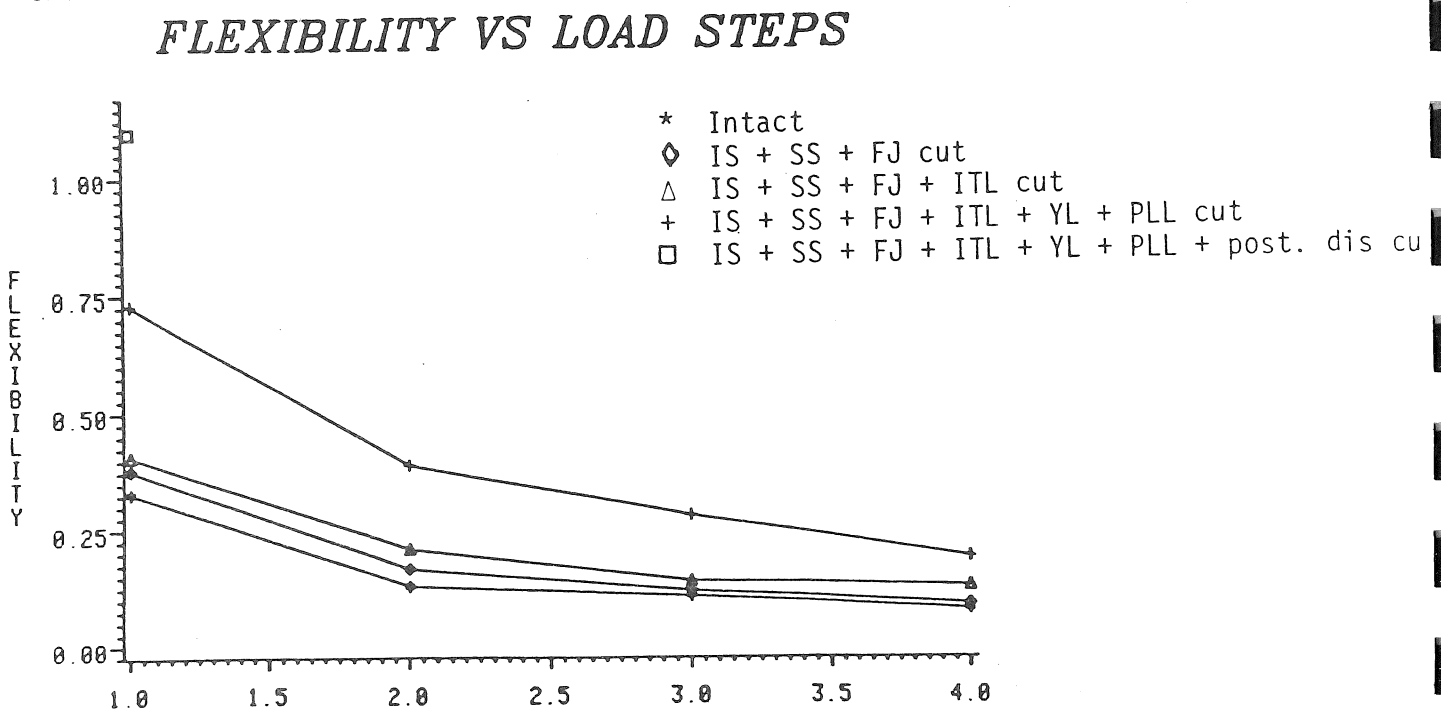

Figure 1.a. Load Steps for Flexion Load

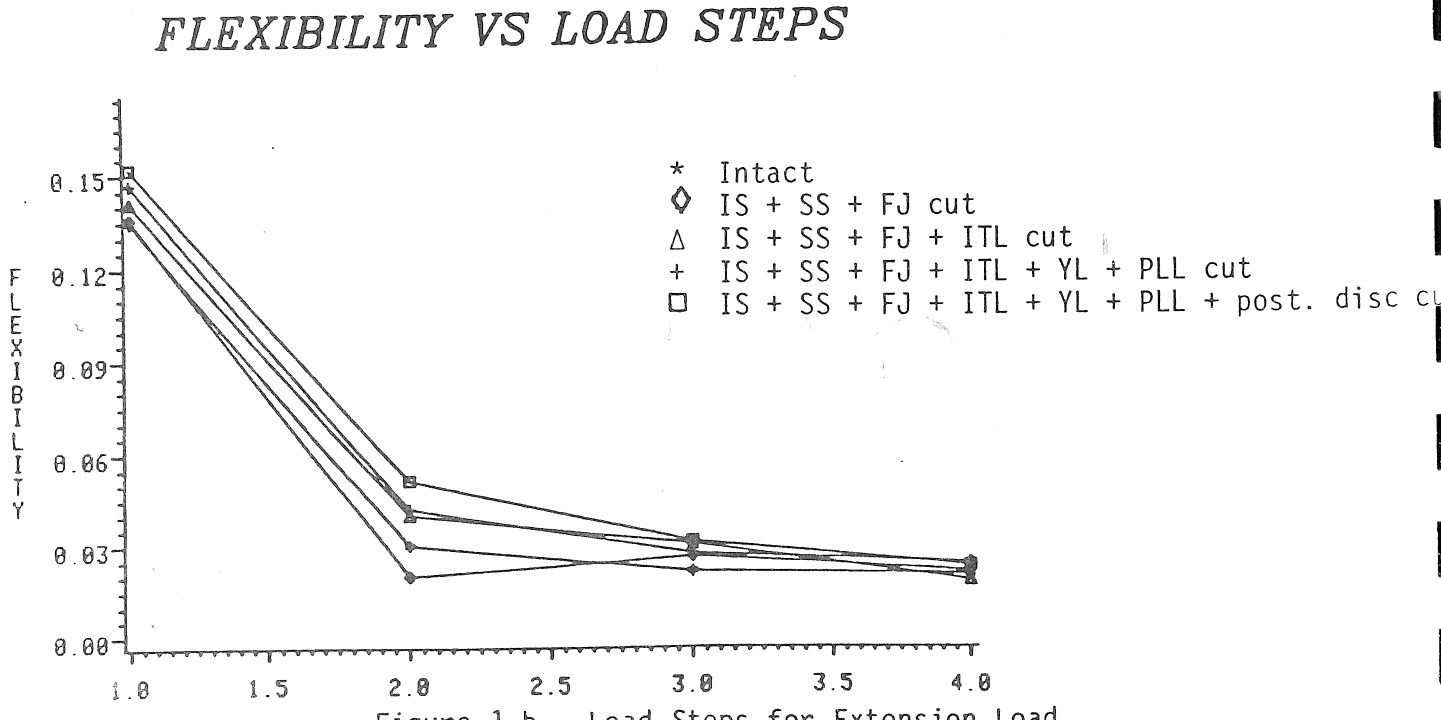

Figure 1.b. Load Steps for Extension Load

The authors wish to acknowledge the support of OREF Grant 273 which made this study possible.

LATERAL MOVEMENT OF THE UPPER BODY IN RESPONSE TO STATIC LATERAL MOMENTS

T. Jakobs, J.A.A. Miller and A.B. Schultz

Department of Mechanical Engineering
University of Michigan
Ann Arbor, MI 48109-2125

Little is known about the strategies used to control upper body posture. This study examined postural control in a simple, familiar task. The postural response of the upper body to static moments in the frontal plane was examined in twenty female and twenty male volunteers between the ages of 18 and 25 years. The group consisted of equal numbers of University gymnasts and non-gymnasts. Subjects held a 2.5 kg weight in one hand with both arms stretched laterally, or a 10 kg weight in one hand with arms at their sides, for periods ranging from 10 seconds to 3 minutes, while seated on a fixed seat with eyes closed. The trunk lateral motion that occurred in response to this was measured using a mark over the T1 spinous process. The motion was expressed as the angular deviation about S1 from the midline. Similar experiments were conducted with subjects balancing on a pivoted seat. Use of this device required that the center of mass of the upper body and weight held be kept over the pivot axis.

The pivoted seat experiments showed that the subjects holding the 10 kg weight used their upper body weight to balance 100% of the approximately 20 Nm lateral moment imposed by the weight about the lumbar spine by leaning fully 11.3 ($\pm$ 3.2 deg). Females leaned significantly further than males ($P < .001$) perhaps due to their smaller stature and lower body mass.

In the mean, subjects leaned only 1.6 (SD $\pm$ 1.0) deg away from the midline and the weight while seated on the fixed seat holding the 10 kg weight. No differences were found between females and males. Thus, in contrast to the pivoted seat response, on the fixed seat subjects used their upper body weight to balance only 14% of the approximately 20 Nm moment imposed about the lumbar spine by the weight. The remainder was balanced chiefly by contralateral trunk muscle contractions.

Analysis of the results suggests that the postural control system initially placed more emphasis on restricting lateral tilt of the upper body than on minimising trunk muscle activity, or on equilibrating seat pressures bilaterally, or on maximizing seating stability by locating the seat reaction force vector symmetrically on the midline. However, as time elapsed body tilt was increased (by nearly 50% at three minutes), in apparent recognition of some or all of these mechanical effects. No differences were found between gymnasts and non-gymnasts in any of these tasks.

Comparison of an "in vivo" Spondylolysis Fracture to Those Obtained "in vitro"

John M. Lipka and H.S. Ranu

Department of Biomedical Engineering
Louisiana Tech University
Ruston, LA 71272

The spondylolysis fracture of the human vertebra is a fatigue fracture of the neural arch occuring in the pars interarticularis region. The fracture most commonly occurs in the lower lumbar region (L4/L5 and L5/S1), because these intervertebral joints must sustain the largest loads. Both an axial loading force and an anterior shear component must be withstood by the spinal disc and the facet joints when subjected to load. The degree of disc degeneration is important when considering the number of cycles to fracture.

Spondylolysis fractures were first obtained experimentally (Cyron et al, 1976.) by subjecting a verbra to both acute (compressive) and fatigue (cyclic) loads.

To obtain "in vitro" spondylolysis fractures the vertebra was held inverted on an inclined plane and the inferior facet was loaded by applying a sinusoid perpendicular to the plane of the facet joint. This cyclic load was applied to the inferior facet until a fracture, which resembled the spondylolysis fracture, was obtained. The fatigue lifes obtained are comparable to those obtained by Cyron (Cyron et al, 1978.) for similar aged specimans.

These experimentally obtained fractures are then compared to the x-rays of persons suffering "in vivo" spondylolysis fractures. The positive correlation between the fracture site and propagation of the fracture experimentally to the "in vivo" fracture will allow the mechanics of spondylolysis as a function of fatigue to be modeled as part of an ongoing attempt to develope a usable finite element model of the spine.

1. Cyron, B.M., Hutton, W.C., Troup, J.D.C., Spondylytic Fractures, Journal of Bone and Joint Surgery, Vol. 55-B(4), pp. 462-6, 1976.

2. Cyron, B.M., Hutton, W.C., The Fatigue Strength of the Lumbar Neural Arch in Spondylolysis, Journal of Bone and Joint Surgery, Vol. 60-B(2), pp. 234-8, 1978

PARAVERTEBRAL MUSCLE RECRUITMENT PATTERNS IN THE THORACIC AND LUMBAR SPINE

J.A.A. Miller[1], H. Steen, L.B. Skogland and A.B. Schultz[1]

Biomechanics Laboratory, Sophies Mindes Orthopaedic Hospital
University of Oslo, Norway
and [1]Department of Mechanical Engineering
University of Michigan

Few data have been collected on the extent to which the intrinsic paravertebral muscles can be separately recruited along the length of the spine. Such data are useful in, for example, patients with and without idiopathic scoliosis or Scheuermann's disease. The purpose of this study was to gather such data in healthy adults.

METHODS. Two healthy males and 5 healthy females between the ages of 20 and 48 years were tested. Bipolar fine wire electrodes were inserted to within 5 mm of the underlying bone, 2 and 4 cm to the right of the spinous processes, at each of the T1, T8, T12 and L3 levels. The eight intramuscular myoelectric signals were amplified, rectified and low pass filtered, then displayed on strip charts. Subjects stood throughout the tests with their pelvis supported externally. The position of T1 was monitored in the transverse plane using two LEDs and a Selspot optoelectronic system. Three subjects performed calibration tests. A strap was passed around the head, or around the trunk at the T11 level. The subjects were asked to pull against the strap in extension or lateral bending at 5, 25 and 100% of maximum effort. All subjects then performed 33 tasks for at least ten seconds. Mean values of myoelectric activity were measured over four seconds.

RESULTS AND DISCUSSION. In the calibration experiments each myoelectric signal level was linearly correlated with the magnitude of the head strap tension ($P < 0.001$) and therefore with the lateral bending or extension moment at that spine level. The corresponding results obtained when the strap was at T11 confirmed that activity at T1 and T8 was reduced up to 80%, and that the T12 and L3 level muscles could be recruited maximally with little recruitment of the muscles above the T11 level.

All subjects participated in the 33 standardised tests designed so we could estimate the recruitment of the paravertebral muscles in familiar, everyday tasks. Less than 10% maximal myoelectric activity was found in any muscle in relaxed standing, in ipsilateral inclination of the head (15°) or trunk (5°), with a 2 cm contralateral foot lift or when the pelvis was maximally inclined backwards. Less than 50% activity was found when leaning the head forwards (15°) or the trunk (5°) contralaterally, twisting 45° to the right or with a 2 cm ipsilateral foot lift. Less than 30% activity was found when leaning forwards (5°), twisting 45° to the left, tilting the pelvis forwards or holding the ipsilateral arm in 90% flexion. Less than 40% activity was found in maximally increasing or decreasing sagittal curves, or holding the contralateral arm in 90° flexion. Less than 50% activity was found in 90° abduction of the contralateral arm or both arms.

In general, rank correlation coefficients were higher between myoelectric activity measured at electrodes at the same spine level than between those at different levels, suggesting some independence in longitudinal muscle recruitment patterns, particularly among the T1 and T8, or T8 and T12 levels. These deep muscles appear to be recruited in proportion to the bending moment placed on the spine at a given level. The results showed the muscles caudal to T11 could be recruited independently of those cranial to this level when this was mechanically appropriate. This is a necessary capability in controlling progression of a double scoliosis curve where unilateral contractions along the spine would tend to decrease one curve but increase the other.

POROELASTIC STRUCTURAL MODELS FOR HUMAN SPINAL MOTION SEGMENTS

B. R. Simon*, J. S-S. Wu*, J. H. Evans,** and L. E. Kazarian†

*Aerospace and Mechanical Engineering, University of Arizona, Tucson, AZ 85721, USA
**Strathclyde University, Glasgow, Scotland, U.K.
†AFAMRL/BBD, WPAFB, Dayton, OH, USA.

The mechanical response of a spinal motion segment (SMS) plays a key role in the biomechanical behavior of the spine. A finite element model (fem) can provide quantitative data regarding deformations, strains, and stresses, provided suitable constitutive laws are available to describe the properties of the materials in the SMS. Poroelastic material laws and associated fem's give a view of the mechanical behavior of the intervertebral disc (IVD) that includes a fluid phase flowing relative to a deformable porous solid phase in the material. Here, we extend our earlier study [1] to develop steady-state and transient creep fem's of human SMS's based on a poroelastic theory.

The governing field equations describing the initial-boundary value problem are coupled dynamic equilibrium equations [$L^T\sigma + \rho b = \rho\ddot{u} + \rho^f\ddot{w}$ and $\nabla\pi + \rho^f b = \rho^f\ddot{u} + (\rho^f/n)\ddot{w} + k^{-1}\dot{w}$], strain-displacement relations [$e^s = Lu$ and $e^f = \nabla^T w$], and a constitutive law [$\sigma = De^s + \alpha m\pi^f$ and $\pi^f = \alpha Q m^T e^s + Q e^f$]. Here, the matrix notation is similar to [2]; e.g., u = solid displacements, w = relative fluid displacements, σ = total stress, π^f = pore fluid pressure, and the material properties are D, α, Q, and permeability k. Spatially discretized field equations based on a fem are of the form [$M\ddot{x} + C\dot{x} + Kx = X$], where M, C, K, and X are consistent mass, damping, stiffness, and load matrices with $x^T = [u^T w^T]$ = nodal solid and fluid displacements. Here, steady-state analyses [$x = x_0 \exp(j\omega t)$, etc.], transient creep [solution of $C\dot{x} + Kx = X$], and long-time creep [$x = K^{-1}X$] were carried out using axisymmetric fem's.

An analytical model of a poroelastic column was used to determine disc material parameters, i.e., E, ν (in D) and α, Q, and k. A comparison of Kazarian's data [3] for normal (N) and degenerated (D) IVD's with analytical model predictions (see Fig. 1) suggested that disc permeability may be increased in the degenerated IVD (e.g., $k = 5 \times 10^{-16}$ m^4/N·s, normal disc; whereas k may be as high as 5×10^{-13} m^4/N·s, degenerated disc). Increased k is accompanied by increased flow and associated changes in the mechanical response of the SMS. Steady-state fe analyses ($1 \leq \omega \leq 50$ Hz) were compared with impedance data [4] for human SMS's. The poroelastic steady-state fem results agreed well with experimental data (see Fig. 2). Fluid motion was insignificant in the normal disc, indicating an "undrained" response. Increased flow was predicted in the disc when k was elevated to simulate "degenerated" conditions.

Creep was studied in SMS's using axisymmetric fem's (see Fig. 3) that included a number of flow boundary conditions (e.g., flow prevented or allowed through the "exterior" of the annulus) in order to determine the associated flow fields. These two cases (see Fig. 4) exhibit significant differences in the long-time creep flow field. Similar results were seen in transient creep studies. In all cases, there is flow from disc to the vertebral body through the end plate. When flow is prevented through the "exterior" of the annulus (Fig. 4a), there is flow in through the top of the nucleus, radial flow outward from nucleus to annulus, and flow up from the annulus into the vertebral body. If flow is allowed at the external annular surface, then fluid flows in through that surface and out of the disc through the end plate (see Fig. 4b). These flow trends reverse when creep loads are removed. Such fluid motion could be related to tissue nourishment in the IVD. Discal radial bulge and creep displacements were smaller when radial flow was prevented through the exterior of the annulus. Fem stress analysis predicted stress concentrations that correlate with observed structural failure modes of SMS's.

1. Simon, B. R., et al., ASME-WAM, Boston, Mass. (1983).
2. Simon, B. R., et al., I. J. Num. Anal. Meth. Geom. (1984).
3. Kazarian, L. E., Orth. Cl. N. Am., 6, 3-18 (1975).
4. Kazarian, L. E., Acta Ortho. Scand., Suppl. 146 (1972).

Acknowledgment: Support of AFOSR 1983 RISE Grant.

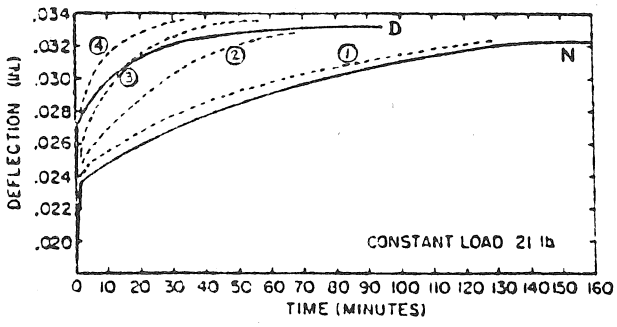

Fig. 1. SMS creep deflection vs. time (exp. data [3] for D = degenerated disc, N = normal disc and ---①→④= analytical models with $k_1 = 5 \times 10^{-16}$, $k_2 = 5 \times 10^{-15}$, $k_3 = 5 \times 10^{-14}$, and $k_4 = 5 \times 10^{-13}$ $m^4/N\text{-}s$).

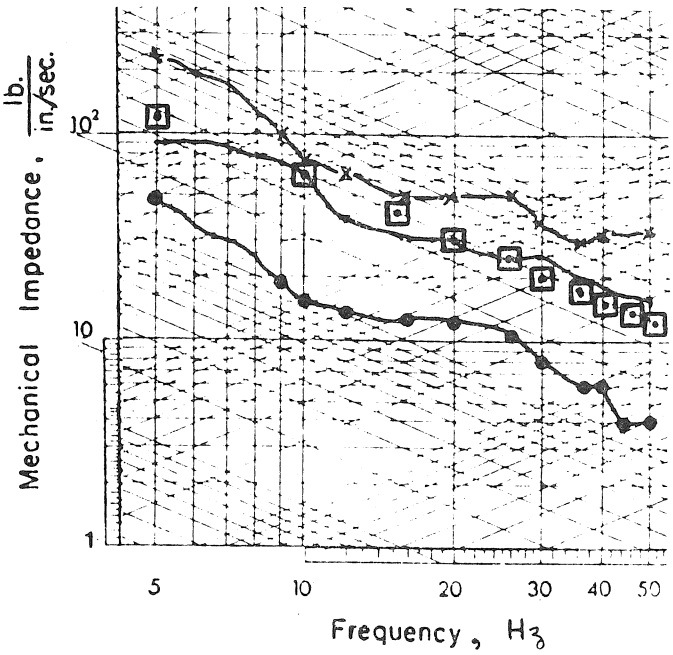

Fig. 2. Mechanical impedance vs. frequency for human SMS (——— = exp. data [4] and ⊡ ⊡ ⊡ = fem results).

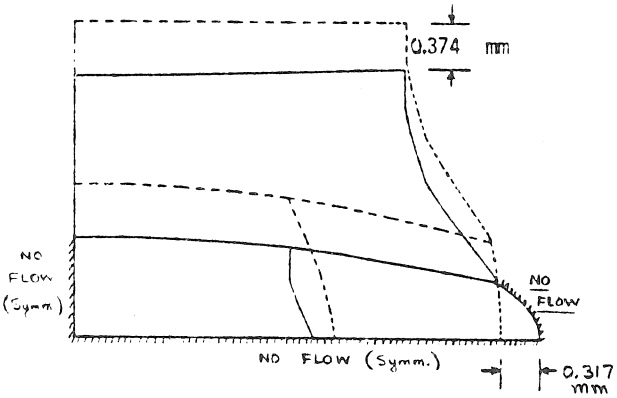

Fig. 3a. Fem overall deformations, $\tilde{u}$ (no flow at exterior annular surface).

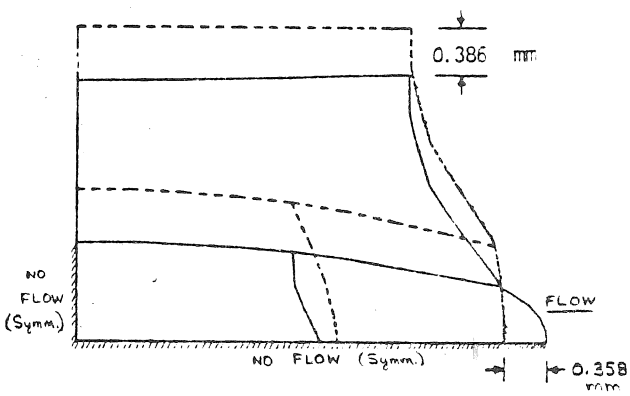

Fig. 3b. Fem overall deformations, $\tilde{u}$ (flow allowed at exterior annular surface).

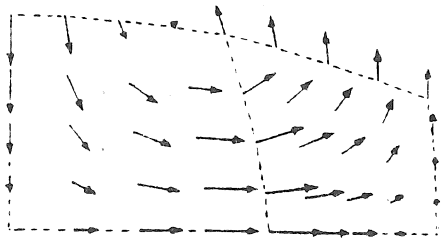

Fig. 4a. Fem IVD relative fluid displ., $\tilde{w}$ (no flow at exterior annular surface).

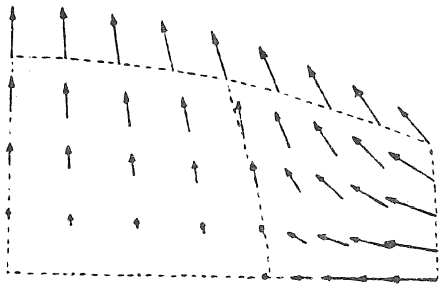

Fig. 4b. Fem IVD relative fluid displ., $\tilde{w}$ (flow allowed at exterior annular surface).

STRUCTURAL-MECHANICAL INDICATORS OF LIMB SPECIALIZATION IN PRIMATES

David B. Burr and Mitchell B. Schaffler
Departments of Anatomy and Orthopedic Surgery, West Virginia University
Morgantown, WV 26506

INTRODUCTION: Forelimb-hindlimb usage in primates differs widely, even within "behaviorally homogeneous" groups. In general, pronograde animals have little forelimb-hindlimb functional differentiation, and habitually place about 50-60% of their body weight on the hindlimb. Antipronograde animals demonstrate marked functional differentiation of the extremities, with the forelimb as the principal propulsive element. The objective of this study was to examine functional differentiation of the extremities using structural and geometrical analyses of the femur and humerus from primates representing a wide spectrum of habitual locomotor activities.

METHODS: Photon absorptiometry was used to determine area moments of inertia at midshaft for intact femora and humeri from Macaca nemestrina, Macaca fascicularis, Presbytis cristatis, and Hylobates lar. Locomotor behaviors in these animals respectively include terrestrial quadrupedalism, arboreal quadrupedalism with either occasional or extensive leaping behaviors, and arm-swinging (brachiation). The study specimens were from wild caught adult animals of both sexes and of known body weights. Least squares regression analysis using log-log plots of femoral and humeral bending rigidity on body weight were employed to assess relative usage of the limbs in weight bearing and propulsion. Comparison of slopes was used to assess significant differences between groups.

RESULTS: Among the pronograde animals, M. fascicularis, M. nemestrina, and P. cristatis, average bending rigidity of the femur and humerus increased similarly with body weight. In the antipronograde gibbon, bending rigidity of the principal propulsive limb element, the humerus, increased more rapidly with body weight than did bending rigidity of the femur.

In both macaques, average bending rigidity of both the femur and humerus increased similarly with body weight (Table 1). In both species the slopes averaged about 1.46, which is close to the expected slope based on previous work ($I \alpha BW^{1.43}$). However, in P. cristatis, bending rigidity in both skeletal elements increased with body weight more rapidly than expected (Table 1). The explanation of this may lie in the nature of the locomotor differences between relatively cursorial macaques and leaping-oriented monkeys. Presumably, frequent leaping activities, such as those in P. cristatis, subject skeletal elements to larger, more impulsive loads than do more cursorial activities. Thus it appears that the relationship of average bending rigidity to body weight in locomotor skeletal elements of Hylobates and Presbytis are different from those in macaques and other generalized quadrupedal mammals, and that this relationship reflects both the extent of forelimb-hindlimb differentiation and the dominant propulsive limb.

TABLE 1
Body Mass - Related Changes in Average Bending Rigidity ($J/2=bx \cdot Mass^{k}$)

Species	Humerus		Femur	
	k	r	k	r
M. fascicularis	1.45	0.81	1.34	0.88
M. nemestrina	1.62	0.98	1.41	0.93
P. cristatis	1.87	0.84	1.98	0.85
H. lar	1.77	0.85	1.44	0.69

Expected K for generalized mammals = 1.43

The ratio of humeral to femoral bending rigidity, normalized by body weight, also provided a measure of forelimb-hindlimb usage (Table 2). Suspensory animals (H. lar) had the highest value, indicating greater relative bending rigidity in the humerus; the most pronounced leapers in the study group (P. cristatis) had the lowest value. The macaques are intermediate, consistent with relatively less functional differentiation of the extremities.

TABLE 2
Ratio of Humerus to Femur Average Bending Rigidity ((J/2)/BW)

M. fascicularis	0.778
M. nemestrina	0.860
P. cristatis	0.609
H. lar	0.917

These structural-mechanical data indicate that:

1. Average bending rigidities of humerus and femur reflect forelimb-hindlimb functional differentiation
2. Deviations of average bending rigidities from expected geometric similarity suggest functional variations from typical primate quadrupedalism
3. The ratio of humeral to femoral bending rigidity identifies trends for hindlimb or forelimb dominance in locomotion

With the accumulation of more comparative data on living primates, structural mechanical techniques may hold considerable promise for interpreting primate locomotor specializations.

ELASTIC RECOIL IN THE MARLIN BACKBONE

J. H. Hebrank and S. A. Wainwright

Duke University Marine Laboratory

Beaufort, North Carolina 28516

ABSTRACT

The backbones of marlin and sailfish are unique in that each vertebra overlaps and fastens tightly to the one before it. Each intervertebral joint remains flexible, but much force is required to bend it and the entire backbone recoils from a bend elastically, like a carpenter's sawblade.

We determined the resilience of whole backbones of blue marlin as follows: each backbone was suspended by the ends in a horizontal position with the median vertical plane parallel to the ground. With a recording force gauge, we pulled downward at the midpoint of the backbone and allowed it to oscillate freely, recording the lateral displacements against a millimeter ruler with a video camera. Two replications of each experiment were done bending to the right, two more to the left, on each of three backbones 120, 155 and 180 cm long from animals weighing 268, 287 and 312 kg respectively.

Resilience of the backbones was 96%. In static experiments, the largest backbones could be bent 180° by 18 kg force applied perpendicular to one end. We also determined that, in spite of the six bony structures overlapping each intervertebral joint, these joints are the flexible points of the backbone.

We conclude that the extraordinary overlapping vertebrae in the marlin backbone allow bending of the fish's body to be stiffened elastically by the six thin bony plates. We find the 96% resilience of the entire complex backbone structure to be high, especially when compared with the resilience of samples of pure elastomers such as elastin and resilin whose maximum resiliences are 93%. We suggest that elastic energy stored and released by the marlin backbone during a body bend contributes to locomotion by accelerating the first few degrees of unbending when actin-myosin overlap in the swimming muscle is minimal. This would increase the power output of the fish in leaping and rapid swimming.

Growth Dynamics of Bacterial Macrofiber Fragments

Neil H. Mendelson

University Department of Microbiology and Immunology
University of Arizona, Tucson, AZ 85721

The helical macrofiber system in Bacillus subtilis is being developed as an experimental system in which biomechanical aspects of bacterial growth and structure may be explored in relationship to the molecular biology of cell wall growth. (1,2,3). The system is based upon the use of cell separation suppressed mutants that grow initially from single cell inocula to produce long cellular filaments consisting of chains of cells. Although the shapes of these individual cells are cylindrical, as are wild-type cells of B. subtilis, the cellular filaments turn about their long axis as they elongate. Whip-like motions result in distortion of the cylindrical shape until the filament bends back and touches itself. The helical shape deformation, and the entire production of multistranded macrofibers is predicated upon such contact. At the point of contact a cell-cell interaction occurs that binds the structure initially in the form of a loop with two tails. The helical turning associated with growth rapidly converts this structure into a double strand helix. Time-lapse films studies of these dynamics indicate a cooperative process in which the initial point of contact propagates bringing more and more cell surfaces into contact as the loop closes into a helix. The degree of order in the helix structure becomes progressively greater as additional cell surface interactions lead to greater restraint on the growth associated cellular rotation. The helical shape deformation has been interpreted therefore as a result of cylindrical rotation produced by insertion of the cell wall polymers along a helical path during growth of the individual cells coupled with a block of rotation due to binding of the cell surfaces to one-another.

The production of macrofibers from the small double stranded helical structures described involves the reiteration of a folding cycle that increases the number of cellular filaments aligned parallel to each other along the length of the fiber. Since folding can occur at either end the mature macrofibers have loops at both ends. Although the topology of folding can be complex, each fold always results in the wrapping together of a super-structure helix of the same helix hand as that produced by all previous folds tracing to the initial fold that generates the first double stranded structure. This fact indicates that folding is driven by negative twist.

The twist of macrofibers can be precisely defined using measurements of either static structures or dynamics of macrofiber growth. The theory of uniform yarns has been applied and it was shown that in any given macrofiber all cells grow with constant twist. A spectrum of twist states exists that ranges from tight right through neutral to tight left handed structures, depending upon the genetic composition of the strain, composition of the growth medium, temperature, and ionic environment (3). In certain strains a fiber produced at one temperature transferred to another will undergo a helix hand inversion. We have studied kinetic aspects of helix hand inversion coupled to molecular biology manipulations in an attempt to probe the events that go on in the cell wall during such changes. So far as mechanics are concerned, the presence of loop end constraints complicates matters and we have therefore developed methods to study fiber fragments in which the loops are removed. This communication describes some of the initial properties of fiber fragments in terms of growth, folding, splicing and helix hand inversion.

The general form of a macrofiber fragment is shown in Fig. 1. The individual cellular filaments protrude from the severed ends of the excised section of a right-handed macrofiber.

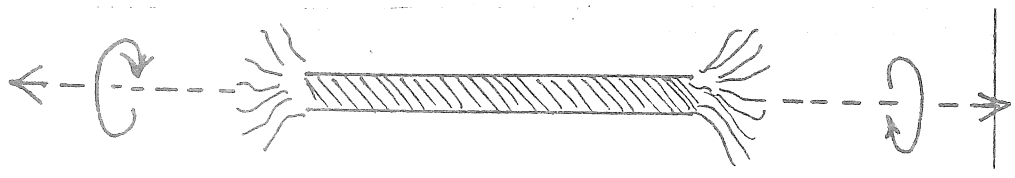

Time lapse films of such structures reveal the helical rotation of individual cell filaments within the array as the entire array elongates at an exponential rate. Fragment growth eventually results in folding as shown in Fig. 2.

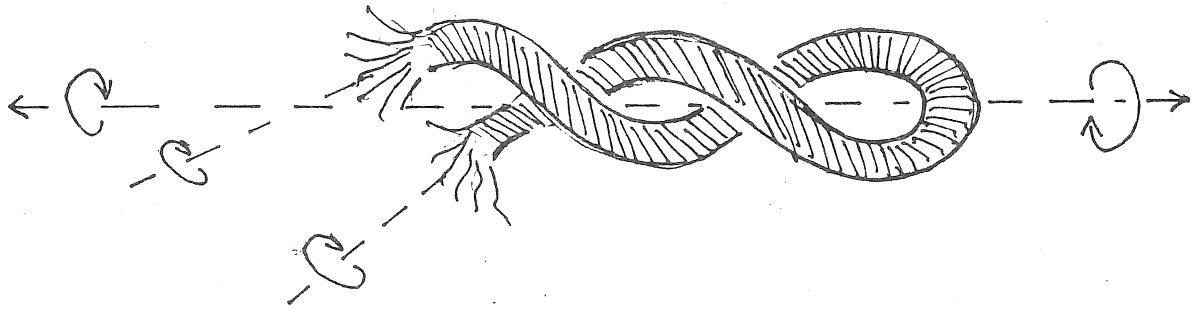

The dynamic behavior of folded fragments appears identical to that of conventional macrofibers, consequently attention is focused primarily on fragment growth only until the initial fold is achieved. Fig. 3 diagrams the basic mechanics of temperature-induced helix hand inversion.

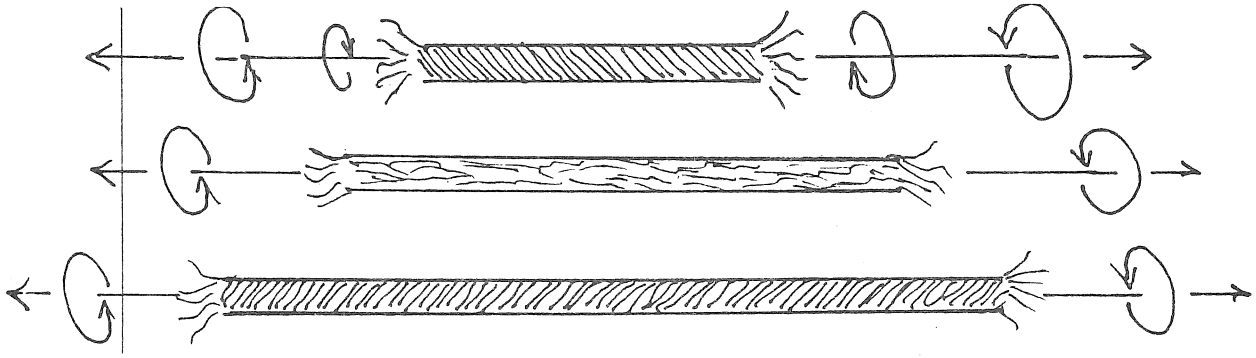

In such structures it is possible to trace the fate of individual cellular filaments throughout the inversion. A helix phase inversion of all the individual filaments within the fragment can be documented. Finally, fig. 4 illustrates the appearance of a butt-spliced fragment consisting of two tandemly joined fragments.

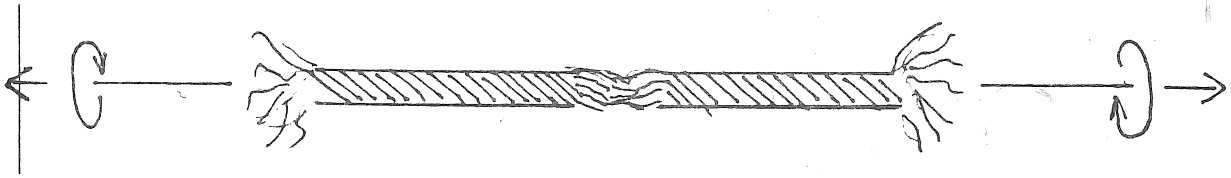

The spliced structure behaves mechanically as a single entity in terms of transmission of whip-like motions, growth turning, and even temperature-induced helix hand inversion. Time-lapse films of live macrofibers will be shown to document the events illustrated in figs 1-4. Although the cell-cell interactions required for induction of the helical shape deformation, folding initiation, and butt-splice formation must be of sufficient magnitude to restrain growth, such interaction do not hinder the cell surface reorganization required for helix hand inversion. The manner by which fiber fragments maintain structural integrety during these processes
remains to be revealed.

References

1. Mendelson, N.H. 1976. Proc. Natl. Acad. Sci. USA 73:1740-1744.
2. Mendelson, N.H. 1978. Proc. Natl. Acad. Sci. USA 75:2478-2482
3. Mendelson, N.H., D. Favre, and J.J. Thwaites. 1984. Proc. Natl. Acad. Sci. USA. 81:(in press June issue).

Mary Ellen Morbeck
Department of Anthropology
University of Arizona
Tucson, Arizona 85721

Biomechanics and Human Evolution

The principles of biomechanics contribute directly to the interpretation of human evolution. Direct evidence from fossils shows the sequence of structural changes in form-function relationships of dental and skeletal systems throughout geological time. The primary task of researchers who study form-function relationships in past human and prehuman groups is to sort the morphological variation observed in the fossil record in a context of time, space and environment.

Fossils of our ape-human ancestors and immediate progenitors allow us to focus on: 1) size, shape and position of occlusal features of teeth and related jaw structures; 2) size and shape of joint surfaces that permit directions and ranges of movements between body segments; 3) skeletal links that function as levers as related to origins and insertions of muscles that cross joints and affect power and speed of movement; and 4) size and shape of cross-sectional areas of limb bone shafts that reflect loading conditions during an individual's lifetime. Fossil teeth, jaws and limb bones, especially those from associated skeletons, provide information on chewing and postcranial movement capabilities and, therefore, inferred diet and positional behavior (locomotion and posture).

Fossil bones and teeth, which are mineralized during the change from the biosphere to the lithosphere, are parts of once-living organisms. They represent the product of growth and development at one point in their lives, ie., the time of death. Species-defined characters (based on evolutionary history), genotype (including sex) and environmental influences (e.g., positional behavior and substrate use, diet and nutrition, disease and pathology) affect the speed and duration of growth, development and aging. Individuals may vary within the phylogenetic limits of a species' structural plan and the mechanical constraints of the musculoskeletal system, but general form-function relationships provide information on habitual and/or exceptional movement patterns.

Form-function analyses of fossils depend on knowledge of the mammalian musculoskeletal system, comparative primate anatomy, movement capabilities, expressed behavior and habitat use in growing and adult animals. Ranges of variation within and among groups based on large samples from both living primates and osteological collections supplement detailed biomechanical analyses of individual specimens.

Material properties (e.g., bone mineral content) are destroyed during fossilization and soft tissue anatomy (e.g., actual distribution of weight in body segments, variation in cartilage thickness, ligament placement, or tendon insertion angles) and details of the biomechanics of movement (e.g., force magnitudes and acceleration as related to limb position) only can be estimated. This also is true for expressed behavior, ie., we will never know the actual percent of time spent in particular activities in particular habitats.

Biomechanical analysis of Proconsul africanus, 17.5 million year old possible ape-human ancestor from Africa, serves as an example here. Based on linear, angular and joint surface area data, limb proportions, muscle attachment sites and details of the elbow, wrist, hand, ankle and foot joints show that Proconsul was an eclectic quadruped with grasping hands and feet and its positional capabilites were unlike later human ancestors (Morbeck 1984). Analysis of limb bone shaft cross-sections via sectioning of fossils or using high-powered noninvasive techniques such as computerized tomography, which show the distribution of now-fossilized bone tissue around an axis, can

be used to determine loading conditions as has been demonstrated in living animals and interpreted in fossil limb bones (e.g., neanderthal tibiae). In some cases, trabecular patterns, cortical thickness and bone changes due to injury or pathologies may contribute to an understanding of the mechanical history of a bone. Analyses of jaw and tooth function focus on cusp morphology and mechanics as related to shearing facets and crushing basins and study of jaw mechanics as related to size and shape of the skull, face and muscle attachments.

Anthropological studies of large samples of primarily adult skeletons emphasize linear variables and, most recently, include smaller samples that use body segment weight and joint or cross-sectional shaft area data. In addition, comparative studies of living animals include: 1) "natural experiments" with observations of free-ranging groups (e.g., similar animals in different habitats or different animals in similar habitats), and 2) laboratory studies in which; a) the forces, muscle activities and loading conditions are monitored (e.g., force plate analysis, electromyography, strain gauge techniques), b) where local or whole bone loading conditions are altered (e.g., resectioning of bones, exposure to hypergravity and controlled application of stress), c) movement between segments is documented (e.g., high speed film including cineradiography) or d) energy costs are calculated (e.g., measured by oxygen consumption). Research results are combined with theoretical biomechanics studies to explain form-function relationships. Since growth is important in producing adult form, these data need to be enhanced by including more young, growing primates and old, aging individuals in addition to "typical" adults.

Two current studies at the University of Arizona have potential for contributing to biomechanics and, thus, to interpretations of the human fossil record. Investigations of a large sample of human femora of both sexes, fetal to old age, from the Grasshopper Pueblo archaeological series emphasizes external angles, bone mineral content and geometric properties that show changes in form accomodating function during growth, development and aging (Sumner 1984).

A longitudnal study of growth, development and aging in chimpanzees, a phylogenetically close human relative, and complementary body segment analysis from cadaver dissections is in progress in cooperation with the Primate Foundation of Arizona and other insititutions (Morbeck, Marzke and Fritz 1984). This project assesses variation (ie., changes in body weight, its distribution and composition, segment lengths, breadths and circumferences, bone mineral content, hand and foot ossification, dental eruption and secondary sexual characters) as related to sex and age differences and the effects of nutrition, social stress, disease and physical environment on the duration and speed of growth, development and aging. These data will provide crucial information about both the pattern and timing of growth and aging in form and related function in different body segments.

Comparative morphology, physiology, biochemistry and behavior indicate close phylogenetic relationships among the African apes (ie., chimps and gorillas) and humans. Many researchers reconstruct features of the ape-human common ancestor primarily from characters observed in living groups in order to explain human origins and evolution. However, only the fossils can provide the test for hypotheses generated from data on living populations. Direct fossil data are interpreted in the context of the principles of biomechanics and compared to broad samples that confirm these principles and yield ranges of variation within species' patterns.

BONE MICROSTRUCTURE: A STUDY IN COMPARATIVE LOCOMOTION

Mitchell B. Schaffler and David B. Burr
Department of Anatomy and Orthopedic Research Laboratory, West Virginia University, Morgantown, WV 26506-6302

INTRODUCTION: Mechanical factors are important in the control of osteonal remodelling of cortical bone. Examination of primates, because of their physiological and genetic similarity and extreme locomotor diversity, provides a unique comparative anatomical approach to assess the relative importance of mechanical versus biological factors in determining microstructural organization in cortical bone. Using a primate sample, we sought to determine whether differences in locomotor behavior, and in mechanical loading, affect the osteonal organization of primate cortical bone.

METHODS: Midshaft cross-sections of femora from twenty primate species were cut with a metallurgic saw, hand ground to 150μm and stained for light microscopy. Each section was analyzed by point counting with a $1cm^2$ grid at 100X magnification. Data were collected for the proportion of bone cortex occupied by osteonal bone (percent osteonal bone) and average osteon density (osteon/mm^2) for the entire cortex of each specimen. Only secondary osteons with intact Haversian canals were counted.

RESULTS: The present study indicates that differences in percent osteonal bone exist among primate species and these differences are related to how the animal uses its limbs in locomotion. Increasing percent osteonal bone delineates four groups of primates, coincident with different locomotor patterns among the animals studied (Table 1). Analysis of variance indicates that percent osteonal bone significantly distinguishes these groups ($p<0.01$). Based on kinesiological studies, non-human primate locomotion can be classified into two broad patterns[1]. The first, characterized by greater forelimb-hindlimb functional differentiation and relative hindlimb dominance in walking, is comprised of chimpanzees, orangutans and spider monkeys. The second pattern is defined by less functional differentiation of the extremities and adaptations to quadrupedalism. Human locomotion is entirely hindlimb dominated and differs from the two non-human primate locomotor groups. In our study, groups which coincide with those kinesiological groups are defined by percent osteonal bone (Figure 1). This similarity in group definition suggests some cause and effect relationship between primate movement patterns and their bone's microstructural organization.

As primates do not differ significantly with respect to calcium metabolism, mineral homeostatic factors do not adequately explain the observed variation in percent osteonal bone. Percent osteonal bone in some closely related species differs by a factor of two, while more distantly related forms, such as chimpanzees and spider monkeys, each have almost the same amount; therefore phylogenetic factors also fail to explain the observed diversity. Mechanical factors provide the best explanation for differences in percent osteonal bone seen among animals in this study.

These results support the hypothesis that the osteonal organization in cortical bone is characteristic of the biomechanical environment and loading history of a bone. The knowledge that percent osteonal bone is related to the way a limb is loaded may be a valuable adjunct to understanding bone tissue response to its mechanical environment and to interpreting the locomotor biomechanics of various species.

REFERENCE:
(1) Kimura, T., et al., IN: Environment, Behavior and Morphology: Dynamic Interactions in Primates. pp. 297-313, 1979.

TABLE 1

	% Osteonal Bone	
	$\bar{x} \pm$ s.e.	Range
Arboreal Quadrupeds*	6.79±0.61	3.50-9.50
Terrestrial Quadrupeds*	12.72±2.22	6.80-19.00
Suspensory Animals*	26.93±1.15	23.50-28.40
Bipeds*	45.3	-----

*All group differ significantly ($p<0.01$)

FIGURE 1

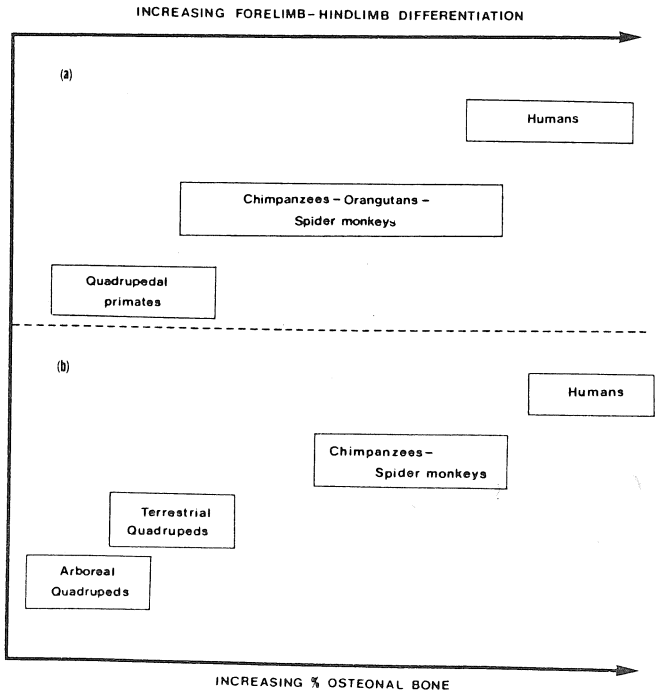

This research was supported by the WVU Medical Corporation and NIH Biomedical Research Grant RRO-443-18.

MECHANICAL BEHAVIOR OF FETAL DURA MATER IN AXISYMMETRIC BIAXIAL TENSION

D. I. Bylski (Biomechanics, Trauma, and Sports Medicine Laboratory, The University of Michigan, Ann Arbor, MI 48109 U.S.A.)
T. J. Kriewall (Surgical Products Division, 3M Company, 270-2A-10 3M Center, St. Paul, MN 55144 U.S.A.)
N. Akkas (Department of Civil Engineering, Middle East Technical University, Ankara, Turkey)
J. W. Melvin (Department of Mechanical Engineering, The University of Michigan, Ann Arbor, MI 48109 U.S.A.)

During birth, the shape of the fetal head is changed due to mechanical loading of the skull. In severe cases, this skull molding may result in mental deficits or death. This study continues a series of studies aimed at quantifying the loads typically exerted on the fetus during delivery, and at defining the response of the fetus to these loads. Specifically, material properties are proposed for fetal dura mater, the tough, fibrous membrane which connects the bones of the fetal skull. Our model assumes that dura mater is an isotropic, nonlinearly elastic, incompressible, and homogeneous material undergoing large static deformation.

Two axisymmetric biaxial tension tests were performed on the dura. The inflation test has been used for material characterization of membranes. A second biaxial tension test was specially designed to simulate the constraints imposed by the cranial bones on the dura mater.

For the inflation tests, circular specimens of dura were clamped into a circular fixture and stamped with a grid pattern. The membrane was inflated in slow, discrete increments, and photographs taken from above. Opposing mirrors and a calibration hemisphere allowed for the three-dimensional grid point reconstruction, assuming spherical deformation. We tested a total of nine specimens of dura mater from eight individuals by inflation.

The second test fixture consisted of a pair of clamps, an inner disk and an outer concentric ring, into which we clamped a circular specimen of dura. The ring of free dura had a circumference on the order of suture lengths and a width near the suture width of a full-term fetus. The outer clamp was mounted to the crosshead of an Instron machine; the inner disk was connected to a load cell. A LVDT measured displacement. Each specimen was cycled to increasingly higher loads at 0.02 mm/s, then failed. We tested 11 specimens from 7 fetuses.

Analyses of the two test geometries are similar. Principal directions of stresses and stretch ratios are in the circumferential, meridional, and normal directions. The equilibrium, compatibility, and constitutive relations are solved via a Runge-Kutta numerical integration scheme.

The experimental stiffness results were compared to analytic results obtained from two published strain energy functions, one defined by Mooney and Rivlin, the other by Skalak, Tozeren, Zarda, and Chien. For both tests, the latter strain energy relations fit the experimental results consistently well. The means (standard deviations) of the STZC stiffnesses for the inflation test and the constraint simulation test, in g_f/cm, are 3400 (1070) and 2000 (840), respectively.

IMPACT FORCES UPON LANDING FROM A HEIGHT IN CHILDREN

Richard N. Hinrichs, Peter H. Werner, Judith E. Rink,
Thomas W. Jackman, and Russell A. Josephs
Department of Physical Education
University of South Carolina
Columbia, SC 29208

One hundred twenty-five (125) second-grade children (66 boys, 59 girls, mean age 7.9 years, mean height 126 cm, mean weight 256 N) performed three different jumps onto a Kistler force platform. The first was a normal two-footed vertical jump, the second was a step from a 46 cm high box placed 5 cm away from the nearest edge of the force platform (Box 1), and the third was a step from the same box placed 66 cm away from the force platform (Box 2). The children performed all jumps in bare feet. Strips of white athletic tape were placed in a matrix across the surface of the force platform to prevent slipping.

In the case of the vertical jump, the children were instructed to "jump as high as you can and make a good landing on the platform with two feet." In the case of the two boxes, the children were instructed to "step off the box with two feet at the same time and make a good landing on the platform with two feet." All non-symmetrical trials (i.e., taking off or landing with one foot before the other) were repeated until two good trials of each jump were obtained.

The vertical component of ground reaction force was measured and displayed on a storage oscilloscope after each trial and saved on magnetic tape for future reference. The peak force at impact with the platform was noted and expressed as a multiple of the child's body weight (BW). Each trial was filmed using videotape with the camera placed 3.6 m to the right side of the subject. The videotape was used to make qualitative assessments of technique as well as quantitative measurements of the vertical displacement of the body center of mass (CM) from the peak of the jump to the instant the toes first touched the platform.

The peak forces were adjusted to take into account the differences in the heights from which the CM fell. The assumption was that if all else were equal, a larger vertical displacement would create a larger velocity at impact which in turn would require a proportionately larger resultant force to stop. A landing index (LI) was created which gave an indication of the "efficiency" of the landing independent of the vertical displacement. Since the velocity at impact is proportional to the square root of the vertical displacement, the landing index was defined as follows:

$$LI = (F-1) / \sqrt{H}$$

where F is the peak vertical ground reaction force expressed in body weights (F-1 is the resultant force) and H is the magnitude of the vertical displacement of the body CM from peak to impact.

The results of the study are summarized in Table 1.

Table 1 -- Results

		mean	std dev	min	max
Vertical Jump					
	F (BW)	5.09	1.87	2.50	12.60
	H (m)	.188	.051	.070	.310
	LI ($BW/\sqrt{m}$)	9.64	4.35	3.20	22.69
Box 1					
	F (BW)	6.97	2.10	3.20	15.1
	H (m)	.385	.075	.170	.590
	LI ($BW/\sqrt{m}$)	9.71	3.39	3.89	20.63
Box 2					
	F (BW)	8.77	2.69	3.30	15.80
	H (m)	.406	.068	.240	.570
	LI ($BW/\sqrt{m}$)	12.31	4.44	3.59	25.01

The results showed surprisingly large forces with little or no discomfort to the children. The peak forces reached nearly 16 BW in some cases. A common factor in the 'inefficient' landers (those who showed large values of LI) was the inability to keep the heels from 'crashing down' onto the force platform. In some cases the children hit the platform heels first or flatfooted, in other cases the heels hit the platform hard after the balls of the feet hit first. The most 'efficient' landers (those who showed the smallest values of LI) seemed to land on the balls of the feet and control the dorsiflexion of the ankles to keep the heels from crashing down. These observations support those of Melvin Jones and Watt (1971) who found that controlled landings were characterized by preparatory muscular activity in the triceps surae prior to impact.

Some children demonstrated large knee and hip flexions after impact as if they had been taught to land that way, yet received large forces because their ankles did not control the initial jolt of the heels hitting the platform. It seems that many of our children are not being taught how to land properly. It is hoped that the results of this study will motivate additional research in this area to further identify the factors which contribute to safe and efficient landings in children and adults.

REFERENCE

Melvin Jones and D.G.D. Watt. Muscular control of landings from unexpected falls in man. (1971). J. Physiology 219:729-727.

USE OF FORCE PLATE DATA TO SCREEN YOUNG PIGS FOR OSTEOCHONDROSIS

Gerald J. Pijanowski, DVM, PhD[1]
Rodger V. Allhands, DVM, PhD[1]
Steven A. Kincaid, DVM, PhD[2]

[1]Department of Veterinary Biosciences and Bioengineering Program
College of Veterinary Medicine
University of Illinois
Urbana, IL 61801

[2]Department of Anatomy
School of Veterinary Medicine
Purdue University
West Lafayette, IN 47907

Osteochondrosis is a nonfatal disease of high morbidity that affects the growing porcine skeleton. It is characterized by the disruption of endochondral ossification by the blockage of vascular invasion resulting in abnormally thick mineralized hyaline cartilage. The pathological process begins sometime before 4 months of age. It may lead to severe distortions of th cartilaginous and synovial articulations, culminating in skeletal deformation, secondary osteoarthritis or, in some cases, healing of the lesions. The joints most commonly affected are the elbow, stifle (knee) and lumbosacral joints. The disease often results in varying degrees of lameness. The lameness results in an economic loss to the pork industry, particularly when it occurs in valuable breeding stock. To date, no reliable on-the-farm methods have been developed to screen growing pigs for the presence of osteochondrosis before the onset of clinical lameness.

The objective of this investigation was to determine if force plate data could be used to detect the presence of osteochondrosis in growing pigs before the onset of clinical lameness. This would allow the producer to eliminate the animal from breeding stock consideration.

Twenty-seven pigs, 10 kg to 80 kg, were trotted over an AMTI Model OR6-3A force plate. An LSI 11/2 computer was used to digitize the output from the force plate at 200 samples per second. Data was collected for each limb of each animal. The data was normalized with respect to time and an average force waveform computed for each limb. The Fourier coefficients were computed for each waveform.

The animals were euthanized and the elbow joints processed for enzyme histochemical evaluation. The severity of the osteochondric lesions were graded from 0 (normal) to 2 (severe). The animals were grouped by lesion grade and discriminant analysis employed to form the discriminant functions.

Thirty more pigs were treated the same except that the discriminant functions were used to predict the lesion grade before the joints were evaluated histochemically. The ability to correctly predict the correct lesion grade was tested statistically.

Discriminant analysis based on the vertical force waveform proved to be a simple and reliable method to separate the classes. The discriminant functions were well separated. Inclusion of the other force components increased the cost of the analysis without adding substantially to the discrimination. The calculated discriminant functions proved to be highly reliable predictors of actual lesion grade.

It appears that the technique can be used to screen pigs for osteochondrosis. A practical "on-the-farm" system must now be developed and tested on commercial pork production farms.

This work was supported by USDA Grant AGR-82-CSR-2-2035.

MODELING OF THE HUMAN SKIN WITH PARTICULAR REFERENCE TO RADIOTHERAPY EFFECTS.

Harcharan Singh Ranu
Department of Biomedical Engineering
Louisiana Tech University
Ruston, Louisiana 71272

Skin is a viscoelastic material, whose properties modify with age. They are also changed by some diseases and certain therapeutic treatments. The elasticity of skin is associated with cosmetic appearance and with the skin's ability to withstand trauma.

A portable apparatus described by Ranu et al (1974) was used to measure the elastic properties of the human skin *in vivo*. The measurements were made on female patients being treated for carcinoma of the breast. Two areas of skin were selected for study on each patient, one in the irradiated area and the other on the contra-lateral breast, which was not treated.

A theoretical model for human skin has been developed which is based on the information derived by means of this device. The model incorporates the elastic as well as the viscoelastic behaviour of the human skin. The skin was visualized as a series of spring and dashpots whose properties are dependent on the viscosity of the dashpot and elastic modulus of the spring. The model takes into consideration the role of elastin, collagen and other elastic constituents of the skin.

Previous *in vitro* studies by Ranu et al (1975) and Ranu (1979) have shown that load extension curves for normal and irradiated skin are identified with the alignment of the collagen fibres and then their subsequent stretching.

An equation of the form shown below has been developed which describes the complete experimental curves of the *in vitro* elastic properties of the normal and irradiated human skin.

$$E = a_o + a_1 \log L + a_2(\log L)^2 + a_3(\log L)^3$$

where E = Extension and L = Load, a_o, a_1, a_2 and a_3 are constants. These constants are very much dependent on the dose of radiation.

The *in vivo* model can be used to predict the viscoelastic characteristics of the skin of humans undergoing radiotherapy treatments. A curve-fitting technique is used to determine the best constants. These constants can further aid the diagnosis and therapy.

Conclusions drawn from this study are that it is possible to theoretically model the normal and irradiated human skin both *in vivo* and *in vitro*. The two types of models have been found to accurately represent the actual behaviour of irradiated skin. These techniques can further aid the clinicians in the diagnosis and progress of therapy.

REFERENCES:

Ranu, H. S., Burlin, T. E. and Hutton, W. C. (1974) The Effects of Radiotherapy on the Elastic Properties of Human Skin. Radiation Research, Vol. 59, No. 1. pp. 245-246.

Ranu, H. S., Burlin, T. E. and Hutton, W. C. (1975) The Effects of X-irradiation on the Mechanical Properties of Skin. Physics in Medicine and Biology, Vol. 20, No. 1. pp 96-105

Ranu, H. S. (1979). The Mechanical and Structural Response of Skin to Irradiation. J. Biomechanics, Vol. 12, No. 8, pp. 601-608.

An *In Vivo* Determination of the Mechanical Characteristics of the Human Heel Pad

Gordon A. Valiant, Nike Sport Research Laboratory, Exeter, NH
Peter R. Cavanagh, Biomechanics Laboratory, Penn State Univ.

It has been recognized that the primary function of the human heel pad is to protect the heel from sudden impacts and excessive pressure. It was the purpose of this study to determine the mechanical characteristics of the heel pad, and to describe the mechanism by which it achieves its primary function.

Twenty-four males, 12 runners and 12 nonrunners, aged 18-36 years, served as subjects. The heel pad of the right foot was impacted with an instrumented ballistic pendulum. The right leg rested on a small platform and was flexed beyond 90 degrees with the femoral condyles firmly pressed against an immovable wall. Acceleration records for three trials for each of three impact velocities, 0.8, 1.0 and 1.2 m/sec, were sampled by a 12 - bit converter at 12.5 kHz. The average acceleration record was integrated twice and the resulting displacement was plotted against force. The rising phase of the force deformation curve was divided into two approximately linear regions. The slopes of these two regions, K1 and K2, were interpreted as estimates of the stiffness of the heel pad tissue. For two trials at each impact velocity, double-exposure 35 mm photographs were taken from three different directions using strobed illumination. The first exposure was made at the instant of impact and the second exposure occurred at the approximate time of peak force. The displacement of skin markers between the two exposures was determined in three-dimensions using the DLT.

None of the variables which were measured during the pendulum impacting revealed any differences between the two groups of subjects. Shown in Figure 1 is a typical averaged force-deformation curve for the 1.0 m/sec impact condition. It reveals an energy loss of 88.5% indicating that the energy absorbing potential of the heel pad is high. For all subjects, percent energy loss ranged from 84% to 98%. The peak force averaged 313 N and was approximately linearly related to the square of the impact velocity. These forces were considerably less than those that have been measured with a force platform during running, but were in some cases close to a pain threshold for many of the subjects. Table 1 shows how the different variables changed with impact velocity.

Table 1

Impact velocity [m/sec]	Peak force [N]	% Energy absorption	Maximum deformation [mm]	K1 [kN/m]	K2 [kN/m]
0.8	216	90.9	9.0	7.6	72.5
1.0	313	92.7	9.8	7.1	104.0
1.2	422	93.8	10.4	7.4	136.0

The 3-D data describing the displacement of the skin markers on the heel was accurate to approximately 0.6 mm. The large cranial

excursion of the impacting pendulum during the time span between exposures resulted in a corresponding cranial excursion of lines drawn across the achilles tendon of only 25% or less of the pendulum displacement. This indicates that the tissue of the heel pad is relatively incompressible and so large excursions of the pendulum into the soft tissue region of the heel pad must be accompanied by displacements of the tissue in directions other than the direction of travel of the pendulum. The most distal skin markers demonstrated displacements in all three principal planes. Proceeding in the cranial direction, the medial and lateral displacements were greatly reduced, as were the posterior displacements. The cranial displacements were reduced as well, but to a lesser extent. There were no differences between resultant skin marker displacements on medial and lateral sides of the heel pad.

The three-dimensional kinematic results suggest that displacement of the tissue in medial/lateral and posterior directions is a mechanism for the absorption of energy if the heel pad does not return to its original shape immediately upon release of the load. In order to investigate this mechanism further, three pendulum impact trials, one at each of the three different impact velocities, were performed with a heel restraining device clamped around the heel pad region. The firm clamping of the fairly rigid device will have the effect of reducing the amount of displacement in the medial/lateral dimension.

Figure 2 shoes the force-deformation curves for restrained and non-restrained conditions for one subject for the 1.0 m/sec condition. The heel restraint resulted in a decrease of only 1% in the amount of energy absorbed, but it did decrease the maximum deformation of the tissue by 10%. It appeared that a reduction in the deformation within the initial portion of the force-deformation curve accounted for the total decrease in deformation. This suggests that the stiffness of the tissue is greater in the initial impact phase, but remains unchanged in the second rising phase of the curve. This apparent increase in stiffness would also account for the 7% measured increase in peak force.

It was concluded that the human heel pad is a highly shock absorbing structure exhibiting nonlinear viscoelastic characteristics. A characteristic two-phase force-deformation curve was identified. Each phase could be approximated by linear slopes which were interpreted as estimates of the elasticity of the soft tissue. It was assumed that the medial/lateral and posterior displacements of the distal skin markers contributed to the low initial heel pad stiffness.

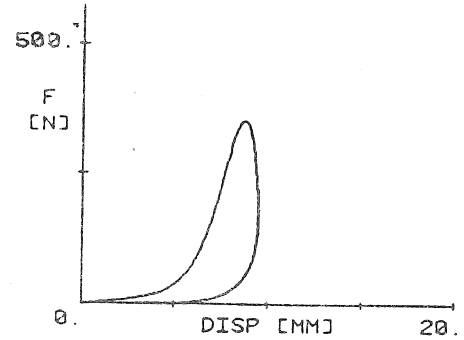

Figure 1.

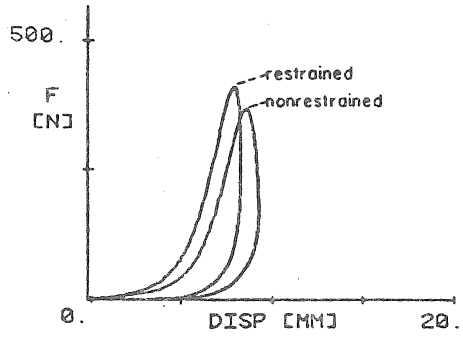

Figure 2.

Total, External and Internal Work for Human Movement

Sergei Yu. Aleshinsky

Biomechanics Laboratory, The Pennsylvania State University

Different methods currently in use for computing the mechanical energy of human movement give radically different results (Williams and Cavanagh, 1983). Among these methods one of the most popular is the determination of two functions of time: 1) the system mass centre energy ("external") and 2) the energy level of the limbs relative to system mass centre ("internal"). Then the increases and decreases of each of these functions are added to give "total" work (Fenn, 1930; Ralston and Lukin, 1960; Cavagna, Saibene and Margaria, 1964; Cavagna and Kaneko, 1977 and many others).

Let us follow the consequences of these operations describing each step mathematically for the simplest case of a one-link model motion under the action of the force $\vec{F}_0\{F_0^x; 0\}$ (nomenclature and a diagram are at the end of the abstract). The equations of motion will be

$$m_1\ddot{x}_{C_1} = F_0^x \qquad m_1\ddot{y}_{C_1} = -m_1 g \qquad I_{C_1}\ddot{\varphi}_1 = F_0^x a_1 \sin\varphi_1 \tag{1}$$

Multiply these equations by $\dot{x}_C = \dot{x}_{C_1}, \dot{y}_C = \dot{y}_{C_1}, \dot{\varphi}_1$ respectively. Taking into account $\dot{x}_C = \dot{x}_0 - \dot{x}_{0/C}$ and $a_1 \sin\varphi_1 \dot{\varphi}_1 = \dot{x}_{0/C}$ we get

$$\frac{d}{dt}\left(\frac{m_1\dot{x}_C^2}{2}\right) = F_0^x\dot{x}_C \qquad \frac{d}{dt}\left(\frac{m_1\dot{y}_C^2}{2}\right) = -m_1 g\dot{y}_C \qquad \frac{d}{dt}\left(\frac{I_{C_1}\dot{\varphi}_1^2}{2}\right) = F_0^x\dot{x}_{0/C} \tag{2}$$

or

$$\frac{d}{dt}\left[\frac{m_1(\dot{x}_C^2+\dot{y}_C^2)}{2} + m_1 g y_C\right] = F_0^x(\dot{x}_0 - \dot{x}_{0/C}) \qquad \frac{d}{dt}\left[\frac{I_{C_1}\dot{\varphi}_1^2}{2}\right] = F_0^x\dot{x}_{0/C} \tag{3}$$

The expressions in square brackets are "external" and "internal" energy, respectively. Obtaining "external" and "internal" work (adding increases and decreases of two curves) means, in mathematical terms, integration of the absolute values of (3) over time:

$$W_{external} = \int_{t_1}^{t_2}\left|\frac{d}{dt}\left[\frac{m_1(\dot{x}_C^2+\dot{y}_C^2)}{2} + m_1 g y_C\right]\right| dt$$

$$W_{internal} = \int_{t_1}^{t_2}\left|\frac{d}{dt}\left[\frac{I_{C_1}\dot{\varphi}_1^2}{2}\right]\right| dt \tag{4}$$

This corresponds (because of the righthand sides of (3)) to

$$W_{total} = \int_{t_1}^{t_2}\left|F_0^x\dot{x}_0 - F_0^x\dot{x}_{0/C}\right| dt + \int_{t_1}^{t_2}\left|F_0^x\dot{x}_{0/C}\right| dt \tag{5}$$

At the same time it is clear that the value of work (taking into account the irreversible character of muscular activity) is equal to $\int_{t_1}^{t_2}|F_0\dot{x}_0|dt$ but this does not correspond to expression (5).

Using the above methods it can be shown that in the more common case of multi-link planar movement under the action of external forces and internal (muscular) moments the following relationships exist:

$$W_{total} = W_{external} + W_{internal} =$$

$$= \int_{t_1}^{t_2} \left| (F_0^x \dot{x}_0 - \underline{F_0^x \dot{x}_{0/c}}) + (-F_N^x \dot{x}_N + \underline{F_N^x \dot{x}_{N/c}}) + (F_0^y \dot{y}_0 - \underline{F_0^y \dot{y}_{0/c}}) + (-F_N^y \dot{y}_N + \underline{F_N^y \dot{y}_{N/c}}) \right| dt \quad (6)$$

$$+ \int_{t_1}^{t_2} \left| \underline{F_0^x \dot{x}_{0/c}} - \underline{F_N^x \dot{x}_{N/c}} + \underline{F_0^y \dot{y}_{0/c}} - \underline{F_N^y \dot{y}_{N/c}} + \sum_{i=1}^{N-1} M_{i,i+1} (\dot{\varphi}_{i+1} - \dot{\varphi}_i) \right| dt$$

Similarly underlined terms in (6) correspond to components of external and internal energies which always fluctuate out of phase with each other requiring no energy supply (as was the case in the simplest example). If one follows the traditional way of calculation of total work he unintentionally includes the energy cost of these fluctuations twice.

In addition, the absence of the absolute values signs inside of the summation " $\sum$ " in (6) admits the complete energy transfer between all the "muscular sources" independent of their disposition. This leads to an erroneous result.

In conclusion, it has been shown that "total work" calculated as the sum of "external" and "internal" work leads to incorrect results although the total energy presentation as a sum of external and internal components is correct.

Note All the formulae here have assumed an equal cost for positive and negative work. The validity of this assumption does not influence the conclusion.

Nomenclature :

N - number of the links in the system
m_i - mass of the i-th link
I_{c_i} - moment of inertia at center of gravity of the i-th link
x_{c_i}, y_{c_i} - coordinates of the mass centre of the i-th link
x_c, y_c - coordinates of the system mass center
$\varphi_i, \dot{\varphi}_i$ - angular position and velocity of the i-th link
$\vec{F}_0, \vec{F}_N$ - external forces (support reactions)
$M_{i,i+1}$ - net joint moment
$x_{0/c}, y_{0/c}$ - correspond to $x_0 - x_c$, $y_0 - y_c$
t_1, t_2 arbitrary moments of time

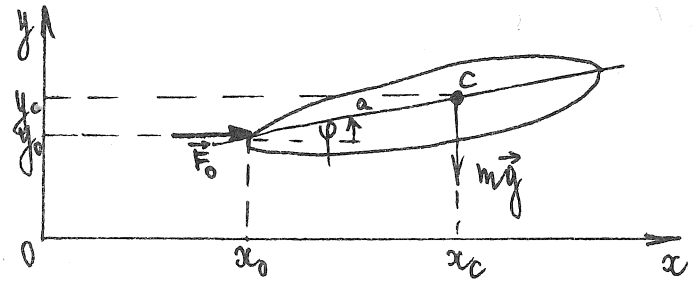

Mechanical Work Done on the Lower Extremities During the Recovery Phase of Loaded Running

Philip E. Martin
Department of Health and Physical Education
Arizona State University
Tempe, AZ 85287

INTRODUCTION

The effect of carrying load on the body has been the subject of considerable research in the past. Early research efforts primarily dealt with the effect of carrying load on the trunk in the form of backpack loads. More recently, the influence that the weight of footwear has on sports performance has become an interest of sports scientists and manufacturers of sports shoes because of possible performance benefits to be gained by wearing lightweight footwear. Most of the published research studies related to load carrying, particularly those considering the effect of footwear weight, have been evaluations of the physiological consequences of carrying additional load. While the physiological consequences are fairly well established, there has been little research which has considered the effect of load on the mechanical characteristics of movement. It was the purpose of this research to evaluate the effect of loading the lower extremities on the mechanical work done on the foot, shank, and thigh during the recovery or nonsupport phase for moderate speed running.

PROCEDURES

Fifteen men, all of whom were considered to possess a high level of physical fitness, performed eight-minute runs on a treadmill at 12 km/hr under five load conditions. These included: 1) no added load, 2) 0.25 kg added to each thigh, 3) 0.25 kg added to each foot, 4) 0.50 kg added to each thigh, and 5) 0.50 kg added to each foot. The extra loads were added to the lower extremities in the form of packets of lead shot. Running shoes and shorts, which were specially adapted to receive the loads, were provided for the subjects. Estimates of the inertial properties of the lower extremity for each subject were generated using the procedures of Clauser et al. (1) and Hanavan (2). These values were then adjusted for the footwear worn by the subjects and for the added loads.

A sagittal plane view of the subjects' running motions was recorded near the end of each eight-minute run with a single Locam camera operating at 100 frames per second. Film coordinate data representing the locations of the toe and heel and the ankle, knee, and hip joint centers were first corrected for treadmill speed and then digitally filtered. The smoothed coordinate data were then used to calculate the kinematic characteristics of the segmental movements. Values for the positive and negative work done on the foot, shank, and thigh were derived by calculating the increases and decreases in the mechanical energy level of each segment. Changes in the total energy level of the leg as a single unit were also quantified. Analysis of variance was used to statistically analyze the mechanical work data to determine the effects of the magnitude and positioning of the loads. The Tukey WSD test was used for all follow-up testing.

This research represents a portion of the doctoral dissertation of the author. The research was conducted in the Biomechanics Laboratory at Penn State University, University Park, PA.

RESULTS

Table 1 contains the mean values for the positive and negative work done on the foot, shank, thigh, and total leg for each of the five load conditions. The results demonstrated that when load was added to the thighs, changes in the positive and negative work done on the segments were limited to the thigh. There were no significant changes in the mechanical work done on the shank and foot when the thighs were loaded. There was a tendency for the work done on the leg to increase as the load was increased but these changes were not statistically significant. When the feet were loaded, there were no significant changes in the positive and negative work done on either the thigh or shank. The work done on the foot and the leg as a whole, however, did show significant increases as the load on the feet was increased. Consequently, the results clearly indicate that the increases in the positive and negative work observed when the load applied to the lower extremity was increased were limited to the segment to which the load was added. The effect of adding load to the feet on the mechanical work measures, however, was considerably more marked than the effect of adding load to the thighs.

Table 1. Positive and Negative Work Done on the Lower Extremity

	LOAD CONDITION				
	NO LOAD	0.25 THIGH	0.50 THIGH	0.25 FOOT	0.50 FOOT
Foot - Positive	41.7J	41.8J	42.1J	47.1J	52.7J
Foot - Negative	-45.6	-45.7	-45.5	-51.3	-57.1
Shank - Positive	42.6	42.1	42.2	42.1	42.9
Shank - Negative	-49.8	-48.7	-48.7	-49.3	-49.8
Thigh - Positive	22.5	23.4	24.9	22.5	23.5
Thigh - Negative	-36.2	-36.8	-39.4	-36.9	-38.1
Leg - Positive	84.0	85.2	87.4	87.6	93.8
Leg - Negative	-108.7	-109.0	-111.9	-113.3	-119.5

When considered in combination with the results of physiological evaluations of the effect of lower extremity loading, the results of this study provide greater insight into the reasons for an increased metabolic demand under loaded conditions. Physiological results, which were presented previously (3), demonstrated that oxygen consumption increased as load magnitude increased and that the changes in oxygen consumption due to foot loading - approximately 0.7% for each 100g of load - were nearly twice as great as those for thigh loading. Because the changes in mechanical work were limited to the loaded segments, the results suggest that the pattern of movement for the lower extremity was quite consistent for all load conditions. The increased physiological demand, therefore, can be attributed almost totally to the inertial changes in the lower extremity and not to some major modification in the pattern of movement. These results have important implications not only for the demands placed on the leg musculature but also for the mechanisms by which the nervous system controls the locomotion process.

REFERENCES

1. Clauser, C.E. et al. (1969). Weight, volume, and center of mass of segments of the body (AMRL-TR-69-70). Wright-Patterson Air Force Base, Ohio.

2. Hanavan, E. (1964). A mathematical model of the human body (AMRL-TR-64-102). Wright-Patterson Air Force Base, Ohio.

3. Martin, P.E. (1984, May). The effect of lower extremity loading on mechanical and physiological measures of running performance. Paper presented at the American College of Sports Medicine annual meeting, San Diego, CA.

RESULTS

Table 1 contains the mean values for the positive and negative work done on the foot, shank, thigh, and total leg for each of the five load conditions. The results demonstrated that when load was added to the thighs, changes in the positive and negative work done on the segments were limited to the thigh. There were no significant changes in the mechanical work done on the shank and foot when the thighs were loaded. There was a tendency for the work done on the leg to increase as the load was increased but these changes were not statistically significant. When the feet were loaded, there were no significant changes in the positive and negative work done on either the thigh or shank. The work done on the foot and the leg as a whole, however, did show significant increases as the load on the feet was increased. Consequently, the results clearly indicate that the increases in the positive and negative work observed when the load applied to the lower extremity was increased were limited to the segment to which the load was added. The effect of adding load to the feet on the mechanical work measures, however, was considerably more marked than the effect of adding load to the thighs.

Table 1. Positive and Negative Work Done on the Lower Extremity

	LOAD CONDITION				
	NO LOAD	0.25 THIGH	0.50 THIGH	0.25 FOOT	0.50 FOOT
Foot - Positive	41.7J	41.8J	42.1J	47.1J	52.7J
Foot - Negative	-45.6	-45.7	-45.5	-51.3	-57.1
Shank - Positive	42.6	42.1	42.2	42.1	42.9
Shank - Negative	-49.8	-48.7	-48.7	-49.3	-49.8
Thigh - Positive	22.5	23.4	24.9	22.5	23.5
Thigh - Negative	-36.2	-36.8	-39.4	-36.9	-38.1
Leg - Positive	84.0	85.2	87.4	87.6	93.8
Leg - Negative	-108.7	-109.0	-111.9	-113.3	-119.5

When considered in combination with the results of physiological evaluations of the effect of lower extremity loading, the results of this study provide greater insight into the reasons for an increased metabolic demand under loaded conditions. Physiological results, which were presented previously (3), demonstrated that oxygen consumption increased as load magnitude increased and that the changes in oxygen consumption due to foot loading - approximately 0.7% for each 100g of load - were nearly twice as great as those for thigh loading. Because the changes in mechanical work were limited to the loaded segments, the results suggest that the pattern of movement for the lower extremity was quite consistent for all load conditions. The increased physiological demand, therefore, can be attributed almost totally to the inertial changes in the lower extremity and not to some major modification in the pattern of movement. These results have important implications not only for the demands placed on the leg musculature but also for the mechanisms by which the nervous system controls the locomotion process.

REFERENCES

1. Clauser, C.E. et al. (1969). Weight, volume, and center of mass of segments of the body (AMRL-TR-69-70). Wright-Patterson Air Force Base, Ohio.

2. Hanavan, E. (1964). A mathematical model of the human body (AMRL-TR-64-102). Wright-Patterson Air Force Base, Ohio.

3. Martin, P.E. (1984, May). The effect of lower extremity loading on mechanical and physiological measures of running performance. Paper presented at the American College of Sports Medicine annual meeting, San Diego, CA.

JOINT TORQUE PATTERNS OF BELOW-KNEE AMPUTEES DURING RUNNING STANCE[1]

Doris I. Miller
Faculty of Physical Education
University of Western Ontario
London, Ontario

Carolyn F. Munro
Department of Kinesiology
University of Washington
Seattle, Washington

Resultant hip, knee and ankle joint torques of below-knee amputees running at speeds ranging from 2.3 to 6.0 m/s were computed during stance to gain insight into compensatory mechanisms employed by these individuals to offset leg loss.

The running patterns of four unilateral below-knee amputees were filmed at 90-100 fps with a Locam camera located 20 m back from the major plane of the motion. Ground reaction force was obtained from a Kistler Z4852 force platform (.9 m in the running direction) mounted flush with the surface of a 20 m runway. The platform was connected on-line to a PDP 11/34 computer and sampling was at a rate of 1000 Hz. Ground reaction data and segmental endpoint coordinates digitized from the film were combined into computer data files and input to a program which calculated resultant joint torque-time histories utilizing a planar link segment model (Miller & Nelson, 1973, pp. 61-72).

In general, resultant hip, knee and ankle joint torques of the noninvolved limb of the amputees during stance were similar in both pattern and magnitude to those reported previously (Mann, 1981; Mann & Sprague, 1980; Winter, 1983). There was, however, an initial dominant dorsiflexor torque immediately following foot-strike which was absent in the records of Mann and Winter.

In nonamputee runners and on the noninvolved side of the amputees, dominant hip extensor torque was observed at the beginning of stance and was related to a continuation of the muscular torque pattern used to slow and reverse thigh rotation at the end of the swing phase in preparation for stance. The resultant hip extensor torque on the amputee involved side during stance, however, was greater in magnitude and duration than its counterpart on the intact limb. By exerting a torque which tended to rotate the thigh backward, the hip extensors on the amputated side appeared to be assisting the control of residual knee flexion following foot-strike and then helping with knee extension during the middle half of stance (Figure 1).

After a brief initial flexor torque, the dominant torque about the knee joint was extensor for the remainder of stance for the three subjects who displayed flexion of the residual knee at the beginning of stance. These residual knee torques tended to be smaller in magnitude than those generated about the knee by the musculature of the intact limb. In sharp contrast was the pattern of the fourth subject who exhibited an overly straight residual knee during stance on the prosthesis. His intact and

---

[1]Supported in part by VA Contract No. V663P-1254 awarded to D.I. Miller, M.W. Passer and E.M. Burgess

residual knee joint torques were almost mirror images of one another. While the intact knee displayed the anticipated dominant extensor torque during most of the first 75% of stance, the residual knee was characterized by a dominant flexor torque throughout virtually the entire stance period.

The analysis of resultant joint torques of amputee runners during stance suggested that the hip extensors on the amputated side, through their action in promoting backward rotation of the thigh with respect to the hip, help to compensate for the lower than normal knee extensor torques generated by the residual limb.

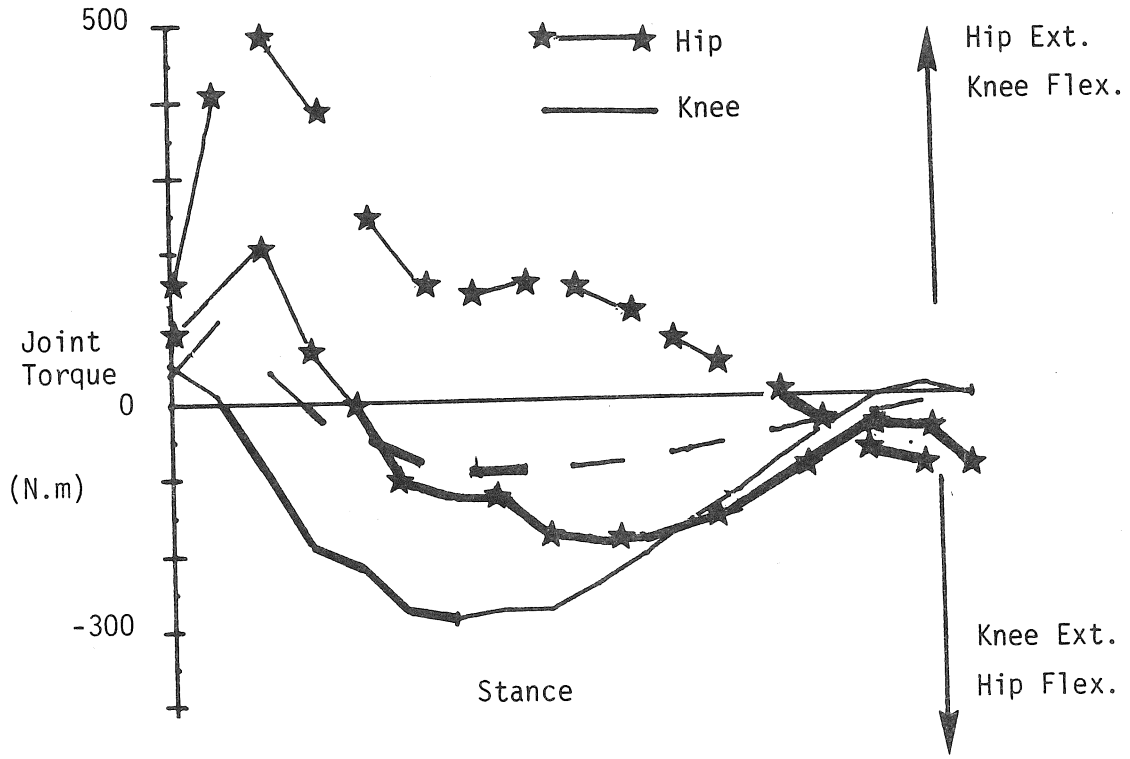

Figure 1. Resultant hip and knee joint torques during stance of a skilled amputee runner (5.4 m/s). Solid lines represent the intact limb and broken lines, the residual limb. Thickened lines designate eccentric phases of contraction.

References

Mann, R.V. A kinetic analysis of sprinting. Medicine and Science in Sports and Exercise 13 (5): 325-328, 1981.

Mann, R. & Sprague, P. A kinetic analysis of the ground leg during sprint running. Research Quarterly for Exercise and Sport 51 (2): 334-348, 1980.

Miller, D.I. & Nelson, R.C. Biomechanics of Sport. A Research Approach. Philadelphia: Lea & Febiger, 1973.

Winter, D.A. Moments of force and mechanical power in jogging. Journal of Biomechanics 16 (1): 91-97, 1983.

Segment Interaction in Treadmill Running at Four Different Speeds

C.A. Putnam School of Physical Education
Dalhousie University, Halifax, Nova Scotia

Recovering the leg between steps of a running cycle is an example of a swinging motion of the lower extremity in which segments rotate in a sequential fashion. The kinematics of this motion is ultimately determined by the initial conditions at toe-off, external forces applied to the lower extremity system and the resultant joint moments (RJM) at the hip, knee and ankle. By virtue of the fact that one segment is set in motion, it will influence the motion of all other segments in the system. The nature of this intersegmental interaction is a function of the relative orientations, angular velocities and accelerations, and inertial characteristics of the involved segments. The purpose of this study was to examine the interaction between the thigh and the lower leg plus foot (hereafter referred to as the leg) during the swing phase of treadmill running, and to determine the effect of running speed on the relative roles of the segment interaction and RJMs in bringing about angular velocity changes in the two segments.

Six trained, male runners were filmed at high speed while running on a treadmill at 3.0, 4.0, 5.0 and 6.0 m/s. Joint coordinates digitized from the film images were smoothed with a digital filter and used in a link segment analysis to arrive at resultant joint forces and moments at the hip and knee. The resultant joint force was divided into components, each a function of a single kinematic parameter of the system. The moments of these component forces, relative to the segment center of mass, were used to express the segment interaction as a function of the system kinematics.

The total time of the swing phase ranged from 0.45 to 0.57 seconds with subjects demonstrating a slight tendency to decrease their swing phase time with increases in running speed. Segmental angular velocities and accelerations and RJMs increased in magnitude with increases in running speed while the overall patterns of these parameters remained quite similar across running speeds. During the middle two quarters of the swing phase, the angular velocity of the leg increased. The RJM at the knee accounted for 16% of this increase at 3.0 m/s and 40% at 6.0 m/s. The relative influence of the thigh motion on the leg which was a function of the thigh's angular velocity also increased by similar magnitudes with increases in running speed, while that of all other interactive terms decreased.

During the final 25% of the swing phase the angular velocity of the leg decreased in preparation for foot strike. At 3.0 m/s the RJM at the knee was responsible for 89% of this decrease, assisted by the interaction moment which was a function of the thigh's angular acceleration. As running speed increased, the segmental interaction changed in such a manner that it no longer aided in decreasing the leg angular velocity. By 6.0 m/s the angular impulse of the knee RJM was 105% of the total impulse necessary to decrease the leg angular velocity.

During the first one-third of the swing phase the RJM at the hip was at its highest magnitude in the direction of hip flexion, causing, in part, thigh angular acceleration in this direction. The angular impulse of the hip RJM was approximately four times that necessary to bring about the increase in thigh angular velocity because of the effect of the segment interaction on the thigh motion. The relative role of the hip RJM changed very little with increases in running speed.

During the final one-third of the swing phase, the hip RJM was very large in the direction of hip extension. However the thigh did not necessarily

accelerate in this direction. Instead, the hip RJM worked primarily against the interactive moment which was a function of the leg angular acceleration, and tended to angularly accelerate the thigh in the direction of hip flexion. The relative influences of the hip RJM and this interactive moment changed with running speed such that at 3.0 m/s the influence of the hip RJM on the angular acceleration of the thigh was about 75% of that of the interactive moment, while at 6.0 m/s it was 90% of that of the interactive moment.

In conclusion, the relative roles of the RJMs and the interactive moments in causing changes in segment angular velocities appear to be a function of running speed. In general, the roles played by the RJMs relative to those played by the interactive moments tend to increase with increases in the speed of the recovery leg action.

Changes in Rearfoot Motion Associated With Systematic Variations in Running Style

K.R. Williams and J.L. Ziff, Human Performance Lab, University of California, Davis, CA., 95616

Excessive rearfoot pronation is commonly implicated as a condition which may lead to the development of lower extremity injuries during running, though exact causative relationships have not been established. While variations in foot structure and function are often cited as a cause of over-pronation, the affect that differences in running style might have on pronation is a relatively unexplored area. It may be that there are aspects of running style which cause or exacerbate pronation-related problems, and that changes in selected parameters might alter pronation enough to relieve symptoms. The purpose of this study was to examine the influence of stride length (SL), stride width (SW), and shoulder rotation (SROT), on measures of rearfoot motion.

Methods

Eight male runners experienced at running on a treadmill were filmed at 200fps from the rear while running at a speed of 3.57 m/s in each of nine conditions. Each subject was given a preliminary training session to familiarize them with the procedures used to vary SL, SW and SROT. The same model of a neutral running shoe was used for each condition. Changes in the lower leg, heel, and rearfoot angles during contact were derived from the film for each experimental condition. When stride length was varied, subjects first ran at their chosen SL, and then were constrained to run at chosen SL+10% leg length (LL), and chosen SL-10%LL by making contact to the beat of an electronic metronome.

SW and SROT were systematically varied to provide data over a normal range of values for each of these parameters. During SW and SROT trials subjects received constant qualitative feedback from the experimenter as to relative SW, or the amount of SROT, to ensure that all subjects ran with similar variations in each parameter. Cine film was taken at 50fps from the front during SW trials. Foot position during contact, relative to a central line of progression derived from markers on the center of the trunk, was averaged over 10 running cycles for each SW condition. During SROT trials film was taken from above at 50fps and mean shoulder rotation maximums for 5 cycles determined and averaged.

Results and Discussion

Though SL varied significantly over the three SL conditions (Table 1a), no significant differences were found in rearfoot angle at foot strike (RAFS), rearfoot angle at maximal pronation (RAMP), maximal pronation velocity (MPVEL), or amount of pronation (AMTP). Similarly, though wide variations were induced in the three SROT conditions (Table 1c), no significant differences were found in RAFS,

RAMP, MPVEL, or AMTP. In both SL and SROT conditions some individuals did show systematic variations but the nature of the changes were not consistant between different subjects.

Only with variations in SW (Table 1b) were significant differences found for rearfoot movement parameters, with wider SW asscciated with smaller RAMP, MPVEL, and AMTP. No significant differences were found in RAFS. Within each SW condition correlations between SW and either RAMP or MPVEL were low, indicating that SW itself did not determine rearfoot parameters. However, SW was better correlated with RAMP (r=-0.63) and MPVEL (r=0.55) when data across all three SW conditions were used, indicating that manipulations of SW were successful in altering rearfoot motions.

In examining rearfoot data from all nine conditions combined, it was found that RAMP was better correlated with leg angle at initial contact (LAC, r=0.59) than with heel angle at contact (HAC, r=-0.36) or with RAFS (r=0.45). MPVEL, however, was poorly related to LAC (r=-0.26) but highly correlated with HAC (r=0.80) as well as RAFS (r=-0.80). The more supinated the rearfoot angle at contact, the greater the MPVEL.

Results indicate that differences in rearfoot pronation are affected by variations in SW but not influenced in any consistant pattern by large variations in SL or SROT. If certain lower extremity injuries are in fact related to excessive pronation, it still is not known what aspect of rearfoot motion is most responsible, with RAMP and MPVEL the typical variables implicated. The data would indicate that running with wider SW would tend to reduce both RAMP and MPVEL, and that changing the heel angle at contact to a less supinated position may reduce MPVEL. Thus, for those runners who show symptoms related to excessive pronation an alteration in selected running mechanics may be a viable alternative to traditional and more expensive treatment methods.

TABLE 1 - REARFOOT ANGLES AT MAXIMAL PRONATION

	a) STRIDE LENGTH (cm)	a) REARFOOT ANGLE (degrees)	b) **STRIDE WIDTH (cm)	b) REARFOOT ANGLE (degrees)	c) SHOULDER ROTATION (degrees)	c) REARFOOT ANGLE (degrees)
Mean	123.3	14.8	-2.8	*18.3	24.7	15.9
SD	(8.6)	(3.3)	(1.1)	(3.9)	(4.9)	(2.3)
Mean	131.8	15.6	1.6	@15.9	29.8	16.2
SD	(8.5)	(3.1)	(1.3)	(3.3)	(5.2)	(1.7)
Mean	140.6	15.6	5.1	@*12.2	41.5	16.4
SD	(8.9)	(3.3)	(1.6)	(2.8)	(11.8)	(1.7)

@ Significant difference in rearfoot angles ($p<.05$)
* Significant difference in rearfoot angles ($p<.01$)
** Positive value indicates foot contact lateral to midline.

BASEBALL PLAYERS CANNOT KEEP THEIR EYES ON THE BALL

A. Terry Bahill
Systems and Industrial Engineering
University of Arizona
Tucson, AZ 85721.

Ted Williams, perhaps the best hitter in the history of baseball, has described hitting a baseball as the most difficult single act in all of sports. The velocity of the ball approaches 100 mph, producing angular velocities greater than 500 deg/sec as the ball passes the batter. Humans cannot track targets moving faster than 70 deg/sec; yet, professional batters manage to "get a piece of the ball" in over half their swings. In this paper we investigate how they do this by examining a professional athlete tracking a pitched ball, and we demonstrate the superiority of his eye movements and head-eye coordination to those of our graduate students.

Why did we want to study a batter tracking a baseball? We wanted to learn more about how the brain controls movement, and we therefore were searching for a situation in which a human was performing optimally. This condition is fulfilled by a professional baseball player hitting a baseball.

There are four basic types of eye movements: saccadic eye movements, which are used in reading text or scanning a roomful of people; vestibulo-ocular eye movements, used to maintain fixation during head movements; vergence eye movements, used when looking between near and far objects; and smooth-pursuit eye movements, used when tracking a moving object. These four types of eye movements have four independent control systems, involving different areas of the brain. Their dynamic properties, such as latency, speed, and high-frequency cutoff values, are different, and they are affected differently by fatigue, drugs, and disease.

The batter has the potential to use the head-movement system in addition to each of these eye-movement systems. Does he? Earlier studies have suggested several strategies for tracking a baseball: track the ball with head movements and smooth-pursuit eye movements and fall behind in the last 5 ft of flight; track with eyes only, or with head only, and fall behind in the last 5 ft; track the ball over the first part of its trajectory with smooth-pursuit eye movements, make an anticipatory saccadic eye movement to a point ahead of the ball, continue to follow it with peripheral vision, and finally, at the end of the ball's flight, resume smooth-pursuit tracking with the ball's image on the fovea, the small area in the center of the retina that has fine acuity. We will examine each of these strategies.

To discover how well a batter tracked the ball, we had to be able to determine the position of the ball at all times, and thus we could not use a real pitcher or a throwing machine. Instead, we simulated the trajectory of a pitched baseball. We threaded a fishing line through a white plastic ball and stretched this line between two supports, which were set 80 ft apart in order to accommodate the 60.5 ft between pitcher and batter; a string was attached to the ball and wrapped around a pulley attached to a motor, so that when the motor was turned on, the string pulled the ball down the line at speeds

between 60 and 100 mph. The ball crossed the plate 2.5 ft away from the subject's shoulders, simulating a high-and-outside fastball thrown by a left-handed pitcher to a right-handed batter.

We ran several subjects through our simulation, including graduate students, students on the University baseball team, and Brian Harper, a member of the Pittsburgh Pirates; all had 20/20 uncorrected vision. Typically our students tracked the ball well (less than 2 deg error) until the ball was 9 ft in front of the plate. The professional ballplayer keept his eye on the ball longer than our other subjects did. He was able to keep his position error below 2 deg until the ball was 5.5 ft from the plate.

Although the professional athlete was better than the students at tracking the simulated fastball, it is clear from our simulations that batters, even professional batters, cannot keep their eyes on the ball. Our professional athlete was able to track the ball until it was 5.5 ft in front of the plate. This could hardly be improved on; we hypothesize that the best imaginable athlete could not track the ball closer than 5 ft from the plate, at which point it is moving three times faster than the fastest human could track.

Our findings should generalize to other sports. In tennis, for example, the distances are similar, 60 ft for baseball and 78 ft for tennis, as are the linear velocities, 100 mph for a fast pitch and 110 mph for a fast serve. There is often an abrupt change in the ball's trajectory just before the player hits it: the baseball breaks and the tennis ball bounces. Tennis coaches, even more than batting instructors, teach beginners to use the strategy with the anticipatory saccade in order to see the ball hit the racket; this strategy is probably only useful as a learning tool. Therefore, we suggest that neither baseball players nor tennis players keep their eyes on the ball. The success of the good players is due to faster smooth-pursuit eye movements, a good ability to suppress the vestibulo-ocular reflex, and the occasional use of an anticipatory saccade.

VARIABLE FORCE COIL SPRING HAND SPLINT

J. Danoff, W. Schneiderwind, B. Moy, B. Thornton,
L. Gerber, A. Rich, J. Ledermann

Department of Rehabilitation Medicine
National Institutes of Health, Bethesda, Maryland

Medical conditions such as rheumatoid arthritis (RA) can cause severe disfigurement and pain in the metacarpophalangeal (MP) and interphalangeal (IP) joints of the fingers with significant functional loss. In recent years surgical intervention has been applied as a means of regaining function of these finger joints. Many health professionals believe that successful MP joint arthroplasty or capsular and extensor hood repair depend on proper patient selection, adequate operative technique, and good postoperative management.

Various types of hand splints have been used as components of post-operative management in combination with specific exercise protocols. Hand splints are generally designed to apply low forces to the affected digits in such a manner to ensure that functional alignment will be retained after soft tissue healing has been completed. Splints that allow for digit movement are referred to as dynamic splints, and resistive forces are usually generated by appropriately positioned elastic bands. These bands are suspended from wire outriggers above the dorsal hand and attached via short cords to stirrups around the proximal phalanges.

The basic function of the dynamic hand splint is to apply a force at the proximal phalanx which will result in an extension and/or radial torque at the MP joint. This force will then counter any tendencies in the finger to develop flexion and/or ulnar contractures. Ideally the torque at the MP joint should be constant. Applying this criterion (d(torque) = 0) to the geometry of the cord, MP joint, and stirrup location, the best outrigger location can be determined to be directly over the stirrup resulting in a 90° angle between cord and phalanx (θ).

Several factors can modify MP torques. When the MP joint is flexed beyond the initial position, θ decreases leading to a decreasing torque. At the same time the elastic element will be further stretched leading to an increasing torque. The use of a radial force component (towards thumb) to prevent ulnar drift will further decrease the extension torque. In addition to the above effects, a compressive force will be created at the MP joint which may lead to further problems in this joint.

A computer program has been used to generate force values (gm) at the finger stirrup for a representative range of positions with an initial force of 40 gm at MP angle of 0°. "F extension" is based on the case with no radial force component. When a radial correction is applied, the extension force is decreased as indicated. The radial correction was achieved by mathematically tilting the pulley plane 45° out of the extension plane.

MP angle	F compr.	F extension	F extension with radial correction
30°	3.7 gm	39.8 gm	28.2 gm
40°	10.8	39.2	27.8
50°	17.4	37.6	26.6
60°	23.6	35.0	24.8
70°	29.2	31.5	22.3

Several problems are associated with the use of elastic bands in splints. Elastic bands are not dependably linear through their elastic ranges. Excessive stretch can cause plastic deformation, and elastic is subject to significant deterioration after exposure to the atmosphere, repeated stretching, and aging. It is also difficult to adjust elastic bands for low force ranges.

For these reasons a new hand splint was developed using stainless steel linear coil springs to provide variable forces to each of the fingers. The springs are anchored in a brace over the dorsum of the wrist via blocks which ride on threaded rods. These rods are rotated by thumb screws to set tension in the springs. Spring forces are directed via cords passed over pulleys suspended above the dorsal hand and attached to stirrups around the proximal phalanges. The distal end of the splint can be adjusted in length, flexion/extension angle, and radial/ulnar orientation. This splint is easily calibrated and set for precise loads (gm). It has been used on six different patients for periods up to 14 weeks. Three units are in current use for additional post-surgical patients as needed.

The advantages of this new splint include more precise quantification of MP torques and reproducibility of initial values. Patients will be able to perform functional hand movements while wearing the splint, and active exercises versus small resistance forces will be possible throughout the entire range of MP flexion. Data generated by this splint will be used in the future to improve treatment of patients with hand functional loss.

ASSESSMENT OF FOOTPAD DEPENDABILITY

J. Danoff, T. Waggoner, G. Hunt

Department of Rehabilitation Medicine
National Institutes of Health, Bethesda Maryland

Footpads with electronic switches for monitoring foot-surface contact patterns are used in many current clinical settings. Information is usually provided on contact of the heel, first metatarsal, fifth metatarsal, and first distal phalanx (great toe). These data can then be used to evaluate gait patterns for stance phases, forward velocity, and foot plant patterns.

Commercially manufactured switched footpads are available, but no guarantee is provided of their dependability for continuous clinical use. The following questions must be answered: Do all pads have the same sensitivity to loading? Is each pad uniform in sensitivity across its entire surface? Does pad sensitivity change with increasing use? In an attempt to answer these questions, testing procedures have been developed to assess switched footpad dependability.

The tested footpads consist of a foam insole pad sandwiched between two sets of brass shims. The foam contains regularly spaced holes in which are placed silicon rubber plugs impregnated with tiny brass spherules (100-150 μm diameter). The entire complex is then wrapped with duct tape. External pressure compresses the foam and silicon rubber plugs allowing electrical contact to be made between the upper and lower brass shims. Separate circuits are provided for each of the four foot regions.

Nine similar points were marked on 10 footpads, and each pad was then mounted in a rig under a Chatillon Pressure Gauge. Pad output was monitored by an electric light sensor. The Pressure Gauge was fitted with a 2.8 cm diameter copper dowel milled to a perfectly smooth flat surface for making contact with the pads. The rig was raised until switch closure occurred in the pad as indicated by the light. The reading on the Chatillon Gauge was then noted and recorded.

All locations on each pad were tested on two separate days. Pads were then compared over the two trials by correlated t-tests and linear correlations. Data for all pads were pooled, and these same two tests were then applied to compare each pad location over the two trials. Coefficients of variation (CV = std. dev./mean) were calculated for each pad's nine points to assess internal consistency. Five pads were further tested 10 times, and CV's were calculated for each of these pads over the 10 trials.

Internal consistency of the pads was found to be satisfactory with CV's ranging from 0.119 to 0.273. Five pads had non-significant linear correlations between two trials, but low correlations could be expected due to the truncated samples associated with these low CV values. Only one of the 10 pads resulted in a significant t statistic ($p < .02$) indicating a change in data values from trial 1 to trial 2. This pad also had a low correlation, and based on these statistics (t, corr.) it has been rejected as unsuitable for clinical use. When the five pad subsample was tested 10 times, CV's resulted in the range of 0.041 to 0.13 indicating very good consistency for these pads over multiple trials.

Assessment of the switched footpads in this study was done to determine their usefulness in clinical applications. Gait evaluation is often repeated for patients after rehabilitation procedures have taken place, and it is important that any changes observed not be due to changes in the pads. In addition a busy clinic may reuse a given pad many times in the course of a few months. Periodic retesting is therefore recommended to monitor pads for any possible deterioration. Based on the collected data, these pads can be assumed to be generally satisfactory for clinical applications. However an occassional pad may be found that produces inconsistent results, and this pad should be eliminated from use.

Quantitation of Fuji Prescale Film Pressures Using Digital Image Scanning

Douglas R. Pedersen, Thomas D. Brown, and Robert J. Singerman
Departments of Orthopaedic Surgery and Biomedical Engineering
University of Iowa, Iowa City, IA 52242

Since its introduction into orthopaedic biomechanics research several years ago, Fuji Prescale film has become a commonly used means for measuring contact areas and interfacial contact stress distributions in systems such as articular joints. Fuji film consists of two matched paper layers, one doped with chemical-filled microcapsules which rupture differentially with pressure increases, and the other containing a developing chemical. Upon reaction, these chemicals produce a reddish stain whose intensity (darkness) correlates with the magnitude of local pressure (Fig 1). Most commonly, inference of absolute pressure magnitudes has relied upon either gross visual comparisons with stains produced by known pressures, or upon the output of a pre-calibrated optical densitometer (3 mm diameter view field) supplied by the manufacturer. Since the film is potentially applicable to very small contact regions (e.g., between adult carpal bones or in the juvenile hip), a technique has been developed to assess staining intensity using a high-resolution digital scanner.

An EYECOM II scanner (Spatial Data, Inc.) controlled by a PDP 11/34 computer system was used to digitize Fuji-film images into 640x480 pixel arrays, each with 8-bit grey levels (darkest=0, white=255). The discrete pixel intensity data were encoded in binary form on floppy disk, and were re-read for later image analysis on a VAX 11/730 computer. Since white background predominates on most Fuji-film images, analysis was facilitated by first reversing the grey scale code (i.e., set white=0, darkest=255). Scanned fields are then printed on a Printronix dot-matrix printer (Fig 2) with superimposed Cartesian geometry axes. The operator specifies Cartesian window parameters to isolate regions of interest, for which the pixel intensities are then read into VAX memory. For Fuji stains corresponding to known pressures, histograms of the pixel intensity distributions (Fig 3) reveal a much broader spectrum of grey levels than is apparent to the naked eye. The range of intensities (e.g., 0 to 108 for dot #5) increases approximately 30% over the given pressure range. With increasing pressure, darker pixels become an ever-more-dominant component of the intensity spectrum. A quasi-uniform-pressure indentor was developed, and is used to prepare calibration-dot strips. Each dot's stain intensity is represented by plotting the mean intensity of the pixels, within the dot, whose intensity is greater than a given threshold (Fig 4). As the threshold is increased from zero to the maximum intensity for each dot, the mean value approaches the maximum. The relationship between pressure and stain intensity is nonlinear but is almost threshold-independent for low (threshold <20) intensities. Digital image scanning provides an effective means for greatly increasing the spatial resolution with which absolute pressure contours can be constructed from Fuji stains. But the increased intensity discrimination has not proven capable of appreciably extending the range of pressure sensitivity, since staining saturation occurs due to rupture of essentially all microcapsules.

Financial assistance was provided by NIH grants AM29979 and AM33964.

Fig.1

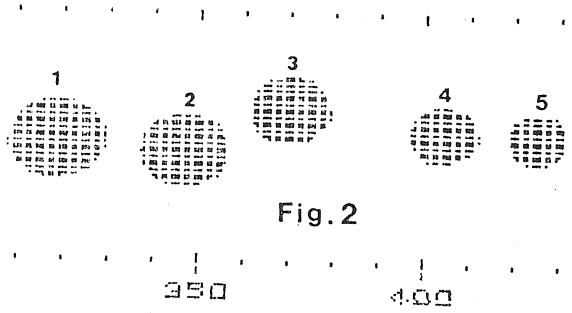

Fig.2

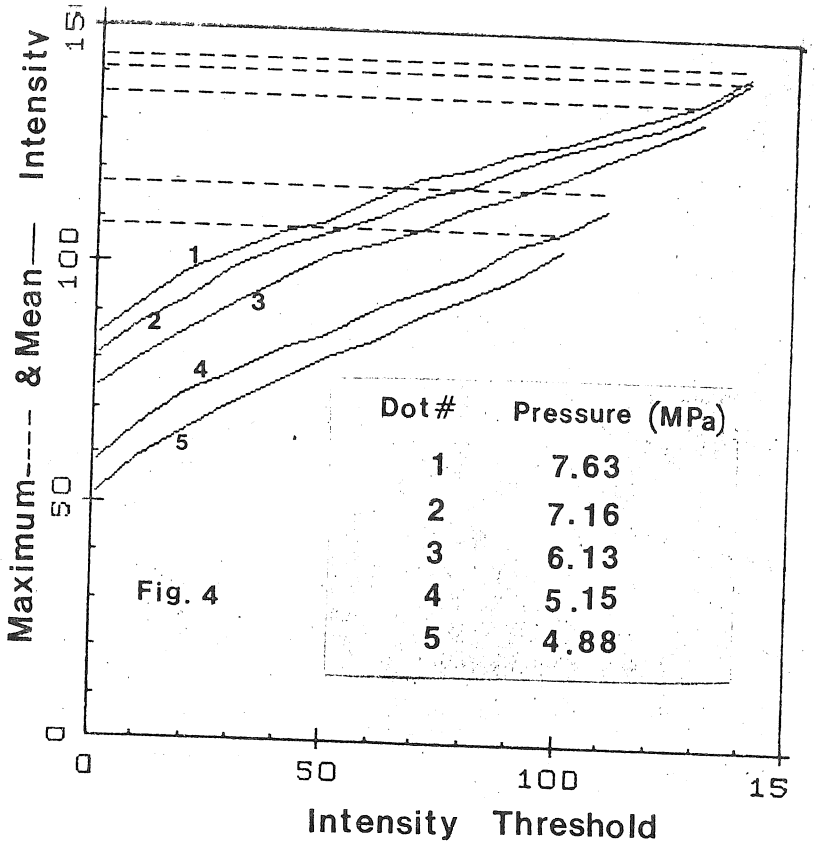

Dot#	Pressure (MPa)
1	7.63
2	7.16
3	6.13
4	5.15
5	4.88

Fig. 4

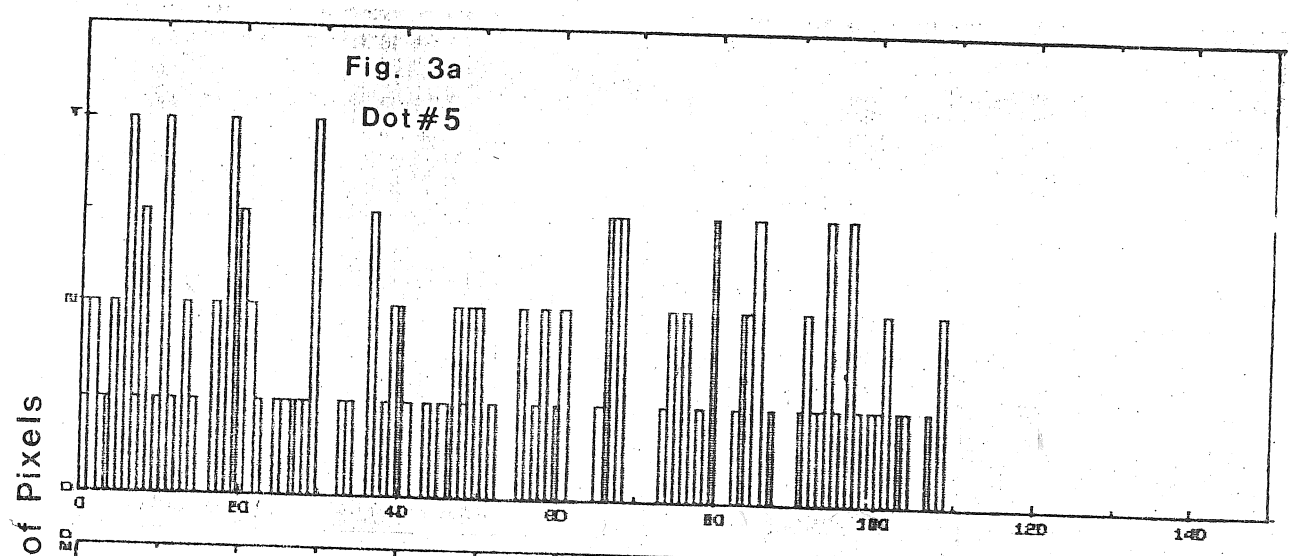

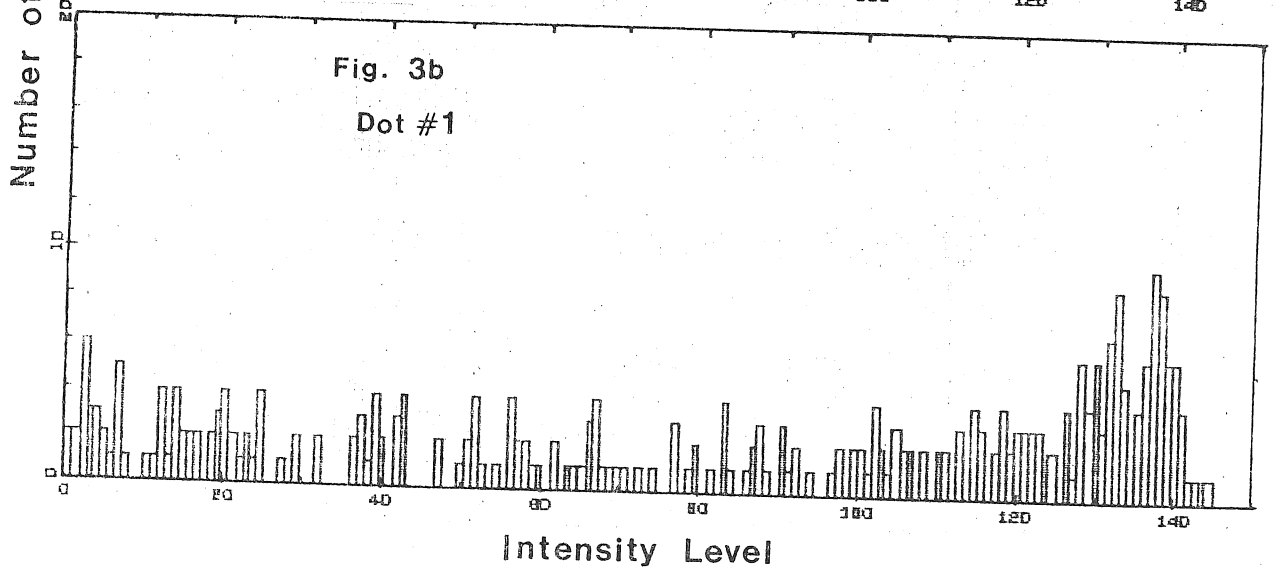

TEMPORAL GAIT ANALYSIS BY INTER-ANKLE DISTANCE MONITORING

M. S. Pinzur, P. Dimonte-Levine, R. Sherman, J. Trimble, and K. Hoog

Rehabilitative Research and Development Center of Hines Veteran's Administration Hospital

and the Department of Orthpaedics and Rehabilitation of Loyola University Medical Center

A new device is presented which is able to provide a temporal recording of gait events including a continuous qualitative monitoring. It can be used with motor point electromyography to perform walking electromyography, an electrogoniometer to record joint position, or other measuring devices to record events relative to phase of gait. The major advantages of this system as compared with available systems are (1) ease of use, (2) decreased patient encumbrance, (3) potential for portability, (4) greatly reduced expense and (5) the potential for digitalizing the signal for computer compatability. Preliminary data are comparable to available accepted norms.

The device is a simple ultrasonic transmitter and receiver system which, with associated electronics, provides a continuous recording of the distance between the "inter-ankle distance" (IAD). Two transmitters and two receiver transducers are snugly attached with Velcro straps just above the medial malleoli. One of the transducers is directed 60 degrees forward and the other 60 degrees rearward. This provides nearly equal signal reception over the entire range of the stride.

The uppermost point on the tracing represents the period of double support and the lowermost point represents mid-swing and initial contact. Initial contact (heel strike) occurs at the time of change in slope of the IAD upward tracing. Toe-off occurs at the downstroke change in slope. Once these events are identified, stance, swing and double support times are easily obtained. The signal which produces this recording can be digitized and calculations performed by a micro-processor.

Forty volunteers between the ages of 24 and 43 were used in the initial study. None of the subjects displayed any gait abnormalities by observational analysis. Each subject was asked to work at his/her self-selected velocity along a twenty-five foot flat linoleum walkway. Four such recordings were performed on each subject. Stance, swing and double support times were determined by the average values from the four recordings.

The average cadence was 102.04 steps per minute with forward velocity of 80.12 centimeters per second. By determining the absolute amount of time spent in each phase of gait, relative percentages of the gait cycle were calculated. Stance phase occupied an average of 61.49 per centimeters of the gait cycle, swing phase 38.51 percent and double support 13.04 percent.

Following initial calibration, specific motor point electromyography was performed during walking in 25 normal and 105 adult hemiplegic patients. Temporal muscle group activity was entirely consistant with previous reports on Inman and Perry.

The object of this study was to validate a new device and suggest its value in temporal recording of gait and specific gait events. Its value is in its (1) ease of use, (2) decreased patient encumbrance, (3) portability, (4) reduced expense, (5) computer compatability and (6) accuracy.

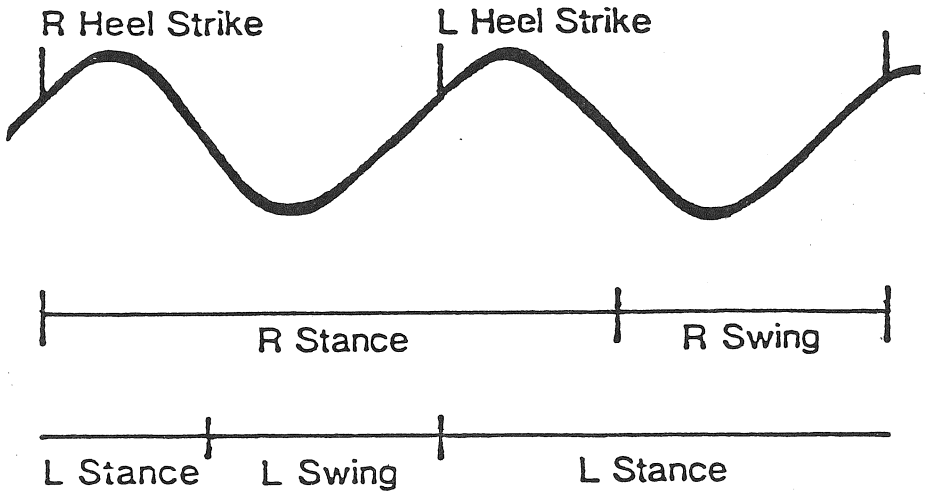

DEPARTMENT OF ORTHOPEDICS
AND REHABILITATION
2160 SOUTH FIRST AVENUE
MAYWOOD, ILLINOIS 60153

ABSTRACT

An application of photoelastic techniques to the measurement of tibial stiffness

J. Richards B.Sc.(Eng.), Ph.D.,
M.I.Mech.E., M.I.E.E.

The research refers to the design and development of a mechanical method for the study of stiffness in fracture healing in the tibia. The device incorporates specially designed links of photoelastic material which respond to axial, lateral and torsional displacements. The design incorporates two major stiffness planes and the frame is capable of adequate support of the fracture in differing stages of healing.

The attachment of the frame to the limb is via the cortical pins for an external fixator, which is subsequently removed, and the variation of stiffness of the frame is shown in relation to pin spacing. The frame has a degree of flexure which is not present in single fixator applications and the calibration of the device is given with respect to axial, lateral and torsional efforts.

A comparison between the photoelastic response and the direct strain measurement from gauges fixed to the links shows that the former technique has acceptable sensitivity and response. The calibration refers to tests on artificial tibia but successful application and measurements have also been conducted on cadaver limbs. The research is complementary to measurements of frequency transmission during formation of the callus.

Department of Mechanical Engineering and Engineering Production,
University of Wales Institute of Science and Technology, Cardiff,
U.K.

Temporal and Kinematic Characteristics of Skilled Tracking Movements

G.L. Scheirman
P.J. Cheetham

Department of Biomechanics and Computer Services
United States Olympic Committee
1750 East Boulder Street
Colorado Springs, Colorado 80909

Success in the performance of an activity requires combining correct movement patterns and correct movement sequencing. Present theory proposes that a motor program for a specific motion contains phasing information, but this pattern as a unit may be accelerated or decelerated to meet specific temporal movement constraints. Running Game Target Shooting is a sport where the participant must track and shoot a target which moves in one of two directions at one of two velocities. Although there are four conditions, the shooter may use similar motor programs. The purpose of the present study was to measure the kinematic and temporal tracking modifications elicited by highly skilled Running Game Target Shooters and evaluate the possibility of motor program phasing.

Three national class Running Game Target Shooters were tested under competitive conditions. Each subject performed fifteen shots at a moving target in each of four standard situations, two horizontal movement directions (left to right and right to left) and two speeds (5.0 and 2.5 m/s). An infrared light emitting diode was placed underneath the rifle muzzle and the horizontal and vertical positions were determined with a SELSPOT Motion Analysis System. Data were sampled at 25 Hz and stored on a microcomputer. Within the tracking time interval, aggregate component displacements and mean velocities were computed. The data indicated there were no temporal or kinematic tracking differences between directions. However, between speed conditions, all subjects tracked the slower target for a proportionately longer duration, a further distance and half the velocity. These results suggest that the subjects learned to specify their movement patterns and duplicate them under directional changes, but the phasing of the motor programs may not be identical for both target speeds.

STRUCTURAL MODELING AND DESIGN OF KNEE ORTHOSES

D. S. Schnur and J. L. Lewis
Harrington Arthritis Research Center, Phoenix, AZ
Northwestern University, Chicago, IL

INTRODUCTION: Knee orthoses are often prescribed for patients with chronic knee ligament laxity. The purpose of the orthosis is to prevent various types of instability during vigorous activity. How a knee orthosis works to reduce these instabilities is unclear; current designs are chosen empirically. This results in no objective basis of comparing different designs, no general guidelines for improving designs, and possibly erroneous concepts taught. For example, it is taught in orthotics training that the method of stabilizing the knee is the three point fixation system; a force applied to the knee is balanced by opposing forces at the thigh and calf. When ligamentous deficit is present, however, it would appear that the limb behaves as two separate segments. Three point support will leave a force uncoupled on one limb segment, causing the segment to rotate about the point of application of the force.

Although some research has been done to improve the joint of the orthosis, there has been no quantitative investigation of the knee orthosis structure as a whole. The goal of this study is to develop structural models that can be used to examine knee orthosis design features. The model results will suggest which design factors to compare with experimental or clinical studies.

METHODS: Three separate models were developed: (1) a 2-D plane strain finite element model, (2) a complete 3-D finite element model, and (3) a simplified rigid body model. The 2-D finite element model was used to evaluate the effects of changing the design parameters on the relative displacement between the femur and the tibia at the knee. The 3-D finite element model, as a more realistic representation of the physical system, was used to verify the 2-D behavior. The rigid body model aided in understanding the finite element model behavior and provided analytical expressions relating the displacement at the joint and the forces at the suspension points to the design variables.

The 2-D finite element model is shown in Fig. 1. The soft tissue and bone of the leg were modeled with 188 2-D quadrilateral elements. The knee was represented by a beam, hinged at both ends. Vertical beam elements were used to simulate the sidebars of the orthosis, and horizontal beams were connected to the sidebars to simulate the function of the calf and thigh cuffs. A simple load case of valgus force at the knee was applied to the model. The design cases included varying fixation, tissue stiffness, sidebar stiffness, attachment of the crossbeams, and cuff size.

The 3-D finite element model is shown in Fig. 2. The model consisted of four element types: (1) 934 3-D bricks for the soft tissue and bone of the leg, and the pads, cuffs, and joints of the orthosis, (2) 33 2-D membrane elements for the straps, (3) 15 3-D beam elements for the sidebars, and (4) a truss for the knee. Six loading situations were considered: varus and valgus

stress, anterior and posterior drawer, internal rotation, and pivot shift. The material properties for the soft tissue and straps were obtained experimentally.

The rigid body model, illustrated in Fig. 18, represents only the portion of the limb below the knee. The tibia was modeled as a vertical bar. Linear springs were attached to the bar, representing the tissue stiffness at the suspension points. A rotational spring attached to the distal suspension point simulated the resistance of the calf cuff to rotation. From the analytical equations of the system, curves were generated to illustrate how displacement and force were affected by suspension stiffness, rotational stiffness of the cuff, and location of the suspension points.

RESULTS: The 3-D finite element model behaved as expected and was thus assumed to be reasonably accurate. The 2-D finite element model agreed qualitatively with the 3-D model for similar load cases. The 2-D model predicted that (1) four point fixation is superior to three point, (2) the ratio of the tissue to sidebar stiffness is an important influence on the direction of the proximal tibial displacement for varus or valgus loading, and (3) the sidebars and the orthotic cuffs do not have to be extremely rigid to provide stability in bending in the medial-lateral plane, but torsional stability may be reduced. The rigid body model demonstrated that (1) the proximal suspension point should be located close to the knee and the distal suspension point far from the proximal for an orthosis with rigid sidebars, and (2) the stiffness at the suspension points should be high for an orthosis with rigid sidebars.

In the future, experimental checks must be made on the model results, and a simple, 3-D rigid body model needs to be constructed to study torsional behavior.

2-D FINITE ELEMENT MODEL

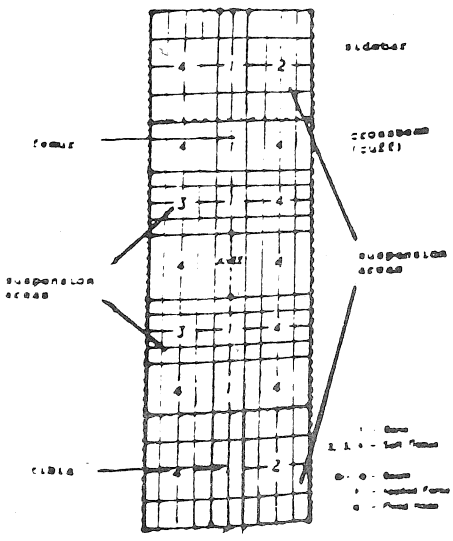

Fig. 1

3-D FINITE ELEMENT MODEL

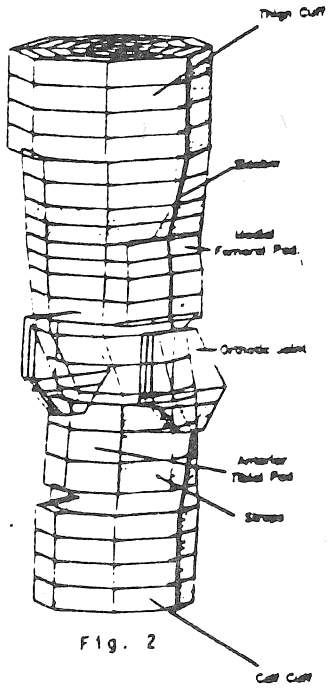

Fig. 2

RIGID BODY MODEL

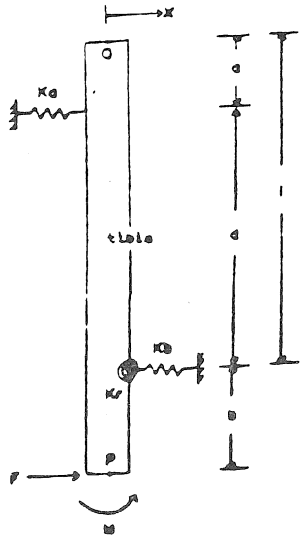

Fig. 3

TWO-LAYER MODEL FOR THE OXYGENATION OF BLOOD IN PULMONARY CAPILLARIES

BY
Maithili Sharan, M.P. Singh and A. Aminataei
Centre for Atmospheric and Fluids Sciences
Indian Institute of Technology, Hauz Khas,
New Delhi-110016, India.

The process of gas exchange leading to oxygenation of blood in pulmonary capillaries is very complex. Blood flow in the pulmonary capillaries is accompanied by several anamolous effects due to its two-phase nature. Capillaries are the smallest vessels in the human circulatory system with the diameters ranging from 2 to 10 microns. Due to comparable sizes of the capillaries and red blood cells, the erythrocytes can travel through capillaries in a single file. Further, they have to deform considerably from their biconcave shape in order to enter the capillaries whose diameters are less than their diameters.

When the blood flows through the narrow vessels, a cell depleted or cell-free-plasma layer has been observed to exist near the wall. The particles near the tube wall tend to migrate towards the axis, the effect being more pronouned in the case of flexible particles.

Recently [(Singh et al. (1980) and Sharan and Singh (1984)] a mathematical model for the oxygenation of blood in the pulmonary capillaries has been developed by assuming the blood as a homogeneous solution. In order to analyze the effect of the existence of a cell-free-plasma layer near the wall on the oxygenation of blood in pulmonary capillaries, a two-layer model has been proposed. The governing equations in the core described the free molecular diffusion, convection and the facilitated diffusion due to the presence of haemoglobin. The corresponding equations in the cell-free layer are based on the free-molecular diffusion and convective effect of the blood.

The governing equations of the model together with the physiologically relevant boundary and interface conditions have been solved numerically. The core is moving with the uniform speed while the flow in the plasma (free from cells) layer will be fully developed. A fixed-point iteration technique is used to deal with nonlinearities arising in the system due to the presence of haemoglobin.

It is shown that, in the immediate neighbourhood of the entry, the amount of dissolved oxygen decreases and the facilitated diffusion is more dominant over the molecular diffusion. As the blood moves away from the entry, the oxygen is slowly replenished from the alveolar air. The concentration of carbon dioxide (oxyhaemoglobin) is shown to decrease (increase) from arterial to venous end of the capillary.

It is found that the blood is completely oxygenated within one-fifth part of its transit and oxygen takes longest and carbon dioxide is the fastest to attain equilibration. Further, it is shown that the core haematocrit and the thickness of the cell depleted layer affect the oxygenation process significantly.

The effects of various physiological parameters on equilibration length have been examined. Finally, the bearings of these results on various physiological conditions such as muscular exercise, meditation, high altitude, fever, anaemia and polycythaemia, etc. have been discussed. This study can provide explanation for some of the borderline respiratory disorders for which apparently no physical reasoning has been put forward so far.

1. Sharan, Maithili and M.P. Singh (1984)
Int. J. Biomed. Computing (press).

2. Singh, M.P., K. Khetarpal and Maithili Sharan (1980)
J. Math. Biol. 9: 305-330.

EFFECTS OF ARM ACTION ON THE HEIGHT ATTAINED IN A MAXIMAL VERTICAL JUMP

J.H. Stegall and L.D. Abraham, Department of Physical & Health Education
The University of Texas at Austin
Austin, Texas 78712

One of the variables associated with vertical jumping which can affect achieved height is the motion of the arms during the jump. Luhtanen and Komi (1978) investigated a straight-arm swing which continued upward during take-off and reported an increase in attained height of as much as ten percent. This increase is probably related to a loading or "weighting" effect in which the inertial reaction to the arm motion improves the power output of the leg muscles. Since athletes in various sports are coached to use different arm patterns during jumping, this study investigated the effects of three common arm patterns on maximal vertical jumps.

Eight volunteer subjects (women, collegiate varsity athletes) performed four sets of four maximal vertical jumps from a standing position. Each set of four jumps was performed using a different arm action: no arm action (NA), full upward arm swing (UA), upward arm swing to a blocked position (BL) with the elbow and shoulder at right angles, and upward arm swing to the blocked position followed by immediate reversal to a downward arm motion at takeoff (DN). The subjects provided informed consent and were allowed to practice each technique. Jump instructions required the subjects to attempt to touch a string target with their heads. Each jump was filmed with a 16-mm cine camera (Locam) at 50 frames/sec from the side. Film analysis included digitizing 21 body segment endpoints for successive frames from the beginning of the jump through attainment of peak height, using a Numonics 1224 graphics calculator and a PDP11/03 laboratory computer. From this data the location of the body center of mass (COM) was calculated (based on tables from Plagenhoef **et al.**, 1983) for each frame. The best (highest) jump by each subject in each condition was selected for analysis of the peak height of the COM and the vertical velocity of the COM during the jump. The latter variable was further analyzed for maximal value and takeoff value. Each analysis involved a 4 x 8 ANOVA, and a Newman-Keuls post-hoc test.

Analysis of the peak height of the COM revealed that the UA condition was significantly greater than the other three ($p < .01$) and the NA condition was significantly less than the other three ($p < .01$). The BL and the DN conditions were not different from each other. While the vertical velocity of the COM at takeoff showed the same relationships (as would be predicted), maximal values for vertical velocity were not different for the NA, BL, and DN conditions. The UA condition, again, was greater than the other three ($p < .01$). This difference reflected a different time of occurrence for maximal vertical velocity relative to takeoff being closest to takeoff in the UA condition and much earlier in the NA condition.

These results support the data that arm swing can contribute to vertical jump height by increasing the maximal vertical velocity generated. In addition, the type of arm action appears to influence achieved height by determining how close to takeoff (the theoretically optimal time) maximal vertical velocity is attained.

Luhtanen, P. & Komi, P.V. Segmental contribution to forces in the vertical jump. **Eur. J. of Appl. Physiol.**, 1978, 38, 181-8.

Plagenhoef, S., Evans, F.G., & Abdelnour, T. Anatomical data for analyzing human motion. **Res. Quart. for Exerc. & Sport**, 1983, 54, 169-178.

SPECTRAL ANALYSIS OF TREMOR PATTERNS ASSOCIATED WITH STUTTERING SPEECH.
E. K. Stauffer, R. S. Pozos and R. F. Pierce*. Departments of Physiology and Communicative Disorders*, University of Minnesota, Duluth, MN 55812.

One feature of stuttering speech that has not received much attention is the stuttering tremor. These periodicities often appear in the later developmental sequences of stuttering and involve the lips, jaw, tongue, and extrinsic muscles of the larynx, but are also known to occur in the eyelids and legs during the attempt to speak. Tremor can also be recorded just prior to the utterance of certain words. A wide variety of stuttering behaviors and symptoms have been noted, however, very little quantitative analysis of the tremor has been reported. In particular, quantification of the preformance of the neuromuscular apparatus is lacking for the various kinds of stuttering behaviors. We have begun a series of studies designed to quantitate the electromyographic activity and movement patterns that are associated with the stuttering tremor. In addition, the effects of delayed auditory feedback (DAF) has been investigated in stutterers to assess its effectiveness in reducing or altering the tremor. Since DAF is reported to induce a stutter-like dysfluency in normal subjects, this method was used to investigate if their responses were similar to that seen in clients who had an overt tremor during stuttering.

Surface electromyograms (EMGs) were recorded from a variety of facial muscles (masseter, obicularis oris, digastric and frontalis). Jaw movement was monitored using an accelerometer attached to the underside of the chin. Electrical and mechanical activity was recorded on magnetic tape for later analysis on a MINC-11 computer. The spectal content of these signals was determined using standard techniques. Records were obtained during (1) conversational speech, (2) reading of a standard phonetically-balanced paragraph, and (3) repetition of a monosyllabic, diadochokinetic sequence. These tasks were done before, during and after DAF. In normals, the tasks were identical except, in addition, they were asked to repeat standard tongue twisters as rapidly as they could (e.g., "Peter Piper picked a peck of pickled peppers ....").

In the stuttering subjects, tremor occurred during two different situations: (1) when they involuntarily assumed a speaking posture wherein the mouth was partially open and the jaw fixed in a nearly isometric position; and (2) when they involuntarily displayed rapid repetitions of the same syllable during the course of speaking. In the first case, the mechanical record of the tremor was characterized by an oscillation whose amplitude monotonically increased until its sudden disappearance. The latter was coincidental with the explosive utterance of a word. The spectral power of this oscillation was contained in a very narrow frequency band at 9 Hz. The EMG pattern in certain muscles was characterized by a bursting of activity, the interburst frequency of which was significantly coherent with the acceleration signal. This bursting pattern occurred simultaneously in a number of facial muscles. In the second case, the acceleration record was distinctly different from the first. The duration of the oscillation was shorter, it was relatively symmetric about the baseline, and its amplitude was significantly larger. However, the overt movements of the jaw which were associated with these larger amplitudes still occurred at 9 Hz. The EMG interburst frequency was coherent with the acceleration record. These two characteristic patterns of of tremor were not changed by DAF, but the number of tremoring episodes per unit time was reduced. Tremors could only be induced in the speech of normals while attempting to say the tongue twisters with DAF. In these situations, oscillations could be identified in the mechanical records. In contrast to the tremor of the stutterers, the acceleration records had complex waveforms. They had low (4-5 Hz) and high frequency (9 Hz) components with most of the

power in the low frequency band. In addition, the EMG patterns lacked the distinct bursts seen in the stutterers. However, spectral analysis did show significant coherence at the major frequencies of the motion record.

Our results indicate: (1) there are at least two kinds of tremor associated with stuttering that can be differentiated quantitatively and qualitatively; (2) DAF has no effect on the quantitative features of the tremor of stuttering; instead, (3) DAF decreases the incidence of stuttering; and (4) DAF in normals does not produce stuttering except when used in conjunction with the subjects' attempt to articulate tongue twisters. Although this latter oscillation subjectively resembles the tremors seen during stuttering, they are quantitatively different. These preliminary observations indicate that the control of the neuromuscular apparatus in stutterers is different from that of normals.

(Supported by the Edward Eddy Foundation)

Accurate Determination of Motion from Plane Films

John J.Iriano, M.A.

University of Illinois and National College, Chicago

The value of being able to determine magnitude and direction of vertebral motion in a functional spinal unit (FSU) in vivo has been acknowledged by many.Recent progress in biplanar orthogonal analysis as well stereoradiographic measures is encouraging but remains encumbered by the need for specialized equipment and increased patient exposure.Plane film analysis of voluntary motion of the spine has been reported by several authors despite uncertainty over the accuracy and reliability of these measures.Error sources include technical considerations in radiographic technique, osseous landmark uncertainty, out-of-plane coupled motion components, and magnification of measurement uncertainty by error sensitive computations.

This study was undertaken in effort to account for these concerns in plane films.Primary error sources were systematically isolated at each stage of data processing. Methods were then devised to minimize each component before proceeding to the next step.Two models of FSU were utilized to sequentially test the reliability of the methods chosen. A radiographic phantom (I) composed of a human lumbar spine and pelvis cast in acrylic was centrally mounted on a platform permitting rotation of the coronal plane about a fixed axis (θz) and vertical axis (θy) positioned through the centroid of the phantom.The second model (II) consisted of a commercially prepared set of two lumbar vertebrae that permitted the placement of rectangular or fixed angle spacers between the vertebral bodies to simulate neutral or flexed intersegmental relationships.This model was also mounted on a platform with two additional capabilities. The vertical column supporting the FSU model was attached to a geared carriage assembly that permitted translation, hinged to permit rotation of the sagittal plane about the X axis (θx) as well as coronal plane rotation about the Z axis.Model I was positioned for a lateral view radiograph with the central ray passing through the L4/5 interspace at a tube film distance of 182.88 cm. and a mid-sagittal subject film distance of 16.34 cm..Amplitude of rotations about both the Y and Z axes ($0 < \theta y < 30; 0 < \theta z < 10$) were systematically varied.Positioned similarly with respect to the xray beam, model II was radiographed with rectangular spacer holding the endplates parallel. A study of radiographic offcentering was conducted by systematic translation of the carriage assembly in 2.54cm. increments (X axis); vertically (Y axis) by movement of the xray tube;and combined equidistant translations along both axes. This series was repeated following the replacement of the "disc" spacer by an angled surface of 8 degrees.Finally, model II with parallel endplates was repositioned and systematic rotations about three coordinate axes were introduced and radiographed ($0 < \theta x < 10; 0 < \theta y < 10; 0 < \theta z < 15$).

Using a combined contour recognition criteria and reference marker system,3 points were identified on the neutral position film for each vertebra.For each change of position, the vertebral shadow was superimposed on its neutral counterpart and reference markers were transfered only after approximating centroid alignment by minimizing intershadow boundary differences resulting from out-of-plane motions.Postion vector data was then entered into a microcomputer (mean of 5 iterated samplings for each marker) by means of a backlighted digitizing pad. Verification of accuracy (>97%) for marker transfer was accomplished by comparison of triangular congruency between positions. Using vector algebra, computation of the true principal motion for simulated flexion was attempted and expressed as total and relative intersegmental angular motion (θz) and translation (X,Y).Sample data is shown in Table I.

Computed motion was compared to induced values by means of linear regression for biaxial displacements($r^2=.978$; $r^2=.958$;S.E.=1.08).ANOVA was used to evaluate overlap in measured distributions ($F=397$;df=4/45). Individual comparisons between consecutative rotational values were also significant for values greater than 2.5 deg. ($p<.05$). Triaxial displacement regression (fig.1) was similarly computed ($r^2=.999$;$r^2=.979$;S.E.=.048). The results of this test suggest that combined contour recognition and marker system criteria permit accurate measure of principal motion despite out-of plane coupled components. By avoiding major sources of uncertainty and error prone computations, results compare favorably with accuracy in biplanar systems.

TABLE 1

	Total Planar Motion					Intersegmental Motion				
	L5	L4	L3	L2	L1	L5	L4	L3	L2	L1
					0^o Axial (Θ_y) Rotation					
X	.05	3.98	7.65	11.3	15.8	3.9	3.6	3.6	4.5	-*
Y	.03	2.03	3.53	4.7	5.3	2.0	1.5	1.1	.6	-
Θ_Z	8.81	7.59	6.92	8.56	7.63	0.0	1.2	.68	1.64	-
					5^o Axial (Θ_y) Rotation					
X	.10	3.35	7.03	11.13	14.18	3.2	3.68	4.1	3.05	-
Y	.25	1.25	2.65	3.92	4.33	1.0	1.40	1.27	.42	-
Θ_Z	8.11	7.45	7.81	5.73	6.9	0	.67	.36	2.08	-

Processed data for planar motion (Θ_Z=8^o) induced in a Lumbar phantom 0 and 5 degrees axially (Θ_y) rotated. Translations (X,Y) in mm.+ rotation (Θ) in degrees.

*No comparison reference available above L1.

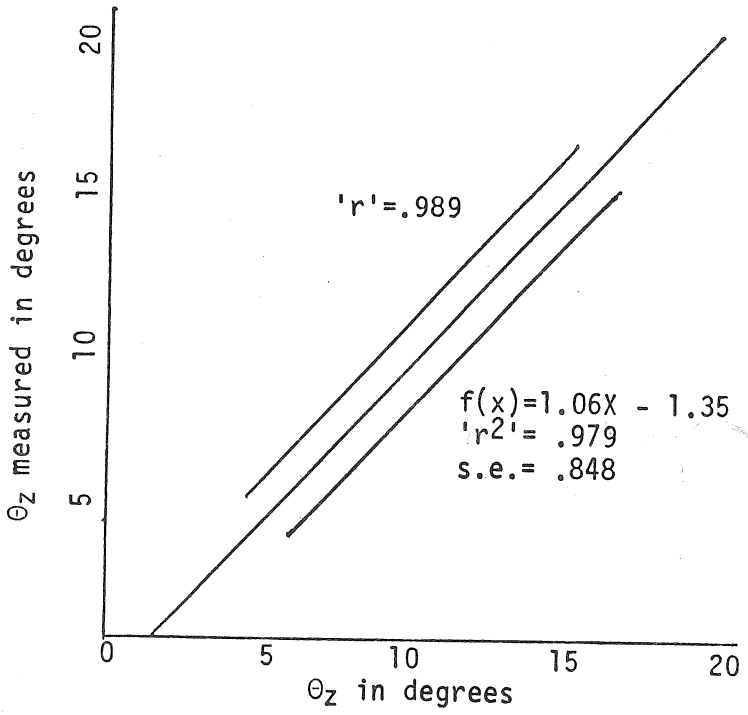

Figure 1

Induced motion (Θ_X, Θ_y, Θ_Z) vs. measured Θ_Z.

SPIN LATTICE RELAXATION TIME OF HUMAN BLOOD: AN NMR STUDY

B. Turan
Faculty of Medicine
University of Ankara
Ankara, Turkey

A. Yilmaz
Department of Physics
University of Dicle
Dicle, Turkey

Harcharan Singh Ranu
Department of Biomedical Engineering
Louisiana Tech University
Ruston, Louisiana 71272

Many investigators have tried to explain the T(1) spin-relaxation time of blood during the past decade. In our study, normal blood samples diluted by its own plasma have been measured by 60 Mhz FT-NMR spectrometer at 30 degrees centigrade. An inversion recovery method was used and selected in 0.4 to 1.8 second intervals. The relaxation mechanism of both the plasma and the diluted blood was interpreted in terms of the parametric iron bounded to the plasma transferrin. For the parametric solutions, 1/T(1) can be expressed:

$$1/T(1) = 16\,(^{99}N^{bb}N)^2\,S\,(S+1)\,N/(15\,n^2\,kt)$$

In case of the diluted blood, by taking N(b) = N(p) [1-HCT] and N(b) - N(p) [1+kHCT], it has been calculated that there is a correlation between the theoretical and experimental values. The relation between the spin lattice relaxation rates and the HCT blood dilution is a linear one. Also, the relative viscosity depends on the diluted blood on HCT.

Analysis of Fundamental Human Movement Patterns by Using In-Depth Antagonistic Muscle Models: Examples for Knee and Elbow Movements

by Jack M. Winters and Lawrence Stark
Dept. of Engineering Science, Bioengineering Program
University of California, Berkeley

Since the early classical work of Hill (1) on isolated muscle and Wilkie (2) on human joint movement, muscle models have traditionally been employed to help test our understanding of fundamental muscle behavior. The basic "classical" elements in the resulting lumped-parameter model structure are: an "active state" element representing electro-chemico-mechanical transduction dynamics; a lightly damped, nonlinear elastic element that is in series with a nonlinear contractile element that accounts for the "force-velocity" property of muscle; a passive nonlinear parallel elasticity and an active "moment-angle" relationship.

More recent, detailed studies of a variety of mammalian skeletal muscles have led to a stronger quantitative understanding of gross muscle material properties. Consequently, by combining muscle material information (such as fiber type composition) with muscle/joint structural data, it is now theoretically possible to estimate the contribution of any given muscle to movement about any joint degree-of-freedom. Conversely, it is possible to start with a global spatio-temporal movement pattern and then estimate the biomechanical contribution of each muscle to the movement. Combined with electromyographic (EMG) data, such efforts allow for a stronger insight into dynamical movement and for better interpretation of EMG information.

In practice, however, there have been surprisingly few efforts in this direction, with research tending toward the two extremes: fundamental muscle "reductionist" work (primarily by physiologists) and limb "macro-modeling" efforts (by bioengineers and biomathematicians). In the former approach, little insight is gained into actual overall human movement, while in the latter case, in which muscle properties are either linearized or ignored as insignificant relative to inertial dynamics, the beauty and benefits of nonlinear muscle filtering properties are missed.

Methods: The present work represents a much-needed compromise between these different approaches, putting forward the most reduced model that can adequately represent basic nonlinear muscle phenomena. An eighth-order, nonlinear model structure is put forward for any single degree of freedom of joint movement. This model consists of two lumped antagonistic muscles, each with: a second order fit for the "active state" response, the output of which is the input to the contractile element; a contractile element which utilizes "Hill's equation" when the contractile element is shortening and an inverted, modified Hill's relation for lengthening muscle; a nonlinear exponential fit for the series elastic relation and the parallel elastic element (based on Fung (3)); and a curve-fitted moment-angle relation (based on the wealth of static curves found in the literature). The two antagonistic muscles then each pull on a passive plant (joint) that is modeled as a simple angular second-order inertia-dashpot-spring system, with the spring element having an exponential-like nonlinear aspect typical for biological soft tissue elasticity (Figure 1a).

The inputs to the model are the neuro-controller signals for the two lumped antagonistic muscles. The outputs are the angular position of the joint (and its derivatives) and the torque that would be measured externally. Different tasks can be accomplished by putting in different input sequences.

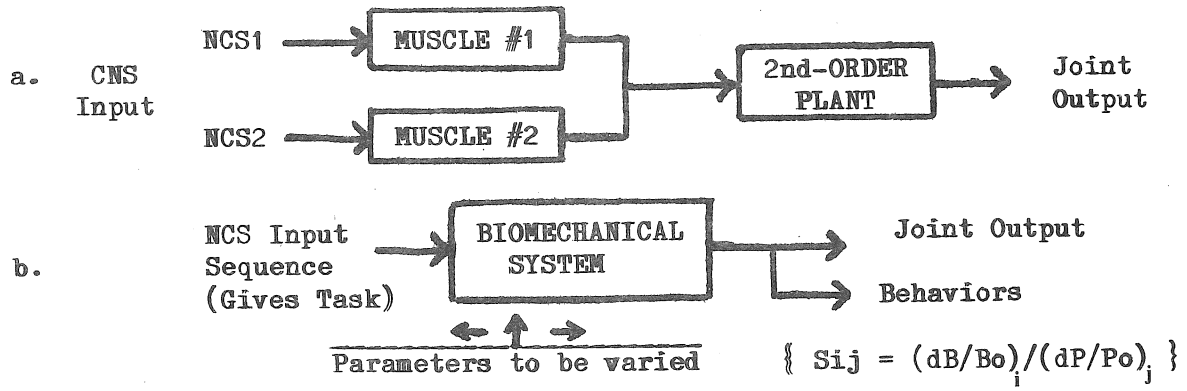

Figure 1: a. Block Diagram of Muscle Model
b. Sensitivity Analysis Schematic

Results: The present work offers two primary contributions. First, model parameter values were obtained for the following human movement systems: elbow, knee, and wrist flexion-extension, head, eye, and wrist rotation. These values were obtained by a series of steps. Initially, default parameter estimations were approximated by using design algorithms that combined material and structural information on the relevant muscles together to form lumped values for the antagonistic muscles. These inital estimates, which were often surprisingly adequate, were modified by three other types of information: first, on any basic experimental data that existed, second, by sensitivity analysis methods, and third, by task-specific biomechanical data in the literature.

Sensitivity analysis methods (Figure 1b), which basically consist of measuring the sensitivity of important output "behaviors" (such as peak velocity) to variation in each internal model parameter, provide a useful tool for in-depth understanding of the underlying causes of the observed behavior. Consequently, such methods have been used extensively to gain insight into the role played by both biomechanical model parameters and neuro-control input parameter variables in effecting relative model performance (4).

The second level of results are the basic findings for important biomechancial tasks such as isometric, isotonic and isokinetic movements, fast-slow movement interaction, movements with complex, time-varying external loads, oscillating movements, or movements with different co-contraction levels. Since elbow and knee flexion/extension have by far the largest amount of experimental data, and are also well modelled, most of the detailed work has been done with these two neuromuscular systems. Besides basic simulations for each type of movement, sensitivity analysis methods are employed for these various tasks.

Conclusions: An antagonistic muscle model structure has been put forward and model parameter values have been obtained for a wide variety of joint movements. These values are of use in simulating many basic human movement patterns. Furthermore, by combining task-specific sensitivity analysis results with experimental data for certain tasks, while having immediate access to all state variables, internal parameter values, and force and energy propogation, a number of insights have been obtained both into muscle/joint biomechanics and into neuromuscular control strategies. Such modeling efforts are needed to help understand the subtle role of muscles in facilitating human movement.

[1] Hill, A.V., Proc. Roy. Soc (London), Ser. B, 126:136-195, 1938.
[2] Wilkie, D.R., J. Physiol. (London), 110:249-280, 1950.
[3] Fung, Y.C., Am. J. Physiol., 213:1532-1544, 1967.
[4] Winters, J.M. and Stark, L., 20th Ann. Man. Contr., NASA AMES, June, 1984.

EFFECT OF HYPOKINESIA ON MAN'S DESIRABILITY IN PERFORMING PHYSICAL ACTIVITIES

Yan G. Zorbas and Ivan O. Matveyev, Istituto di Medicina dello Sport, C.O.N.I., Roma, Italy

The problem of functional state of various organs and systems under the influence of prolonged restriction of motor activity (MA) has acquired general physiological, clinical and applied significance in the last few years. This is related to the fact that a number of special investigations demonstrated the adverse effect of hypokinesia (HK) on several physiological processes in the organism. At the same time, there are not data available about the functional state of man's desirability that regulates the level of performance of physical activity. Against this background, the objective of this experiment was to examine the effect of restricted MA on man's desirability in performing physical exercise on four essentially healthy men, 19-21 years of age. All of the men were subjected to 120 days of HK. Muscular activity was limited by the dimension of a 50-m^2 pressure chamber while their movements were not restricted and the conditions were about the same for all of the men. The workload consisted primarily of operator activity which took up to six hours per day. The muscular activity of the men in the background period (BGP), during their stay in the pressure chamber, hypokinetic period, and in the readaptation period (RP) was determined using pedometers while a daily record of mean number of steps per day was kept and the mean length of the steps was evaluated. Systemic analysis of neurological status which included a specially thorough examination of the neuromuscular system, and, in particular reflexes, was carried out. There was a drastic (3-4 fold) reduction in MA: by a mean of 12,000 steps on the first day constituting 4000 to 5000 steps on the second day with slowly progressing decrease thereafter followed by stabilization of 2000 to 4000 steps per day. The desirability of all men in performing physical exercise (PE) also diminished and they did not want to become more actively involved in it. At some stages of the study, the level of MA increased, and this was primarily related to alterations in working conditions. The number of steps rose with increase in workload, but it did not exceed 5000 per day. Maximum increase in MA was observed on the days that equipment was assembled and overhauled. All of the men, during the morning hours, performed sporadically different forms of athletic exercises at their own initiative, but it was of very limited nature. The length of the steps was also diminished (by a mean of 15% while the men were in the chamber). The obtained results revealed that there was a significant reduction of desire of man to become engaged in physical exercises under the influence of artificially restricted muscular activity. The level of impaired desirability of man to perform any kind of physical activity was markedly related to duration spent under limited motor activity environmental conditions.

THE KINEMATICS AND KINETICS OF SWINGING TWO TYPES OF RAILROAD HAMMERS

Marlene Adrian, Gerald Smith

University of Illinois, Urbana-Champaign

The purpose was to develop a profile of hammer swinging for a skilled male railroad company employee. This male had never experienced injuries to the lumbar or thoracic region of the torso and was selected by his company as a model for other employees. A Lo Cam camera operating at 100 frames per second was used to obtain sagittal views of hammer swinging under two conditions: a spike mallet hammer head and a sledge hammer head. A series of films were obtained as the subject simulated on-the-job performances of striking spikes to secure the railroad tracks to the ground. The results were obtained by means of a digitizing tablet interfaced with a computer, use of smoothing routines, and algorithms of motion.

The legs and feet were stationary throughout the entire action, whereas the trunk was relatively immobile prior to the downswing. Changes in the angle at the hip were a function of flexion of the trunk throughout the downswing. During the downswing all movements of the trunk and arms were planar (either flexion or extension). The movement of the trunk was greater during the sledge condition than during the spike condition. See Fig. 1. Although both performances showed similar speeds of trunk flexion during the majority of the downswing the trunk stopped its movement prior to impact with the spike condition, whereas the trunk decreased its displacement, though not completely, with the sledge condition.

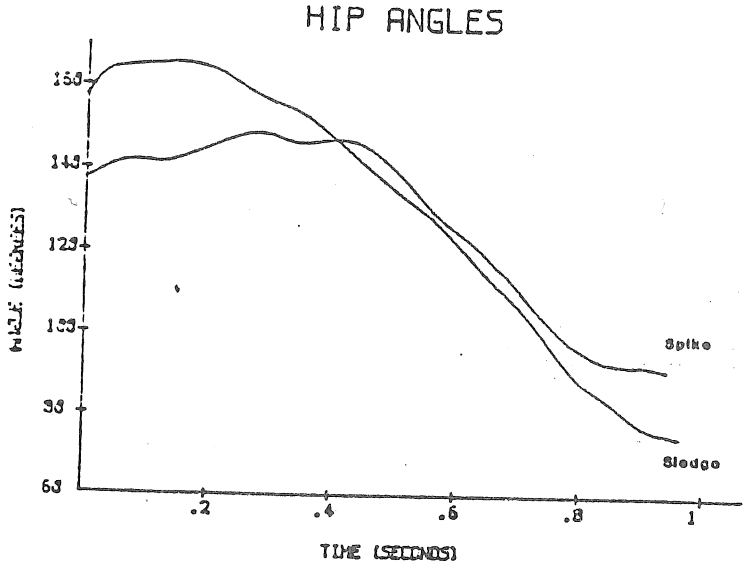

Figure 1

The displacement of the spike and sledge conditions were digitized and velocities and accelerations were generated. Figs. 2 and 3 depict the acceleration of the sledge and spike heads as derived from digitized displacements and calculated velocities. The terminal accelerations of the sledge head was 200 m-sec^{-1} compared with 280 m-sec^{-1} developed with the spike mallet. Torques at the lumbar spine were estimated to be 35% greater for the spike mallet than for the sledge. Since the torque output (based upon no absorption by the shoulders) necessitated considerable manipulation to obtain smooth curves, the validity of the actual values can be questioned. The kinematics of the patterns, however, leads one to believe that most of the forces are dampened at the shoulders thus reducing considerably the forces at the lumbar spine. The output from this subject can be a model for emulation.

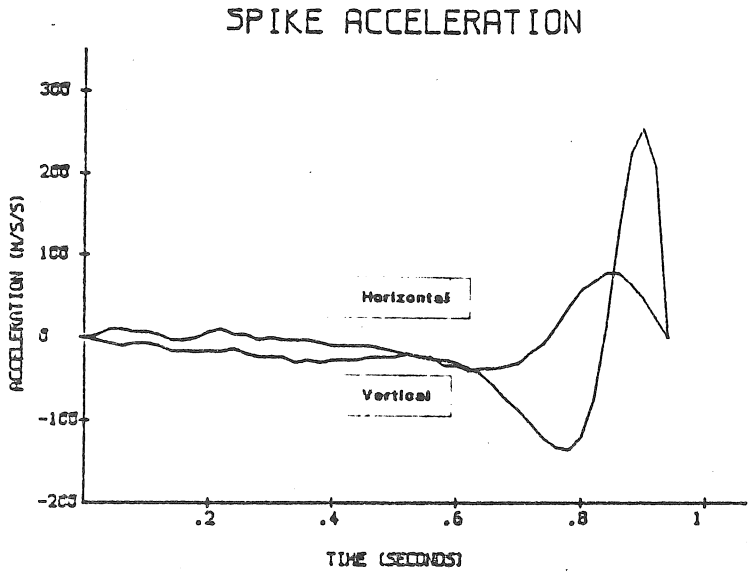

Figure 2

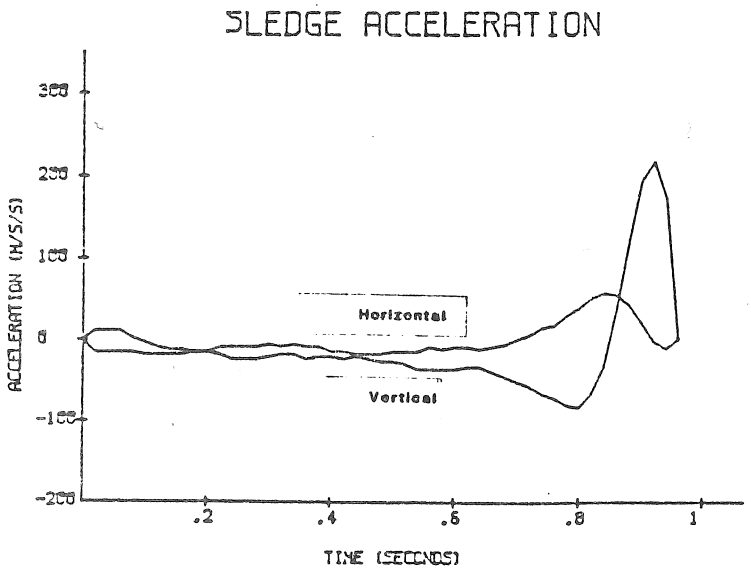

Figure 3

4/26/84

ABSTRACT: A BIODYNAMIC MODEL FOR INVESTIGATING INDUSTRIAL PUSH/PULL TASKS

R.O. Andres, D.S. Bloswick, D.B. Chaffin
Center for Ergonomics, The University of Michigan
Ann Arbor, MI 48109

Carts of various sizes, weights, and configurations are frequently pushed or pulled manually in the tire manufacturing industry, the fiberglass manufacturing industry, commercial laundries, and airlines, to name only a few. A biodynamic model developed by Lee (1982) was used in laboratory experiments to predict two risks associated with push/pull tasks: The risk of back injury and the risk of slipping. The purpose of this report is to describe revisions of the model and results of more extensive model validation experiments run in the laboratory.

The sagittal plane biodynamic model uses subject anthropometry, hand forces exerted against the cart handle, and body joint center positions to calculate reactive forces and moments at each joint, L5/S1 compressive force, and the required coefficient of friction (COF) at the shoe/floor interface. These are not static calculations; the inertial components increase the two major risks mentioned above. To validate model predictions of L5/S1 compressive force and the required COF it is necessary to compare independent observations of these quantitites with the model predictions. Foot forces were measured with a force plate, so comparison was straightforward, but the only way to validate L5/S1 compressive force predictions was through surface electromyographic (EMG) recordings from erector spinae and rectus abdominus muscles. These EMGs were then experimentally related to muscle force in isometric cases and, through a model developed by Chaffin and Baker (1970), eventually to L5/S1 compressive force.

The laboratory validation experiments varied several factors which could affect the model: handle height, cart resistance, speed of push or pull, and subject anthropometry (stature and weight). Ten males and ten females performed the experiment, which consisted of 24 trials for the single replicate. Significant differences between observations and predictions were calculated with ANOVA techniques. These results demonstrate the weak portions of the model predictions, thereby preventing erroneous application in the field. The resulting predictions of L5/S1 compressive force and required COF have several occupational implications: should cart configuration (handle height, wheel size) or loading be changed, should floor or shoe materials be changed, should floor maintenance procedures be revised, should workers of certain size or strength be restricted for certain jobs, among other possible recommendations. The revised biodynamic model will be extensively applied to industrial cart push/pull tasks in the future.

References

Lee, K.S.: Biomechanical Modelling of Cart Pushing and Pulling. PH.D. dissertation in Industrial and Operations Engineering, The University of Michigan, 1982.

Chaffin, D.B., and W.H. Baker: A Biomechanical Model for Analysis of Symmetric Sagittal Plane Lifting. AIIE Trans., Vol. 2(1), 1970.

ABSTRACT: FIELD STUDY METHODS FOR APPLYING A BIODYNAMIC MODEL TO INVESTIGATE INDUSTRIAL PUSH/PULL TASKS

K.L. Kreutzberg, R.O. Andres
Center for Ergonomics, The University of Michigan
Ann Arbor, MI 48109

A biodyamic model was developed by Lee (1982) to predict two risks associated with industrial push/pull tasks: The risk of back injury and the risk of slipping. This model was revised and enhanced by Andres, Bloswick, and Chaffin (1984) and extensive model validation experiments were run in the laboratory. The results from these experiments not only validate the model but also demonstrate the weak portions of the model predictions, thus preventing erroneous application in the field. The purpose of this report is to describe the methods for applying the biodynamic push/pull model in the field and to give an example of applying the model to an actual occupational push/pull task.

The goals of analyzing an actual occupational cart push/pull task are to predict the L5/S1 compressive force (risk of back injury) and to predict the required coefficient of friction (risk of slipping). The sagittal plane biodynamic model described by Andres, et al. (1984) can predict these factors using subject anthropometry, hand forces exerted against the cart handles, and body joint center positions. The equipment required to perform this field analysis would be a video camera and video cassette recorder, portable handles with strain gage instrumentation, an analog-to-digital converter, an IBM compatible portable PC, and a video display.

Once a suitable task is chosen, the instrumented handles are attached to the industrial cart. The force exerted on the handles is amplified and passed through the A/D converter. The subject's joint centers are marked with white markers and positional data is recorded on video cassette. The digitized force signal and a frame counter running at 60 frames per second are synchronously recorded with the positional data using software developed at the Center for Ergonomics for use with the IBM personal computer. Before and after actual testing, a force calibration is performed on the instrumented handles.

The data analysis will take place in the laboratory. The video cassette recording will be sampled 15 times per second or every four frames. The joint center poistions will be digitized using cursor control commands. The digitized position data and the handle force appearing on the screen will be stored in a file. This data, along with the suject anthropometry can then be input to the biodynamic model resulting in predictions of the L5/S1 compressive force and required COF for the given push/pull task. These predictions have several occupational implications concerning cart configuration and loading, floor materials and maintenance, shoe materials and tread design, worker strength requirements, and many other factors.

Field studies will be performed at five different industrial locations. Using the methods described here, the biodynamic model will be used to analyze a variety of actual occupational cart push/pull tasks. The results of one of these studies will be presented in conjunction with this report.

Refereneces

Lee, K.S.: Biomechanical Modelling of Cart Pushing and Pulling, Ph.D. dissertation in Industrial and Operations Engineering, The University of Michigan, 1982.

Andres, R.O., D.S. Bloswick, and D.B. Chaffin: A Biomynamic Model for Investigating Industrial Push/Pull Tasks, Center for Ergonomics, The University of Michigan, 1984.

A SYSTEM FOR ANALYSIS OF POSTURES AND FORCES IN MANUAL WORK

Thomas J. Armstrong, Marcia Robertson, Bryan Buchholz, Bradley S. Joseph, Charles Woolley, Barbara Silverstein (Center for Ergonomics, 1205 Beal, The University of Michigan, Ann Arbor, Michigan 48109)*

Cumulative Trauma Disorders, such as carpal tunnel syndrome and tendinitis, are assoicated with repetitive work, certain postures, and forceful exertions. This paper describes a system designed for analysis of work postures and forces.** A video tape recorder is used to record work activities (see Figure 1). the video tapes are played back in slow motion and the posture of the entire upper extremity is analyzed every third of a second. The posture of the arm is determined by its position about three axes of rotation. Forearm posture and forearm rotation are each determined by the location of the forearm or hand around one axis, and the posture of the hand is detemined by its location about two axes of wrist rotation. The range of posture around each axis of rotation was divided into one to six sectors and assigned a value. One value is recorded for each variable corresponding to an axis of rotaion. Six classes of gripping postures of the hand are defined by finger positions and the location of external loads. Which digits are used is also stored.

Forces are estimated from surface electromyography. The EMG signals are integrated and superimposed on the video tape so that they can be synchronized with postures. A digital time signal is also superimposed on the videotape. Least squares regression is used to determine the straight line passing though the origin for the calibration data for each posture. Forces exerted in different postures can then be estimated from the EMGs displayed on the video tapes by using the appropriate calibration curve for a particular posture.

Figure 2 shows an example of posture and force data for a "hand dipping" job. The task consists of an operator dipping a wax mold into a casting material. During the task the right forearm is flexed 90 degrees or is extended 45 degrees; the left forearm is flexed 90 degrees for most of the cycle. It can be seen that the job requires almost constant pronation of the right forearm and supination of the left forearm. The right wrist alternates between neutral and ulnar deviation. It is extended 45 degrees during 36% of the task, neutral 23%, flexed 45 degrees 30%, and fully flexed 11% of the task. The left wrist is neutral with respect to deviation; it varies between full extension and 45 degrees extension throughout the cycle. Eighty-six percent of the exertions performed by the right hand are less than 5kg; approximately 7% are between 5-10kg, and approximately 7% are greater than 10kg. Sixty-eight percent of the exertions performed by the left hand are less than 5kg; 25% are between 5-10kg, and approximately 7% are greater than 10kg. The forceful exertions (5-10kg and >10kg) for both the right and left hand occur during grasping with the wrist extended 45 degrees or fully extended.

This information can be used to identify stressful postures and corresponding work activities, such as flexion of the wrist

to hold a part. It could also be used to determine the postural requirements for management of restricted workers. With anthropometric information, it could be used to design workplaces and tools that reduce physical stress on workers. In the past tools were customized for the person and the task. With modern technology, tools are standardized for an "average" person. Because of individual variation, these tools may not be appropriate for individual workers or tasks and may be responsible for stressful postures.

*This work was supported by The National Institute for Occuptional Safety and Health and private industry.

**References: Armstrong,T., Chaffin,D., and Foulke,J. (1979) A methodology for documenting hand positions and forces during manual work. J. Biomechanics 12:131-133.

Armstrong,T., Foulke, J., Joseph, B., Goldstein, S. (1982) Investigation of cumulative trauma disorders in a poultry processing plant. Am. Industrial Hygiene Assct. J. 43:103-116.

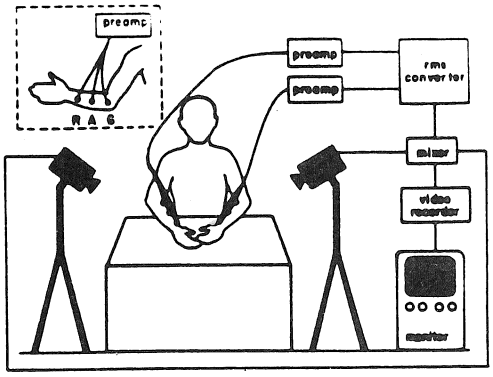

Fig. 1. Schematic of the system for collecting data.

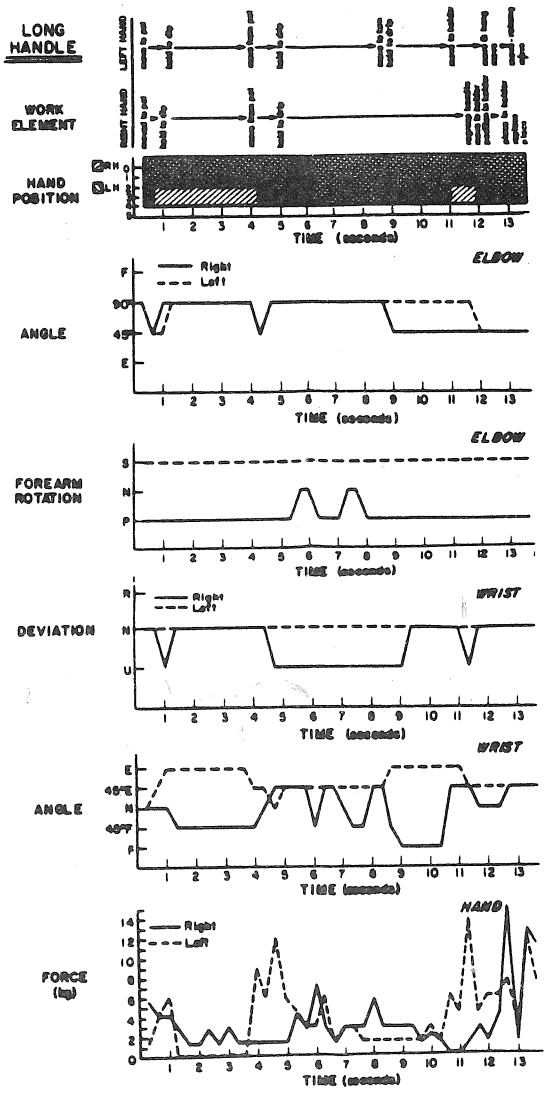

Fig. 2. Raw data for hand dip job: work elements, postures, and forces.

A TEST OF THE HYPOTHESIS OF ABDOMINAL PRESSURE AS A DISC LOAD-REDUCING MECHANISM: A STUDY USING QUANTITATIVE ELECTROMYOGRAPHY.

M. Krag, L. Gilbertson, M.H. Pope, Department of Orthopaedic Surgery, University of Vermont, Burlington, VT 05405

Both the abdominal and thoracic cavities have been reported to become pressurized during strenuous activity. This pressure is believed to force the pelvic wall (floor of the abdominal cavity) and the lung's diaphragm (roof of the abdominal cavity) apart. Bartelink (1957) and Morris, Lucas and Bresler (1961) suggest that this mechanism tends to extend the spine and thus reduce the contraction force required in the extensor muscles. In turn, this force rebalancing is said to reduce the compressive load bearing of the disc. This is controversial since the abdominal muscles must contract, producing a flexion moment in order to produce the IAP.

It is interesting to note that although the information to sustain the "football theory" of spinal support is limited, this theory has received wide acceptance. It is the purpose of this paper to test the fundamental hypothesis that IAP reduces loads in the disc.

MATERIALS AND METHODS: The volunteers used in this study were 9 healthy male subjects aged 18-43, free of any history of low back pain. The volunteers were placed standing in a trunk loading frame which supported the subject at the anterior superior iliac spines. The subject was fitted with a shoulder harness attached to a cable, load cell and loading frame. Tests were done in the upright position, and at 45° of flexion. At each position the subject accomplished a maximum voluntary extension effort (MVEE) followed by a rest. In both the upright and flexed position, the subject performed the trunk loading efforts of 1/3 MVEE and 2/3 MVEE with several states of abdominal pressurization: unspecified intra-abdominal and intrathoracic pressures (termed uncoached lifting effort), Valsalva maneuver, normal breathing, and slow exhalation while maintaining abdominal pressure (termed ½ Valsalva). The subject pulled against the cable for 10 seconds at the desired trunk loading level for each state of abdominal pressurization, followed by a period of rest. The electromyographic activity (EMG) was measured by surface electrodes located bilaterally at the level of L3-L4 at a position 3 cm from the anterior line. In addition, electrodes were placed on one side only at the level of T8, 3 cm lateral to the midline.

RESULTS: IAP was plotted against EMG for all cases. There is much scatter in the data, but some trends emerge. As expected, tests of the subjects exerting 1/3 MVEE yield lower EMG activities than those of the same subjects exerting 2/3 MVEE. These decreases of EMG were not accompanied by any consistent trend of reduction with increased IAP. Smaller IAP levels were recorded for both uncoached lifting and normal lifts as compared to the Valsalva and so-called ½ Valsalva. The Valsalva efforts did not appear to reduce EMG activity as compared with other efforts. The increased intrathoracic pressure was suggested by Morris, Lucas and Bresler (1961) to be a factor in reducing EMG activity, but this hypothesis was not sustained by us.

DISCUSSION: The experiments did not demonstrate a consistent decrease of erector spinae activity with increased IAP. Thus IAP would not decrease the disc pressure by means of the hypothesized mechanism. Further study is needed to understand how intra- abdominal and intrathoracic pressures affect the biomechanics of the spine; it is obvious that the widely accepted simple models are not being supported by the experimental data.

MUSCULOSKELETAL STRESS EVALUATION OF MICROSCOPIST USING ELECTROMYOGRAPHY

Kwan S. Lee, Linda Hall and Frank Chen

Department of Industrial and Systems Engineering
Ohio University, Athens, OH 45701 U.S.A.

ABSTRACT

This paper presents the results of a laboratory study in which electromyography was used to measure the musculoskeletal stress of prolonged sedentary work. Most studies in this field have been restricted to subjective questionnaires obtained during a very short work period. But questionnaire evaluations are not as desirable as objective measures because subjective judgment can be easily biased unless subjects are very cooperative and well trained on how to evaluate their own musculoskeletal stress consistently. These conditions in industry are difficult to attain.

Electromyography has provided objective and quantitative data on strenuous muscle contraction which allows the estimation of musculoskeletal stress. However, no study has been done to adequately assess the appropriateness of electromyogram (EMG) as an indicator of stress in a sedentary type of work with a reasonably long work period.

This study also used questionnaires about musculoskeletal stress during experimentation to find subjective measures. These measures were compared with objective measures derived from the root-mean-square (rms) electromyogram measured during the experiment. To improve the reliability of subjective measures, all subjects were told the purpose of the study and were trained to evaluate their own musculoskeletal stress.

Microscope work was chosen as a task because of frequent complaints of neck, shoulder and back pain by many microscopists. All subjects read microscope slides for blood cell count. EMG's were measured on the skin of four muscles in the right side of the body (the erector spinae, the latissimum dorsi, the trapezius, the neck muscle). The sampling rate was 400Hz. Twelve healthy male and female subjects with normal vision, performed the task for two separate four-hour work periods without a rest break. Three different work periods of four hours each were established (morning, afternoon and evening). Each subject had to perform in two work periods on different days. Subjects were randomly assigned to two out of the three possible work periods.

Subjects were required to give, on a scale from one to eight, their perceived sense of stress in the same muscles from which EMG readings were made. This subject assessment was done every half hour. The microscope work station was equipped with one adjustable binocular microscope (HM-LUX: Letiz, Inc.) and a non-adjustable chair. The data acquisition system consisted of an APPLE IIe microcomputer, an analog to digital converter, a rms-to-direct-current converter, an EMG amplifier and EMG preamplifiers.

This study reveals significant increases in musculoskeletal stress over the time of the experiment by both objective and subjective measures. The average correlation r for objective and subjective measures is 0.93. This indicates that electromyography can be a reliable and quantifiable method for objective evaluation of musculoskeletal stress.

LIGAMENTOUS RESTRAINTS TO ACROMIOCLAVICULAR JOINT MOTION: A BIOMECHANICAL STUDY

K. Fukuda, M.D., K. N. An, Ph.D., E. V. Craig, M.D.,*
R. H. Cofield, M.D., E.Y.S. Chao, Ph.D.
Orthopedic Biomechanics Laboratory, Mayo Clinic, Rochester, MN
*Department of Orthopedics, University of Minnesota, Minneapolis, MN

The acromioclavicular (A-C) joint is susceptible to injury through sprain, subluxation and dislocation in contact sports, as well as in traffic accidents. The treatment of Grade III injuries to the A-C joint, with rupture of all the surrounding ligaments, is yet controversial [Allman, 1967; Rockwood, 1975]. In this study, the relative contribution of each ligament to A-C joint stability under various loading conditions was obtained. This information provides significant data for determining optimal treatment.

Twelve human cadaver shoulder specimens were obtained by either transection of the clavicle at the proximal two-thirds or disarticulation at the sternal end. Specimens were prepared by removing the skin and subcutaneous tissues. Each specimen was then mounted on an MTS testing machine in special fixtures at the proximal end of the clavicle and distal end of the scapula. Specimens were tested under nine separate loading modes: anterior-posterior and superior rotations about the A-C joint; anterior-posterior and superior translations; and axial rotation and translation of the clavicle (Fig. 1). The tests were performed on the intact joint and then repeated following sequential sectioning of the three surrounding ligaments: acromioclavicular (A-C) ligament; and the two components of the coracoclavicular ligament -- the conoid and trapezoid ligaments (Fig. 1). The contribution of each ligament to A-C joint stablity was defined as the decrease in the restraining load after removal of that ligament. The relative contributions were then calculated by normalizing as a percentage of the total decrease of load with complete removal of all ligaments.

For each of the tests, the relative contributions of the ligaments to A-C joint stability at small ranges of displacement may not be the same as those with larger displacements (Table 1). The results indicated that in constraining both anterior and superior displacements, the A-C ligament is the primary stabilizer at the initial phase of small displacement and the conoid ligament increased its contribution from secondary to primary with increasing displacement. In constraining posterior displacement of the clavicle, the A-C ligament played the primary role throughout the entire range of displacement. In constraining superior rotation, both the A-C and conoid ligaments contributed equally at the initial phase of small rotation, while with further rotation the conoid ligament surpassed the A-C ligament. The trapezoid ligament was found to be important only in resisting axial compression of the clavicle against the acromion.

This study demonstrated that the conoid ligament is more important than previously described. It played a major role in constraining anterior and superior displacements and rotation of the clavicle, especially with large displacements. In designing surgical procedures to restore the unstable A-C joint, the direction of joint instability should be identified. The ligaments which provide the primary constraint in the direction of joint instability should be restored prior to the other ligaments.

References:

Allman, F.L.: Fractures and ligamentous injuries of the clavicle and its articulation. J. Bone Joint Surg., 49-A:774-784, 1967.

Rockwood, Jr., C.A.: Dislocations about the shoulder. IN: Rockwood, Jr., C.A. and Green, D. P.: Fractures. Philadelphia, J. B. Lippincott, 1975, pp. 721-756.

Table 1. Relative ligamentous contribution to the stability of the acromioclavicular joint (%).

	n	Small Displacement			Large Displacement		
		Conoid	Trapezoid	A-C	Conoid	Trapezoid	A-C
Anterior Rotation	3	55	20	25	72	20	8
Posterior Rotation	3	55	16	29	47	38	15
Superior Rotation	6	40	20	40	82	5	13
Anterior Displacement	6	35	16	49	70	18	12
Posterior Displacement	6	7	4	89	9	1	90
Superior Displacement	3	23	9	68	62	29	9
Axial Compression	3	40	47	13	9	75	16
Axial Distraction	3	35	0	65	8	1	91
Axial Rotation:Posterior	3	9	28	63	2	15	83

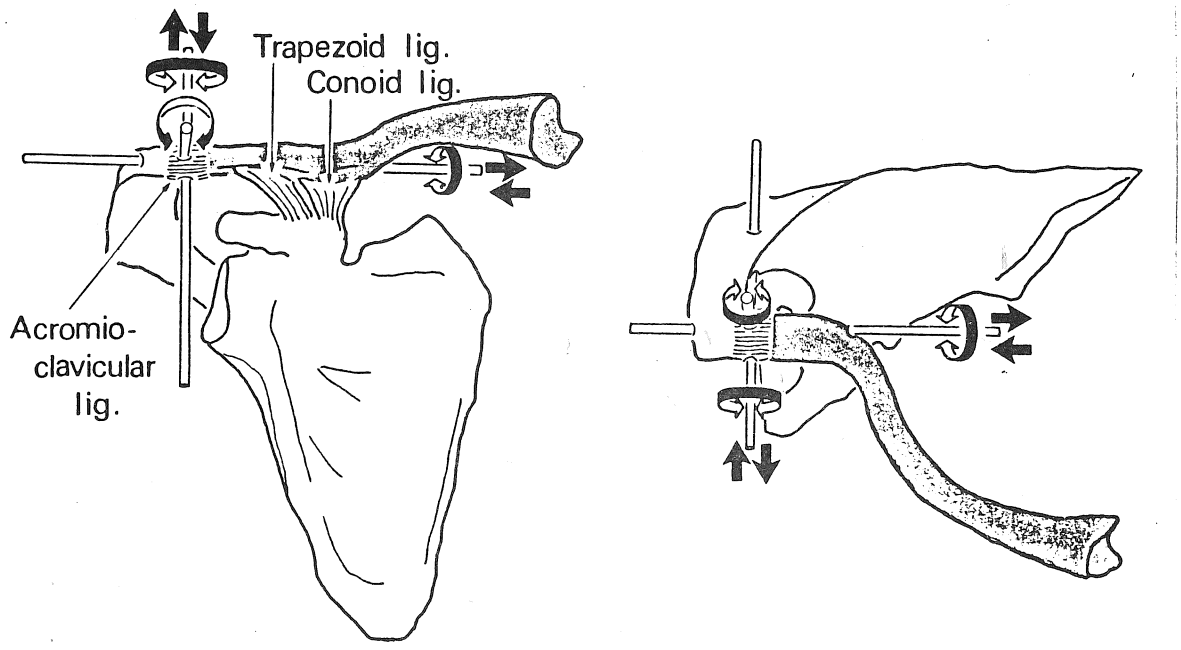

Table 1. Contributions of the trapezoid, conoid and acromioclavicular ligaments to the stability of the acromioclavicular joint are obtained from load-displacment tests. The rotational and translational displacement tests are shown.

A BIOMECHANICAL EVALUATION OF THE FUNCTION OF THE DIGITAL PULLEYS

S.A. Goldstein, Ph.D., T.L. Greene, M.D., D.S. Louis, M.D.,
W.S. Ward, M.D. and L.S. Matthews, M.D.

The Biomechanics, Trauma, and Sports Medicine Laboratory
University of Michigan Medical Center
Ann Arbor, Michigan 48109

The anatomical and functional importance of the digital pulleys has been reported by many investigators. Surgeons, however, continue to be concerned about the integrity of the pulley sheath which must be maintained or repaired after trauma or reconstructive procedures for adequate digital function. Only a few limited studies have addressed the biomechanical consequences of pulley loss. No studies have presented experimental data regarding the relationship between multiple joint performance and pulley loss.

The purpose of this study was to experimentally determine the relationship between tendon load, tendon excursion, joint flexion and randomized serially sectioned digital pulleys.

An experimental apparatus was constructed which enabled simultaneous recordings of tendon load, tendon excursion, MP flexion, PIP flexion and DIP flexion. Sixteen fresh frozen cadaver hands were rigidly fixed in the apparatus by carefully pinning the metacarpals to a specimen block. The hands were maintained at 38 degrees centigrade while being bathed in fluid. Each digit was denuded before testing and pulleys A2, A3 and A4 were carefully identified. The profundus tendon to each digit was secured to a constant speed linear displacement motor which flexed the digit against a constant load attached distally. Flexion at each joint was measured using a specially designed goniometric device. All data was acquired directly on a Tektronix 4054 computer system. The resolution of the system was approximately $\pm$ 1.5 degrees. Each finger was tested and retested according to a randomized order of pulley resections. The pulleys tested were: the proximal half of A2, the distal half of A2, A3 and A4.

The results of the study indicate that many combinations of pulley resections can create significant flexion losses when tendon excursion remains constant. To achieve the same grip position after various pulleys were cut, increased tendon excursion was required. In some cases, this excursion increase could not have been physiologically possible. In general, until all pulleys are sectioned, it takes less force to flex the digits, but at the expense of increased tendon excursion. Specific patterns of joint flexion angles, as a function of tendon excursion, were altered significantly by various resection combinations. Resolved flexion moments and phase lag relationships were also affected.

In summary, the A2 pulley caused the most significant alterations in function when comparing individually sectioned pulleys. Contrary to previous reports, A3 has some importance for maintaining digital performance when several combinations of other pulleys have already been resected.

TORSIONAL LOAD - DEFORMATION CHARACTERISTICS OF THE HUMAN LEG IN VIVO

by

Curtis Johnson
Graduate Student

M. L. Hull
Associate Professor

Department of Mechanical Engineering
University of California
Davis, California 95616

The legs of alpine skiers are subjected to an extremely harsh loading environment. The combination of speed, rough terrain, and coupling between snow, ski, and boot causes severe loading to the leg. Ski safety equipment has been developed and refined, reducing the occurrence of some leg injuries. Yet even the most advanced safety equipment is ineffective in reducing the most common ski affliction, knee injury.

Generally, knee ligamentous injury is caused by over-extension of the joint. Torsional excitation has been singled out as the most damaging input to today's skier. The objective of this study was to explore the quasi-static load deformation of the lower limb in torsion with emphasis on the effects of muscle contraction.

The experimental apparatus consisted of a fixed pivot (i.e. shaft) to which a ski boot was attached. The boot rotation was measured by an instrument potentiometer fixed to the bottom end of the shaft. The torsion input was applied manually via a lever. Tibia and femur rotations were monitored via parallelogram linkages. These linkages allowed accurate potentiometer measurement of axial rotation while decoupling all translations. Inertial bone rotations were measured by fixing one side of the parallelogram linkage to the apparatus frame and the other side to the tibia or femur reference. Positioning of the linkages was adjustable to allow accurate measurement of large displacements.

Quasi-static tests were undertaken for three male test subjects (~ 200 lbs, 25 yrs old) to investigate the dependency of joint load-deformation characteristics on axial loading (i.e. weight bearing) and muscle activity. All tests were run separately in both internal and external rotations. With subject in proper stance, loading was slowly increased in each test until the subject felt pain.

Each joint showed similar trends throughout the testing procedure. Figure 1 shows that the ankle is more compliant in internal rotation than external rotation. This could be caused by the posterior talofibular ligament which, because of its geometry, is only stretched in external rotations. The twisting of the cruciate ligaments of the knee explain the increased stiffness of this joint in internal rotation as opposed to external rotation. This finding is well supported by previous research. The most compliant of the lower limb joints is the hip. This ball and socket joint shows the most rotation and also the most distinct piecewise linear characteristics, especially for internal rotation.

The effect of weight bearing on joint stiffness had good agreement in all tests. Additions of body weight (axial loading) to the tested limb always increased joint stiffness. Figure 2 shows trends towards more linear displacement-torque curves for the increased weight bearing case.

The muscle's ability to stiffen the joints appears in a comparison of relaxed and resisting data (Figure 3). All joints were significantly stiffened when the subjects resisted the leg rotations. The most extreme example of this is the hip, which, with its large thigh and lower back muscles, can eliminate virtually all joint rotation. One conclusion which can be drawn from these observations and the weight bearing tests is that the ski boot does not supply all ankle stiffness. In fact, the ski boot appears to have little effect on the stiffness of the joint.

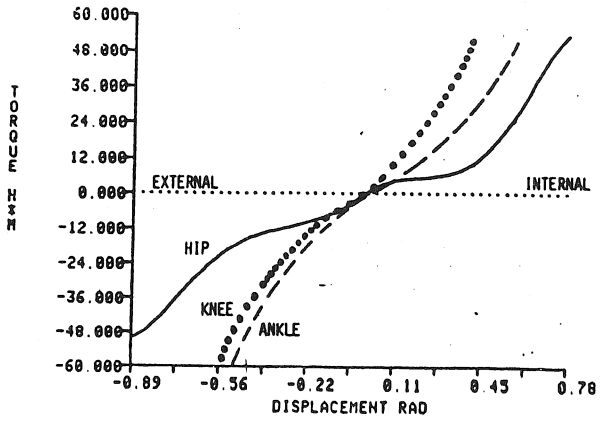

FIGURE 1. TORQUE VS DISPLACEMENT AT 50% WEIGHT, LEG STRAIGHT

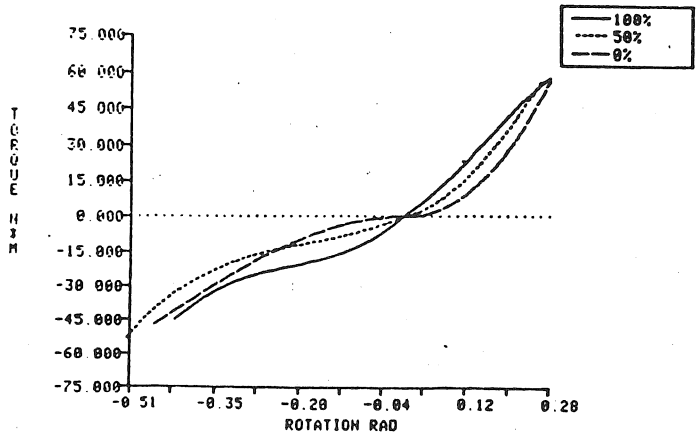

FIGURE 2. EFFECT OF WEIGHT BEARING ON KNEE STIFFNESS

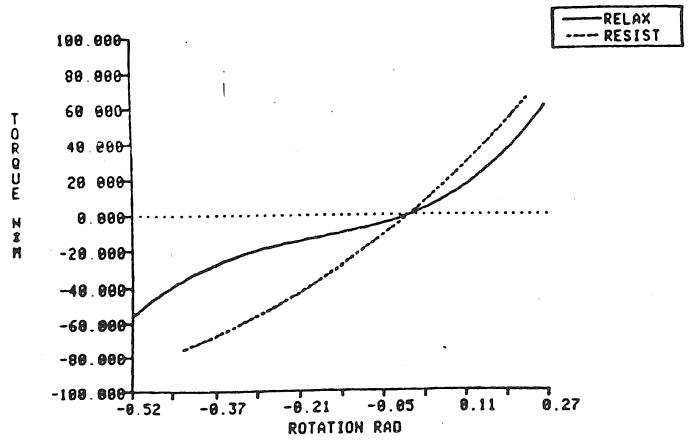

FIGURE 3. EFFECT OF RESISTING (I.E. MUSCLE CONTRACTION) ON KNEE STIFFNESS

ABSTRACT

The Function of the Third Metacarpal Styloid Process: a Force Analysis Employing Magnetic Resonance Imaging

M.W. Marzke, Department of Anthropology, Arizona State University and
R.F. Marzke, Department of Physics, Arizona State University

The third metacarpal in man is held firmly in place at the center of the hand by the adjacent carpal and metacarpal bones and by ligaments. Injuries to the region of its base are rare; dorsal subluxation may occur as the result of traumatic impact on the dorsal aspect of the metacarpal head, and very rarely volar subluxation occurs with severe impact on the volar aspect of the metacarpal head. Because of its invulnerability to injury, the functional morphology of this region has not been extensively analyzed by the medical community.

The stimulus for our force analysis of the region was the discovery that the configuration of joints in the region of the capitate and third metacarpal is unique in man among primates. Three features are noted. (1) A styloid process on the third metacarpal locks against the capitate, which is beveled to accommodate the process. (2) An extension of the pisometacarpal ligament to the palmar aspect of the base of the third metacarpal serves with the ligament from the trapezium to check hyperextension of the metacarpal and volar subluxation of the base. (3) This ligament is accommodated by a groove across the distal aspect of the hamate hook, which lies near the horizontal plane. The bony features of this configuration were found to be absent in hands of 52 primate species examined by MWM in museum collections and in dissections of 26 primate species.

Since the habitual manipulation of large tools distinguishes man

from other primates, we propose that the evolution of the unique configuration and effective resistance of this region to injury in man is related to requirements for resisting marked and persistent stresses incurred by the palm of the hand during the grasping, wielding and throwing of spherical and cylindrical tools such as stone hammers, clubs, and digging sticks. To test one aspect of this hypothesis, a model of the capitate and third finger grasping a spherical object has been constructed and forces on the joint between the capitate and third metacarpal have been calculated. Relative bone lengths, angles between the bones at joints, and moment arms of muscles exerting forces along the third ray are measured on MRI images of hands. Relative flexor forces are derived from measurements with a dynamometer.

Results of the analysis show that forces and moments at the joints of the third finger increase from the distal to the proximal joints; at the carpometacarpal joint, forces normal to the capitate are large and tend to slide the bone dorsally relative to the third metacarpal. The normal component of the reaction force tends to slide the third metacarpal in a palmar direction on the capitate. Both the styloid process and the pisometacarpal ligament are in positions to prevent volar subluxation of the metacarpal base which would result from these forces.

Contact Finite Element Stress Analysis of the Hip Joint and Acetabular Region*

D.J. Rapperport and D.R. Carter

Design Division Department of Mechanical Engineering, Stanford University, Stanford, CA 94305
and Veterans Administration RRnD Center Palo Alto, CA 94304

Two-dimensional finite element analyses were conducted of the normal hip using contact elements at the joint surface. The models were based on a 2-D representation of a section taken through the pubis and normal to the acetabulum. The femoral head and neck was modeled as having a spherical surface which was mated with a congruent spherical acetabular socket. The model consisted of 1120 nodes comprising 1271 four-noded isoparametric quadrilateral elements and 30 contact elements. Frictionless contact elements were incorporated at the joint surface so intraarticular pressures could be calculated as the proximal femur was pushed into the socket.

Many of the studies of contact areas and pressures at the hip joints have imposed boundary constraints which are rigid and/or close to the joint. Such boundary conditions prevent the true deformation of the pelvis and result in the measurement or calculation of incorrect joint areas and pressures. We have analyzed two different sets of boundary conditions: 1) deformable and 2) rigid. In the deformable model the pubic symphysis was allowed to displace in the sagittal plane and was free to rotate. In the rigid model the pubic symphysis was rigidly fixed. For both models the sacro-iliac joint was free to displace in the plane of the joint and the extreme margin of cortical bone in the ilium was rigidly fixed.

Loading directions and magnitudes were chosen as bounding cases. Two resultant femoral load angles were considered and are referred to as case 1 and case 2. Case 1 loading was directed along the ilium and represents typical early phase loading during gait (supero-posterior). Case 2 represents a more medially directed load. A maximum load magnitude of 960 N/cm was chosen such that peak bone stresses were approximately 30% of ultimate strength for case 1 loading. The same maximum applied load was used for case 2.

The mechanism of load transmission was such that contact pressures around the foveal notch were low in both loading directions for the deformable model. The principal stress pattern in the deformable model reflected the trabecular morphology closely. For the deformable model subject to case 1 loading, the highest hip contact pressures were confined to the superior dome of the acetabulum (figs. 1 & 2). This resulted in high compressive stresses in the ilium cancellous bone. Lower contact pressures were also present in the inferior margin. For the deformable model subject to case 2 loading the acetabulum closed in such a manner as to squeeze the head of the femur (figs.1, 3 & 4). High contact pressures were observed at the superior dome and at the inferior cartilage of the pubis. This resulted in significant compressive stresses in the superior dome cancellous bone and in the inferior cancellous bone of the pubis . Bending in the pubis resulted in formation of principal stress "arcades". The curved geometry of the pubis slice provided an excellent mechanism for load transmission of compressive stresses to the sacro-iliac joint. High tensile "membrane" stresses were observed in the superior dome region and in much of the medial surface. The presence of biaxial compression was calculated in the femoral epiphysis. The stress state became more uniaxial around the epiphysis.

The stress distribution in the rigid model was markely different than the deformable model. Rigidly fixing the pubis stiffened the model and caused deviation of principal stress patterns from observed cancellous bone morphology. Bending stresses were transmitted across the pubic symphysis for case 2, which were not reflected in the bone morphology and which one would not expect from this rather flexible joint. Contact stresses around the foveal notch for the rigid model were approximately twice those of the deformable model. Rigidly fixing the pubic symphysis changed the stress distribution around the acetabulum significantly from that of the deformable joint. Based on these results we belive that assumed boundary conditions at the pubic symphysis markedly affect the contact pressures and bone stresses. The use of less constrained boundary conditions better represents normal anatomy.

*Supported by NIH grant AM32378

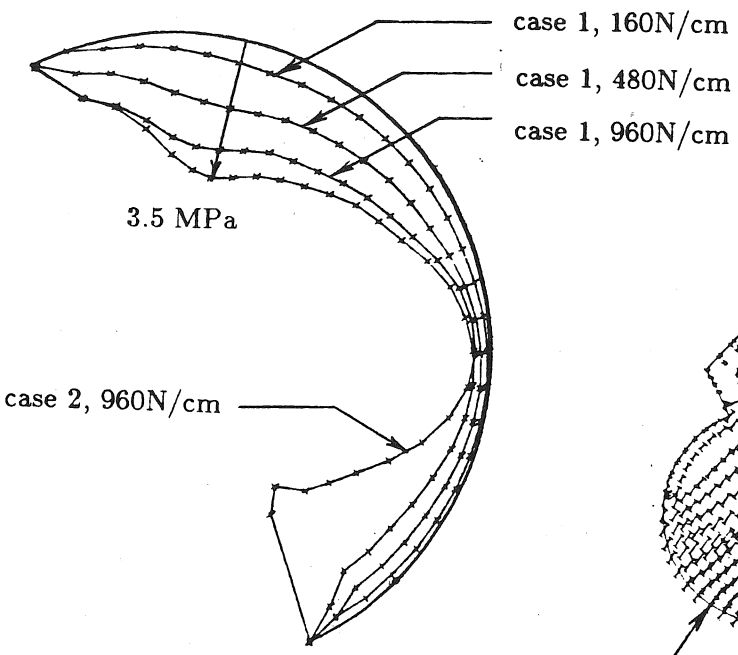

Fig. 1. Pressure distribution across articular surface for various loads.

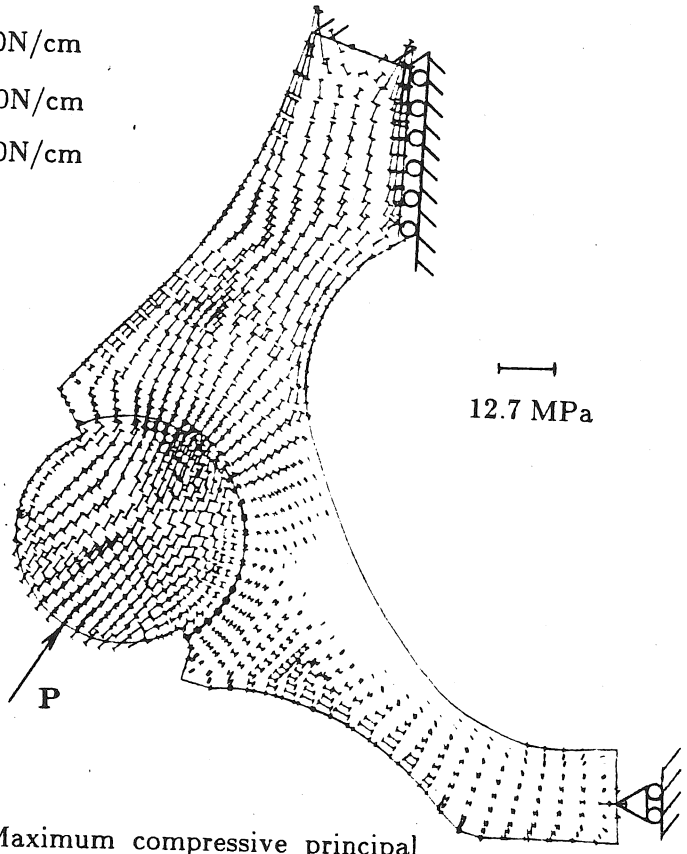

Fig. 2. Maximum compressive principal stresses for case 1 loading of 960N/cm.

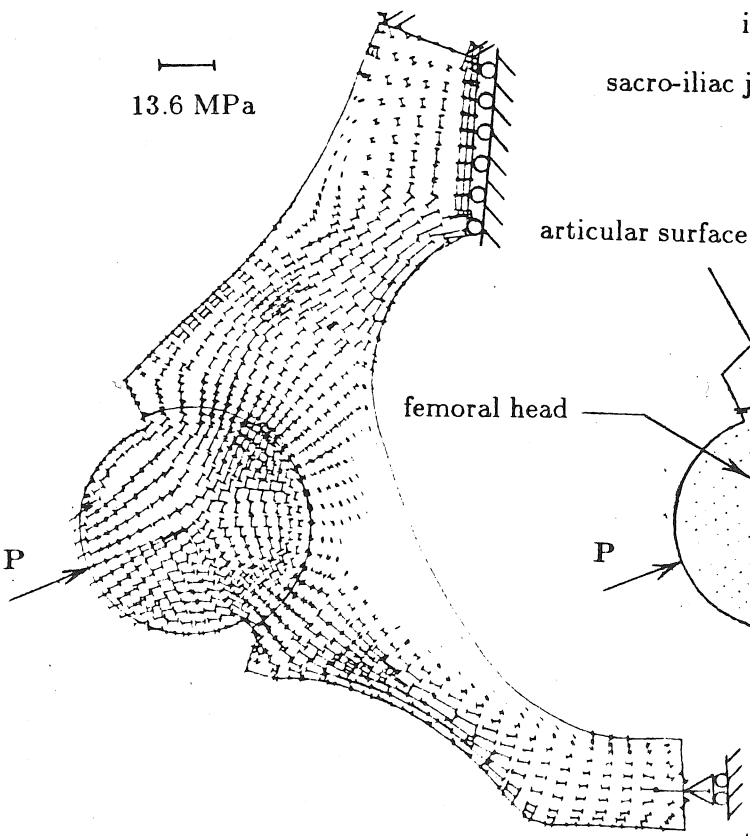

Fig. 3. Maximum compressive principal stresses for case 2 loading of 960N/cm.

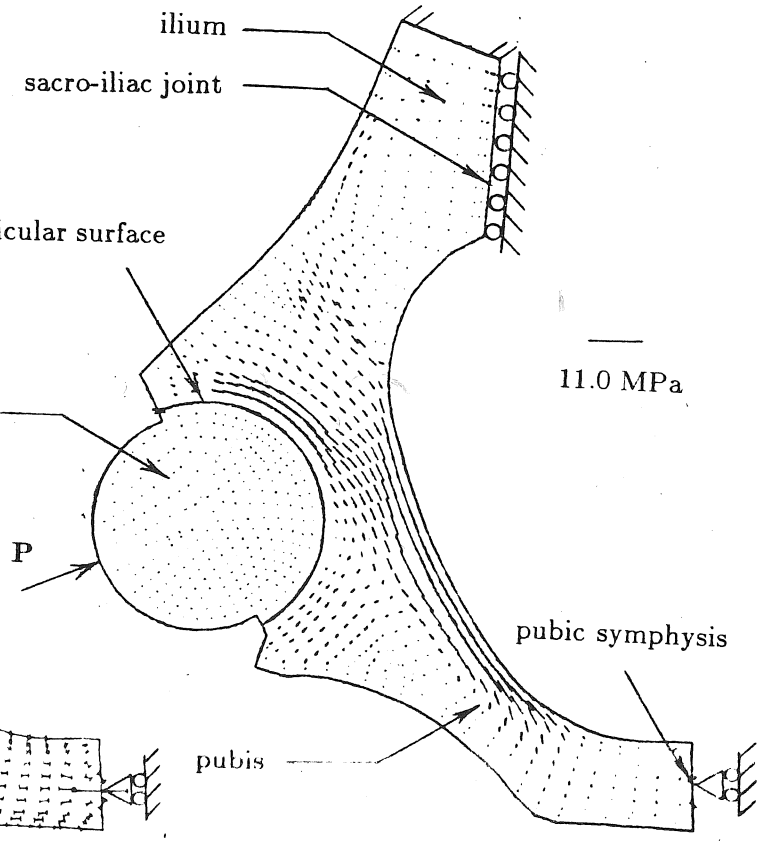

Fig. 4. Maximum tensile principal stresses for case 2 loading of 960N/cm.

The Kinetics of Normal and Prosthetic Wrists

Tolbert JR, Blair WF, Andrews JG, Crowninshield RD; Departments of Mechanical Engineering and Orthopaedics, University of Iowa, Iowa City, Iowa 52240

Descriptions of normal wrist kinetics and the kinetic behavior of currently available wrist prostheses are needed in order to quantify wrist dysfunction, and to evaluate the efficacy of various treatment modalities. The purposes of this study were (1) to describe normal wrist kinetics in cadaver upper extremities, and (2) to investigate the in vitro kinetic behavior of four wrist prostheses (Swanson, Meuli, Hamas, Volz).

Twelve normal cadaver specimens were tested with the wrist restrained in the neutral configuration by load cells oriented in the dorsal-volar and medial-lateral directions. Pronation-supination (P-S) of the hand relative to the fixed forearm segment was first constrained and then left unconstrained. The six major wrist muscles (FCR, FCU, ECU, APL, ECRB, ECRL) were sequentially loaded, and the corresponding equilibrium values of the load cell forces and the P-S torque (or P-S angle) were measured and recorded.

Following this procedure, Swanson implants were inserted and the tendon loading process was repeated. After the Swanson prostheses were removed, four each of the Meuli, Hamas, or Volz prostheses cemented in place, and the tendon loading procedure repeated.

A right-handed, orthogonal coordinate system R:Wxyz was embedded in the hand segment H with its origin at the wrist W (an arbitrarily chosen point located in the center of the capitate). The z axis was directed proximally, the y axis was directed dorsally, and the x axis was directed laterally for right writs and medially for left wrists. Letting $\bar{i}$, $\bar{j}$ and $\bar{k}$ denote unit vectors in the positive x, y and z directions, respectively, the moment contribution about W of each of the wrist tendons was expressed as the product of the known tendon force magnitude and the unknown effective tendon moment arm (ETMA) vector $\bar{d}$, where

$$\bar{d} = d_y \bar{i} - d_x \bar{j} + d_z \bar{k}$$

Here, d_y represents the ETMA about the flexion-extension (x) axis, or the effective tendon location at the wrist (z = 0) in the dorsal-volar (y) direction, d_x denotes the ETMA about the radial-ulnar deviation (y) axis, or the effective tendon location at the wrist (z = 0) in the medial-lateral (x) direction, and d_z represents the ETMA about the P-S (z) axis.

Measurement of the distance from the location of the load cell assembly to the wrist W, together with knowledge of the force and torque transducer readings, permitted the calculation of the ETMA vector $\bar{d}$ using the moment equilibrium equation for the hand segment.

The results of these experiments indicate that all prostheses yielded effective tendon locations that varied randomly relative to those for normal wrists. However, the Swanson prosthesis, with P-S constrained, yielded dorso-volar locations (d_y) that were similar to those for normal wrists. Also, the Hamas prosthesis exhibited P-S torques that were similar to those displayed by normal wrists. Mean values of ETMA lengths, $(d_x^2 + d_y^2)^{1/2}$, for all prostheses also varied randomly relative to normal wrists. Note, in the following table, that all significant ETMA length changes are decreases.

Tendon	Normal	Swanson	Meuli	Hamas	Volz
		Mean ETMA Lengths			
			Constrained		
1	1.62±.207	1.61±.276	1.10±.123 *	1.30±.101 *	1.41±.239
2	1.68±.253	1.44±.189 *	1.56±.142	1.24±.137 *	1.88±.456
3	2.52±.378	2.63±.585	2.24±.205	2.03±.654 *	2.57±.620
4	2.40±.308	1.42±.287 *	1.75±.097 *	2.66±.257	1.60±.264 *
5	1.50±.148	1.34±.205 *	0.93±.183 *	1.59±.323	0.99±.293 *
6	2.06±.186	1.76±.246 *	1.30±.168 *	2.08±.233	1.22±.202 *
			Unconstrained		
1	1.74±.274	1.65±.274	1.13±.109 *	1.44±.205 *	1.43±.233 *
2	1.89±.236	1.54±.241 *	1.82±.241	1.63±.178 *	1.95±.380
3	2.04±.357	1.98±.430	1.93±.159	1.90±.287	2.23±.492
4	1.87±.330	1.33±.235 *	1.44±.135 *	2.01±.165	1.43±.076 *
5	1.61±.090	1.38±.185 *	0.89±.115 *	1.73±.203	0.97±.217 *
6	1.96±.186	1.58±.203 *	1.11±.060 *	2.11±.266	1.18±.231 *

Mean ETMA lengths (cm) with standard deviations, for P-S constrained and unconstrained. Data includes both normal and postoperative specimens. Starred values are significantly different from normal at the $p<.05$ level. Tendon numbers correspond as follows: Tendon numbers 1-6 correspond sequentially to tendons FCR, FCU, ECU, APL, ECRB, ECRL.

The Swanson, Meuli and Volz prostheses decrease the ETMA lengths of tendons located dorsally and radially, while the Hamas prosthesis decreases the ETMA lengths of the tendons located volarly and ulnarly. The results of this study indicate that each of the six major wrist muscles contributes in a unique way to the kinetic behavior of both normal wrists and wrists with embedded prostheses. The statistical comparison of pre- and postoperative kinetic behavior indicates that none of the four prostheses studied preserves normal wrist kinetics.

STRENGTH CURVES FOR MULTIPLE-JOINT SINGLE DEGREE OF FREEDOM EXERCISES

by

J. G. Andrews
The University of Iowa
Iowa City, IA 52242

An isometric strength curve is a plot of the variation of the maximum isometric force or torque exerted by the dominant muscle group at a joint, as a function of an angular variable which describes the joint configuration. Such curves provide the rationale for the design of variable resistance exercise machines, particularly those which allow for the motion of just one body joint (e.g., elbow flexion; knee extension). Many exercise machines, however, require motion at a number of body joints (e.g., bench press; leg extension). The question that then naturally arises is whether the simple strength curve concept, which is well-defined for one degree of freedom (DOF), single-joint exercises, can be generalized to apply to these multiple-joint exercises and furnish the rationale to design the associated variable resistance exercise machines.

For convenience, multiple-joint strength training exercises may be subdivided into those exercises which are realistically modeled as single DOF exercises, and those which are realistically modeled as multiple DOF exercises. The number of DOF of any mechanical system is the number of system coordinates or configuration variables that can be varied arbitrarily and independently without violating any system constraints.

The purposes of this study were (1) to show that the concept of a strength curve for a single joint, one DOF exercise can be generalized to include multiple-joint, one DOF exercises, (2) to define the strength curve for such exercises, and (3) to illustrate how this definition applies with a simple example.

Let the entire body or some portion thereof be modeled as a collection of rigid links interconected by joints in such a way that (a) this linkage system has one DOF, and (b) during the exercise, at least two joints change their configurations. Let N represent the number of moving or active body joints ($N \geq 2$), and let θ_i ($i = 1,\ldots,N$) denote the N angular variables that describe the configurations of these N active joints. Finally, let T_i represent the resultant joint torque component corresponding to the θ_i coordinate which acts on the distal segment at each active joint. Since the linkage system has one DOF, the configuration of any joint θ_i can be uniquely expressed in terms of an arbitrarily chosen, characteristic angular variable θ_j^* called the exercise coordinate.

A plot of the algebraic sum T of these active joint torques T_i vs. the exercise coordinate θ_j^* is defined as the strength curve for this one DOF, multiple-joint exercise.[1] For the case when N = 3, a typical exercise strength

curve might appear as shown in Figure 1 below. Such a curve gives an indication of both individual joint and combined system strength as a function of system configuration, and it represents a reasonable and consistent extension of the concept of a strength curve for a one joint, one DOF exercise.

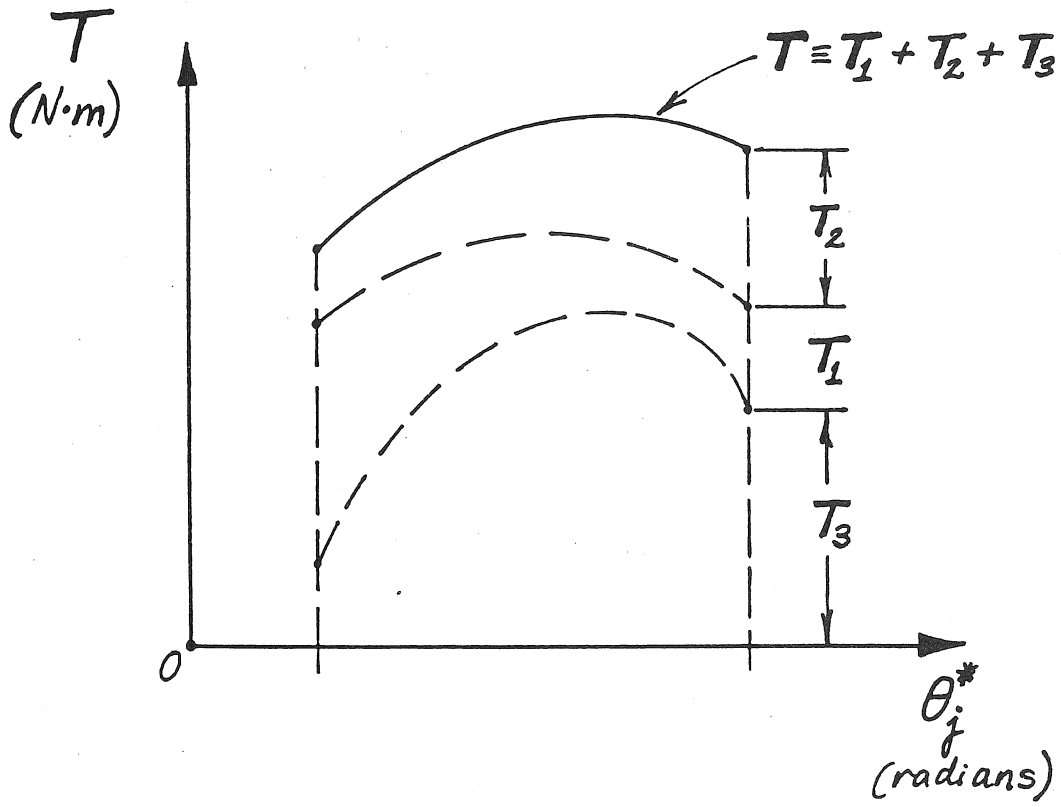

Figure 1

Exercise joint torque T vs. characteristic exercise coordinate θ^*_j for a one DOF exercise with three active joints

FATIGUE INDUCED CHANGES IN STIFFNESS OF THE FLEXOR POLLICUS LONGUS IN HUMAN SUBJECTS WITH INTACT REFLEXES

Patrick E. Crago and Steve V. Zacharkiw

Departments of Biomedical Engineering and Orthopaedic Surgery
Case Western Reserve University, Cleveland, Ohio 44106

INTRODUCTION: The hypothesis that stiffness is regulated reflexly by feedback from muscle force and length receptors has been supported experimentally by the observation that the stiffness of muscle in response to symmetrical lengthening and shortening is very asymmetrical in the absence of reflexes, yet is symmetrical when reflexes are intact[6]. In decerebrate cats this response symmetry has been attributed to compensatory assymetries of muscle mechanical stiffness and muscle spindle primary ending length sensitivity[4], with a negligible contribution from force feedback[5,7]. Stiffness regulation has been tested by examining the dependence of stiffness on initial force prior to length disturbances[3]. Increasing initial force provides an internal disturbance to the hypothesized force feedback pathway by incresaing the inherent (non-reflex) stiffness of muscle. With reflexes intact, stiffness was found to depend on initial force, but not proportionally. The interpretation of these results is complicated by the fact that the motor neuron pool and the reflex pathways may have gains that depend on the level of motor neuron pool output, and force is directly related to this output.

The objective of the current experiments was to induce an internal disturbance to the hypothesized force feedback loop in a way that would allow the comparison of stretch reflexes at the same level of motor neuron pool output. This was accomplished by fatiguing exercise that lowered the muscle gain. Thus, stretch reflexes could be studied at the same level of motor neuron pool output, but at a reduced force, and a correspondingly reduced inherent muscle stiffness. Little evidence was found for reflex compensation for this type of internal disturbance. The stiffness at any level of torque or of motor neuron pool output was not preserved, indicating a low gain of force feedback and poor regulation of stiffness.

METHODS: Stretch reflexes were studied in the flexor pollicus longus (FPL) of adult normal subjects. Regulated joint position disturbances were applied at the interphalangeal joint of the thumb while the subjects contracted the FPL to produce a flexion torque against a crank mounted on the shaft of a position servo motor. The subjects were instructed not to react to the disturbances[2]. Joint position and torque and FPL EMG were measured 500 ms before, during, and 500 ms after ramp disturbances in joint angle. Each contraction for the stretch reflex measurements lasted about 2.5 seconds, with a 30 second rest between contractions. Passive responses were measured with the subject relaxed.

All trials were performed at the same initial angle (usually with the thumb flexed 10 degrees). Groups of stretch reflexes were studied at several initial torques (ranging from 5 to 40 N-Cm) prior to and after fatigue. Ensemble averages of position, torque and smoothed rectified EMG were computed from sets of trials performed at the same torque.

Fatigue was induced by a series of 50 to 100 intermittent isometric contractions at a torque near the maximal torque employed in the stretch reflex studies. Each contraction was 11 seconds in duration, with ten seconds relaxation between contractions. The subjects rested for 45 minutes following the exercise before stretch reflexes were studied again. The median power frequency of the raw EMG power spectral density was measured before the exercise and after the stretch

reflex studies to test for changes in muscle fiber action potential conduction velocity.

RESULTS AND CONCLUSIONS: The torque change induced by a ramp stretch of FPL was also ramplike, with modest overshoot. Stiffness was calculated as the ratio of the torque change to the angle change, either in the steady state (200 to 500 msec following the end of the ramp) or during the ramp. Prior to fatigue, steady-state stiffness and the stiffness measured at the end of the ramp increased with the level of initial torque, but with a decreasing slope for torques above 15 N-Cm.

Muscle gain was assessed as the slope of the relationship between torque and smoothed rectified EMG, calculated from the data measured prior to each stretch reflex trial. This was typically a straight line relationship. The fatiguing exercise reduced the gain by 20 to 50 percent in diffferent subjects. This gain varied very slowly in the post-exercise period[1], allowing the study of stretch reflexes at several initial torques under essentially constant conditions of fatigue. Although there were substantial changes in median power frequency during the exercise, there was complete recovery by the time the stretch reflexes were re-assessed, allowing confidence in the interpretation of the EMG amplitude.

After fatigue, the torque change elicited by muscle stretch was reduced at any given level of initial torque. That is, the stiffness at the end of the ramp or in the steady state was lower than it was prior to fatigue, when compared at the same level of initial torque. The degree of stiffness reduction was related to the degree of muscle gain reduction, as measured by the torque-EMG slope. The stiffness at very short latency (ie prior to any reflex response) was the same as before fatigue, indicating no change in inherent muscle stiffness. Thus , muscle reflexes failed to preserve the mechanical properties at the joint since the relationship bewteen joint torque and joint stiffness was altered by fatigue.

Stiffness was usually also lower when compared at the same level of initial EMG. Thus, for a given level of motor neuron pool output, stiffness is not well regulated to a specific value. EMG responses appeared to superimpose when compared at the same initial value, suggesting that the response was uniquely determined by the initial value of EMG, and was not influenced by feedback from muscle force receptors. Since the total stiffness was lower at the same level of EMG, force feedback should have been reduced and EMG response increased if the gain of force feedback was significant. However, the latter conclusion must be taken as tentative at this time due to the fairly large variance in the EMG responses.

REFERENCES

[1] T.M. Banas and P.E. Crago, Soc. Neurosci. Abstr., 9, 1983.
[2] P.E. Crago, J.C. Houk and Z. Hasan, J. Neurophysiol., 39, 925-935, 1976.
[3] J.A. Hoffer and S. Andreasson, J. Neurophysiol., 45, 267-285, 1981.
[4] J.C. Houk, P.E. Crago and W.Z. Rymer, in Muscle Receptors and Movement, ed. by A. Taylor and A. Prochazka, Macmillan, London, 299-309, 1981.
[5] J.C. Houk, J.J. Singer and M.R. Goldman, J. Neurophysiol., 33, 784-811, 1970.
[6] T.R. Nichols and J.C. Houk, J. Neurophysiol., 39, 119-142, 1976.
[7] W.Z. Rymer and Z. Hasan, Brain Res., 184,203-209, 1980.

ACKNOWLEDGEMENTS: This research is supported by grant no. NS-19135 from NIH.

CONTROL OF HUMAN WRIST MOVEMENTS DURING ADAPTATION TO INERTIAL LOADS. S.L. Lehman, Rehabilitation Institute of Chicago, Chicago, IL 60611

In the course of a series of fast, practiced flexions and extensions of the wrist, I suddenly applied a large (24 Kg) inertial load. The load was produced by a linear motor, servo-controlled to simulate an inertia. Load changed under computer control as the beginning of a movement was sensed, so that there were no prior cues to the subject. I recorded force, velocity, and position of the wrist using the same apparatus that imposed the load.

I found adaptive changes in the forces acting at the wrist, from the first movement on. The changes in force during the first loaded movement were qualitatively different from changes over the next several (loaded) movements. During the first loaded movement, force durations changed drastically, and adaptively. Agonist force was applied for about twice as long as for the unloaded movements. The duration of antagonist force also increased dramatically. Both durations exceeded their fully adapted values during this movement. In the sequence of successive loaded trials, force timings were further tuned, but over a smaller range. Force durations converged on values somewhat smaller than those for the first loaded trial, and much longer than the comparable durations for unloaded movements. Force magnitudes, by contrast, changed only moderately in the first loaded trial. Instead, they increased gradually over the course of several trials. I confirmed the independence of force duration and amplitude adaptations for different sizes of wrist movements (0.5-6.0 cm, or about 5 to 50 degrees), and for a smaller inertial load (4 Kg).

Electromyograms (EMG) of wrist flexors and extensors show qualitative agreement with the force duration changes. EMG activity for these fast movements generally occurs in sharply defined, reciprocal bursts. High agonist EMG activity occurs over a longer period in the first loaded trial, as it does in later trials. Also, the first burst of antagonist EMG appears to be shortened in the first loaded trial.

In order to infer the neural controller signal driving these movements from the forces and EMG's, and to separate mechanical effects from control adaptation, I have modeled the wrist and muscles. The present model consists of a damped harmonic oscillator driven by two Hill-type muscles, agonist and antagonist. I have performed a series of experiments to determine the parameters of this model: passive mechanical parameters of the wrist, force-velocity, length-tension characteristics of (lumped) muscles, and series elasticities. A parameter sensitivity analysis of the model showed that the force-velocity parameters and the series elasticity have profound influences on peak accelerations, velocity and position. I have therefore modified the model to include a more realistic activation-dependent series stiffness. Using a powerful optimization algorithm, I have fit the wrist movement model to the force data, for both loaded and unloaded movements. Allowing parameters to vary within limits established by experimental error in the parameter identifications, I have obtained good matches between model-produced and experimentally-recorded forces. The assumed model inputs are composed of multiple bursts of lumped neural activity (roughly corresponding to EMG). I allowed the timings, durations and magnitudes of the bursts to vary freely. The model trajectories best matching experimental records are driven by nearly reciprocal bursts of reasonable magnitude, with timings quite close to those estimated from electromyograms.

The Mechanical Response of the Active Human Triceps Brachii to Very Rapid Lengthening and Shortening.

by

Shi-Ping Ma and George I. Zahalak
Department of Mechanical Engineering, Washington University, St. Louis, MO 63130

The time-course of the *muscle moment* and myoelectric activity was measured in three normal adult male subjects whose forearms were subjected to small, rapid flexions and extensions starting from a steady isometric contraction of the extensors. These experiments were performed using a versatile testing apparatus, the PLTS, described in (1): a schematic diagram of the experimental arrangement is shown in Fig. 1. The subject's forearm was made as rigid as possible by bracing it with an aluminum surgical splint and a fiberglass sheath, and was tightly clamped to the forearm fixture of the PLTS by a teflon wrist-cuff. Frequency-response tests showed that the dynamic response of this preparation was very well modelled from 0 to 35 Hz as a system consisting of two rigid bodies (fixture and forearm) with a linear viscoelastic coupling at the wrist, and the numerical values of the forearm inertia and coupling stiffness and damping parameters could be identified from these tests. Given this information it was possible to design a numerical algorithm which computed the moment exerted about the elbow by the active, participating muscles from measurements of the external moment applied to the forearm fixture and the fixture acceleration. (Details of this calculation will be provided in a forthcoming publication.)

To check the accuracy of the muscle-moment calculations verification tests were performed as follows. The subject was asked to relax his forearm musculature completely and an "artificial muscle", consisting of a spring in series with a load cell, was attached to the wrist, as shown in Fig. 1. The spring was pretensioned to initial moment values typical of voluntary contraction. Then a fast ramp-and-hold displacement, either flexion or extension, was imposed on the forearm. The duration of the ramp was 25 msec in all cases, and the ramp amplitude was 1, 2, or 3 degrees. The time-course of the moment in the "artificial muscle" was computed and compared to that actually measured by the load cell. The results confirmed that the muscle moment can be predicted accurately (within 5%) from measurements of the external driving moment and fixture acceleration. The "artificial muscle" was then removed and the subject began a test by exerting a prescribed static extensor moment. Ramp-and-hold displacements like those described above were imposed on the forearm and the driving moment, fixture acceleration, and electromyograms from biceps and triceps were measured for approximately one

second following ramp onset. The subject was instructed to "not intervene voluntarily in response to the imposed perturbation", and each test run was repeated ten times for ensemble averaging.

The results showed that the antagonistic flexors exhibited almost no electrical activity, so that the measured mechanical response can be attributed mainly to the triceps brachii. Reflex EMG activity in the triceps commenced 20 to 25 msec after ramp onset, and exhibited complex patterns which will not be discussed here. Typical muscle moment responses are shown in Fig. 2, which displays the muscle-moment perturbations produced by 2 degree forearm rotations in one subject, starting at the pre-ramp contraction levels indicated in the figure. The mechanical response for approximately the first 40 msec can be presumed independent of reflex, and is spring-like; the muscle moment increases with stretch and decreases with shortening, peaking at about 40 msec. This is followed by a second phase, lasting approximately 30 msec, during which the muscle moment returns toward its pre-perturbation level. The last phase of the response is reflex-mediated, and both the muscle moment and triceps EMG approach new post-perturbation steady levels. Attempts to fit the muscle model proposed in (2) to these muscle-moment responses yielded the following results. The intrinsic muscular stiffness K increases with pre-perturbation contraction level, and was higher than identified in frequency-response tests over the range 0 to 10 Hz; this may be due to the higher rates of loading in the current tests. The "viscoelastic" time constant τ_1 had an average value of about 50 msec, which agrees with frequency-response estimates. The "activation" time constant τ_2, however, showed considerable variability and had an average of about 250 msec, -a value much larger than the 50 msec estimated from frequency-response tests. This last result suggests that rapid EMG fluctuations, above 10 Hz, are even less effective in producing contractile force than implied by the model of (2), which may be accounted for formally by expanding the first-order activation dynamics of the model to include higher-order terms.

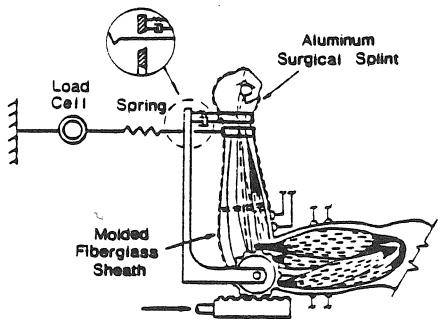

Fig. 1

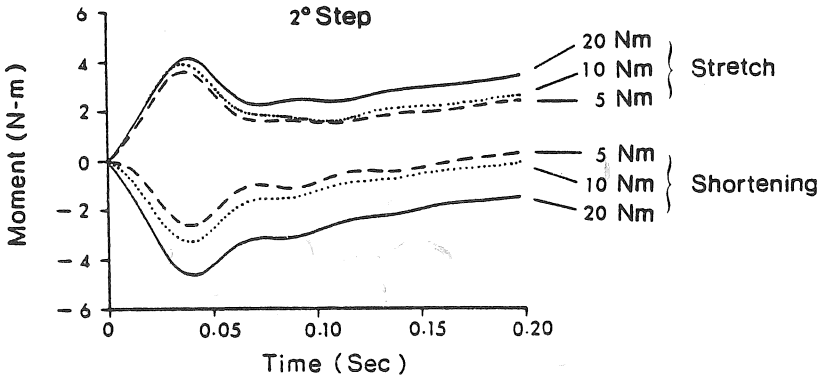

Fig. 2

1. Billian, C. and Zahalak, G.I., "A Programmable Limb Testing System (and Some Measurements of Intrinsic Muscular and Reflex-Mediated Stiffnesses):, Journal of Biomechanical Engineering, V. 105, p. 6, 1983.

2. Cannon, S.C. and Zahalak, G.I., "The Mechanical Behavior of Active Human Skeletal Muscle in Small Oscillations", Journal of Biomechanics, V. 15, No. 2, p. 111, 1982.

BIOMECHANICAL FORCE ANALYSIS OF THE LEG MOTION FOR THE STANDARD AND SUPINE RECUMBENT BICYCLE PEDALLING

Manssour H. Moeinzadeh, L. Daniel Metz & Larry R. White
Department of General Engineering
and
Jack L. Groppel
Department of Physical Education
University of Illinois at Urbana-Champaign
Urbana, Illinois 61801

In bicycling, the joints of a rider's lower limb experience high forces and moments. Particularly in racing, these forces and moments can become large enough to cause injuries, most commonly to the knee joint. Various modifications in bicycle design have been proposed to reduce these potentially injury causing forces.

This study is concerned with the analysis and comparison of the forces and moments generated at the joints of a rider's leg during pedalling motion . This analysis is performed for two different kinds of bicycles --the standard and the supine recumbent . Data were collected on three different riders --a novice cyclist, a serious recreational cyclist and a licensed state-class racer. Applying the U. S. National Team Fitness Test procedures, each cyclist was tested on the standard and supine recumbent bicycles. For each test, the bicycles were adjusted to the riders involved then, mounted on a wind/road load simulator in order to emulate actual riding conditions.

Data were collected through the use of high-speed cinematographic movie analyses. From the film data, five target points were digitized: a reference, the anatomical landmarks for the hip, knee and ankle joints, and the hub of the pedal. A computer and video/graphics display were used for digitization. The reference points were translated to an origin and the pedal motion was analyzed to identify obvious errors such as duplicated or missing frames. A Fast Fourier Transform analysis was performed to determine the harmonic content of the motion of each target point. Data for each target point were then passed through a low-pass, second-order Butterworth filter in both the forward and reverse directions with the cutoff frequency adjusted on the basis of appropriate harmonic content. The filtered data were then scaled to actual units.

Velocities and accelerations were computed for both linear and angular motion using the first central difference formulae. Anatomical data were used in conjunction with the appropriate velocities and accelerations to determine inertial loads on each leg segment. Data on relative pedal forces with respect to pedal position were combined with information on power requirements of the simulator to determine the driving forces. The driving forces were then combined with the inertial loads and the resultant forces and moments were determined at each joint. These results would serve as a qualitative estimator of potential injuries during both kinds of cycling, and would aid the development and design of an optimal pedalling regimen for both the recumbent and standard pedal stroke.

Interaction Between Ongoing Eccentric/Concentric Movement and Fast Movements for the Limb

Jack M. Winters and Lawrence Stark
Dept. of Engineering Science, Bioengineering Group
University of California, Berkeley

In both normal movement and in sports performance most fast movements take place in the presence of slower ongoing eccentric or concentric motion. Most reseach on fast movement, however, has considered the simpler condition of isolated, time-optimal, point-to-point fast movements. Studies of gross human performance suggest that ongoing slower movements effect fast movement trajectories, and that certain muscle properties, especially the force-velocity relation and the series elastic storage capacity of muscle, are of special significance. The purpose of the present study has been to expand recent simulation work on fast-slow eye movement interaction (1) to more complex situations, such as movements about joints such as the elbow and knee, and then investigate interaction phenomena in detail.

Model Description: The eighth-order model employed here uses two antagonistic muscles, each of which includes second-order "active-state" dynamics, a contractile element that includes nonlinear force-velocity relations for both shortening and lengthening muscle, and nonlinear series and parallel elastic elements. The passive elastic and viscous muscle properties are lumped with those of the joint to form a nonlinear second-order inertia-dashpot-spring plant that is controlled by the two antagonistic muscle actuators. Muscle parameter values are based on algorithms constructed from material and structural data, experimental work found in the literature, and on sensitivity analysis findings (2,3).

For each simulation run, the joint model of interest, the two muscle controller signal input sequences, and the external loading with time must be specified. The resulting movement output trajectory, as well as information on internal model states, model parameter values and energy and force propagation, can be plotted as desired.

Results: The simple example presented in Figure 1 shows some basic trends, including: phase lag and position nonlinearities in the early periodic output and differences between trajectories for "with" versus "against" ongoing velocities. Also plotted are the node lengths and velocities for the flexor and extensor muscles (dashed lines). The difference between the node and actual muscle lengths gives one an idea of series elastic energy storage. The node velocities are the instantaneous velocities across the contractile element.

Figure 2 represents, in simplified form, the type of dynamics that must be considered for movement interaction tasks such as throwing a baseball. The controller input signal is kept simple to facilitate understanding of the phenomena. Assuming the zero position to be an elbow angle of 100 degrees, a moderate speed elbow flexion, initiated at 0.1 sec, takes place from the starting positon of -60 deg (160 deg elbow angle) until a 100 ms maximal pulse occurs at 0.4 sec, allowing a fast extension of the arm. The ball inertial load is released at 0.7 ms. Notice the increased entension speed for the condition of the same input signal but no increased load, and the resulting lower muscle force for the opposite concentric movement. In general, one sees that most of the potential muscle force is not passed past the torque-velocity element.

Other model runs include simulations with different combinations of: the magnitude and type of input pulse sequence for fast movements, the magnitude and type of ongoing movements, and the external loading conditions. Also, movements of different body parts must be discussed to complete the complex picture of

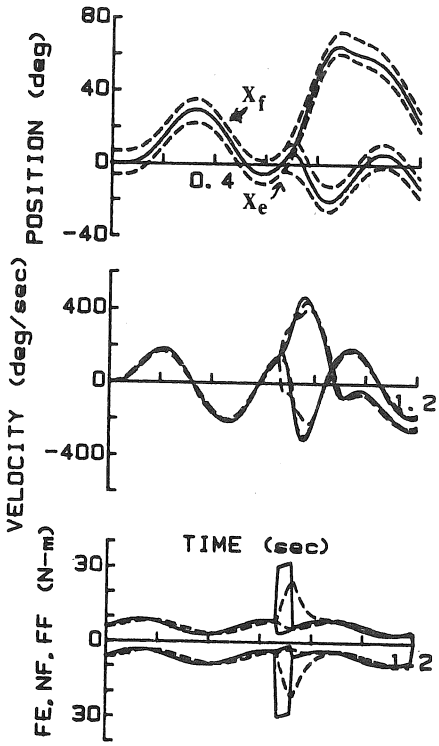

Figure 1: Two superimposed simulation runs for elbow model. Ongoing 2 Hz, 3-9 N-m range sinusiodal input interacting with single-pulse input signals occuring at time of zero position crossing in directions "with" and "against" velocity **Top:** position (solid) and the flexor and extensor node positions vs. time (dashed lines). **Middle:** velocity (solid) and node (contractile element) velocities (dashed) vs. time. **Bottom:** Neural inputs (N-m) and muscle force vs. time.

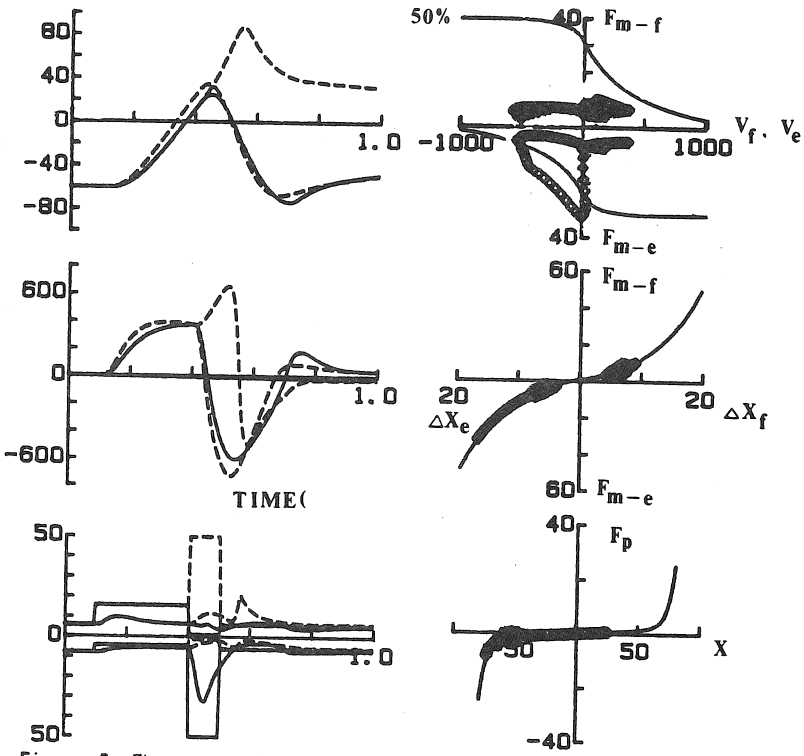

Figure 2: Three superimposed simulations for elbow model. **Left panel:** Solid lines represent a fast movement of short duration (100 ms) occuring during an ongoing moderate speed eccentric movement. External inertial load (a baseball) is released at 700 ms. Dashed lines represent: i) trajectory, for same input signal, if no external load ii) trajectory for inverted input pulse. **Right panel:** Top is instantaneuos torque-velocity behavior for two muscles. Also plotted is torque-velocity relation for 50% activation. Middle and bottom are instantaneous behavior across the viscoelastic series and parallel elements, respectively, with static elastic constitutive relations in thin lines. Position, velocity to right for flexion; Flexor torque up, extensor torque down ordinate.

movement interaction dynamics. Sensitivity analysis results for different interaction tasks also add considerable insight into which model parameters are responsible for any observed behavior (2). Such tools have been used extensively to gain insight into the role played by the various biomechanical model parameters in effecting model performance.

Conclusions: Ongoing velocity, acceleration, and sometimes position conditions, as well as controller signal interaction protocol, significantly effect fast movement trajectories. The relative magnitude of each effect is a function of the task. The most fundamental observations possible are that movement interaction results are especially sensitive to series elastic storage, to force-velocity relation nonlinearities, to system inertia, and to external loadings. These findings show how simulation can be used to gain insight into the nature of movement interaction phenomena. The role of fundamental nonlinear muscle properties on various movement patterns has been ascertained. Such insights also suggest central nervous system control strategies.

[1] Winters, J.M.,Nam, M.H. and Stark, L., Math. Biosci., 68:159-186, 1984.
[2] Winters, J.M. and Stark, L., 20th Ann. Man. Contr., NASA AMES, June, 1984.
[3] Winters,J.M.and Stark, L., 8th Ann. Biomech., this meeting, Oct., 1984.

SYSTEMATIC ERROR IN 3D COORDINATES WITHIN A LARGE OBJECT-SPACE WHEN USING THE DLT AND NLT METHODS OF 3D CINEMATOGRAPHY

Jesús Dapena
Biomechanics Laboratory
Department of Physical Education
Indiana University
Bloomington, IN 47405

The Direct Linear Transformation (DLT) method of 3D cinematography requires a 3D control object of known shape and size to determine the internal and external parameters of the cameras. The unknown accuracy of the DLT method in the calculation of coordinates outside the control object becomes an issue when the activity to be filmed takes place in a large object-space, as control objects much larger than one cubic meter pose stress deformation and transportation problems of difficult solution. In an alternative method, Non-Linear Transformation (NLT), the internal camera parameters are obtained from the images of a cross, filmed at known distances from the cameras; the external camera parameters are obtained from the images of a control object of unknown shape. The "object" is formed by a one-dimensional segment (pole with two targets) placed successively in several arbitrary positions that surround the object-space. The present paper is a comparison of the DLT and NLT methods for the calculation of 3D coordinates within a large object-space.

A 48-point grid (5m x 5m x 2.30m) was set up and surveyed. 3D coordinates were calculated from the film data for each point in the grid using three methods: (a) DLT with a triaxial control object (DLT_T), dimensions = 1.77m x 1.67m x 1.90m (Fig. 1a); (b) DLT with a cuboid control object (DLT_C), dimensions = 1.67m x 1.67m x 1.15m (Fig. 1b); (c) NLT, cross spans = 1.10m, segment length = 2.15m (Fig. 1c). Fig. 2 shows typical results obtained with each method. The error analysis took into account compression, tension, and shear distortion. This permitted the calculation of the eigenvalues, or principal tension-compression values (maximum, minimum, and intermediate) at each point of the grid. The averages of the absolute values of the relative errors in the X, Y, and Z directions were: 3.1% (DLT_T), 1.5% (DLT_C), and 0.8% (NLT). The averages of the eigenvalues (a more meaningful indication of error, as they account for the effects of shear distortion) were: 4.8% (DLT_T), 2.1% (DLT_C), and 2.0% (NLT).

The results indicate that the accuracy of the DLT method is similar to that of the NLT method when a cuboid control object is used, and inferior when a triaxial control object is used. The main advantages of the NLT method over the cuboid DLT are: control object is simpler, cheaper, usually more rugged, and easier to transport and/or assemble. The main advantages of the DLT method are: simpler filming (one shot of the control object is enough to obtain camera parameters, while in the NLT method the one-dimensional segment has to be filmed briefly in different positions, and a shot of the cross is also necessary); simpler computation of camera parameters (the NLT method requires the solution of a set of non-linear equations through an iterative procedure, which requires an initial rough estimate of the solutions); and

shorter computer time for the calculation of camera parameters (because of the direct solution of the set of linear equations).

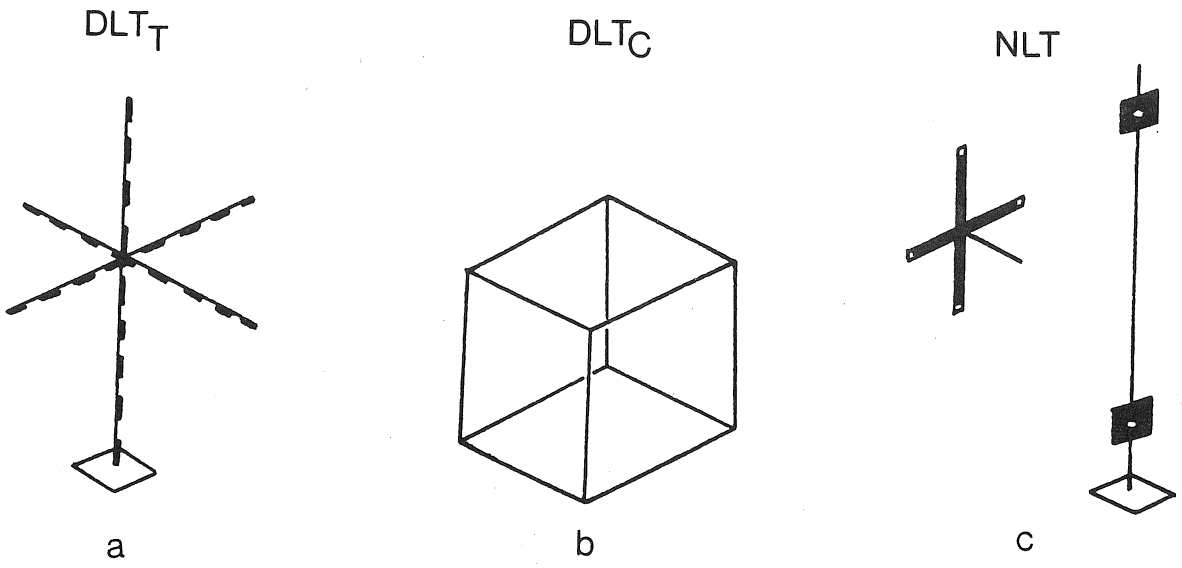

Figure 1. Devices used for each method.

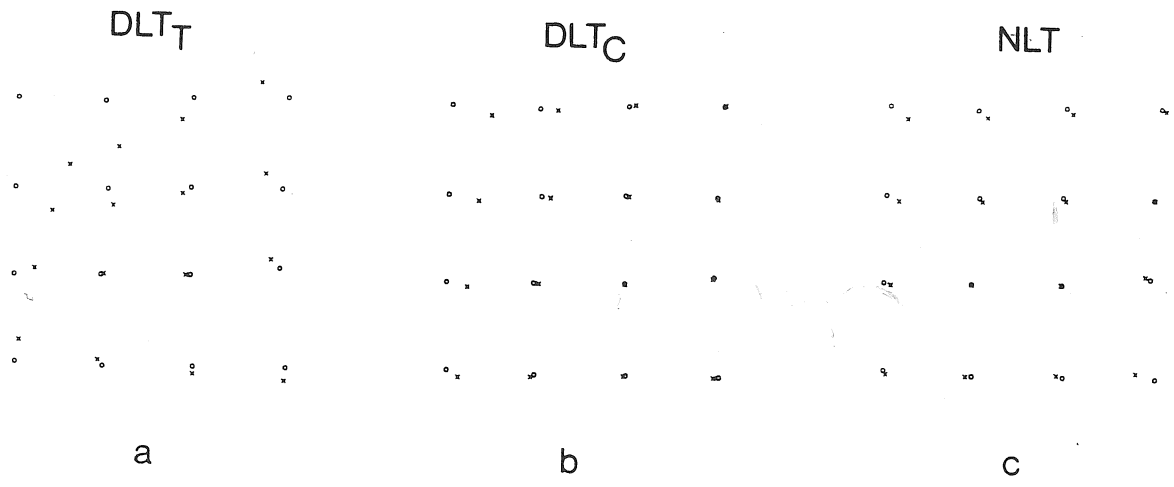

Figure 2. Points of top layer of 3D grid. Surveyed positions of points = O; film-calculated positions = X. NOTE: errors have been exaggerated by a factor of 5 to show the distortions more clearly.

THEORETICAL PREDICTION OF ENERGETICALLY OPTIMAL STEP LENGTH - VELOCITY PROGRAMMING IN BIPED LOCOMOTION

M. Hubbard, E. G. Paterson, A. E. Orcutt
Department of Mechanical Engineering
University of California, Davis

Energy expenditure in biped locomotion depends on many factors. Two of the most important are step length and step frequency or, equivalently, step length and velocity. It has often been experimentally observed [1-4,6] that in free walking, as speed increases, both step length and step frequency increase in a regular, repeatable fashion. That is, at a given speed, there seems to be a preferred step length. In addition, it has been suggested, based on experimental data gathered using both cinematographic and oxygen consumption measurements, that the preferred step length is chosen because, at that velocity, it results in the least energy cost for locomotion.

In spite of the large amount of experimental work involving the above ideas, however, the authors are unaware of any purely theoretical investigations which would predict that the observed step length - velocity patterns are indeed energetically optimal. The purpose of the present study was to examine progressively more complicated mathematical models of biped locomotion in an attempt to see whether the experimentally observed step length - velocity patterns can be shown to be optimal based on these models. A secondary point of the study was to determine how simple a model, if any, might satisfactorily predict the dependence in question.

The simplest model investigated was that due to Alexander [1] which included an approximate analytical expression for mass and distance specific energetic cost in J/(Kg-m) as a function of dimensionless step length λ and velocity u

$$T = \frac{1}{256\eta}\left[\lambda^3 \coth^2\frac{\lambda}{4u} + \frac{256\, mu^2}{3\lambda}\right] \tag{1}$$

Above, η denotes metabolic efficiency, m is the leg-torso mass ratio, and the first and second terms are the energy cost due to the torso and legs, respectively. Necessary conditions for optimality of step length, $\partial T/\partial\lambda = 0$, yield the transcendental expression

$$\cosh^2\frac{\lambda}{4u} - \frac{2}{3}\frac{\lambda}{4u}\coth\frac{\lambda}{4u} - \frac{m}{9u^2}\left(\frac{4u}{\lambda}\right)^4 \sinh^2\frac{\lambda}{4u} = 0\ . \tag{2}$$

Equation (2) was solved numerically for λ vs u. Although the predicted energetically optimal step length versus velocity based on this model was roughly a factor of two too small, the correct trend with velocity was present. The reason for the non-agreement was felt to be the fact that Alexander's simple expressions for energy costs of the torso and legs do not include the effect of energy transfer between segments. Additionally, Alexander's simple compass gait model overestimates the energy loss of the torso at heel strike. If the energy cost of the torso in Eqn. (1) is adjusted downward by a factor of 1/4, more in line with actually observed energy variations in the torso, the theoretically optimal step length vs velocity profile falls nearly in the center of the experimental data.

The next most complicated model investigated, a dynamic one, was a variation of that of Mochon and McMahon [5], composed of plane motion of four rigid bodies pinned at the hips, knees, and ankles. For this model the energy costs as a function of λ and u were determined by:

1) Integrating the equations of motion through swing. This used a shooting procedure similar to that proposed by Mochon and McMahon for the calculation of the set of pre-swing angular velocities which produce the desired step length and step time and assuming that the swing phase was ballistic, i.e. energy conservative.
2) Calculation of the impulsive energy losses during collisions at knee lock and heel strike.
3) Replacement of these energy losses by work done only in the stance phase to return the system to the same preswing angular velocities necessary at the beginning of the next step.

Several variations of the above dynamic model were investigated:

I) A 2 DOF model with straight rigid legs,

II) A 4 DOF model which included straight legs but separate feet and ankling action, and

III) A 4 DOF model which included knees and ankles.

All the dynamic models were improvements on the model of Alexander since all account for intersegmental energy transfer during swing and stance.

The major conclusions of the investigation were:

1) Much of the energy cost of locomotion results from the energy losses in successive collisions with the ground, a fact not clearly pointed out in previous experimental work on the subject.
2) Model I predicts correct magnitudes for λ but not the trend of increasing λ with u.
3) Model II accurately predicts the observed λ vs u dependence for low velocities, $u < 0.4$.
4) Model III, which includes the effects of knees, is the least complicated model which can also predict the observed λ vs u dependence for larger velocities.

References

1. Alexander, R. M., in Scale Effects in Animal Locomotion, (T. J. Pedley, Ed.), Academic Press, London, 93-110, 1977.
2. Cotes J. E. and F. Meade, Ergonomics, 3, 97-119, 1960.
3. Grieve, D. W. and R. J. Gear, Ergonomics, 9, 379-399, 1966.
4. Van Der Welt, W. H. and C. H. Wyndham, J. Appl. Phys., 34, 559-563, 1973.
5. Mochon, S. and T. A. McMahon, J. Biomechanics, 13(1), 49-57, 1980.
6. Zarrugh, M. Y., J. Biomechanics, 14(3), 157-165, 1981, and Euro. J. Appl. Phys., 33, 293-306, 1974.

CONTROL OF HUMAN ELECTROMYOGRAPHIC ACTIVITY DURING DIFFERENT WALKING VELOCITIES. B. J. Jaeger, S. A. Olivares and M. C. Wetzel. Department of Psychology, University of Arizona, Tucson, Arizona 85721.

Although mechanical forces change during human and animal locomotion as a function of forward velocity, few reasons have been given for accompanying changes that may occur in the step cycle. Experiments that are reported here compared the effectiveness of one mechanism, operant conditioning, to alter the configuration of the human step cycle at two different walking speeds.

Results for two subjects who walked on a motorized treadmill at .90 m/sec were compared with data collected previously in the same laboratory for walking at .45 m/sec. A computerized regimen caused a green light to flash at a fixed time after heel strike on every third step. By means of operant training, the light was made to produce a 100-500 msec EMG burst in the rectus femoris (RF) muscle before the end of a 500 msec performance duration.

The test operant (composed of green light as discriminative stimulus, Sd, together with the resulting response, an RF burst) was established as rapidly and successfully at the higher speed as had been true at the lower one (see Fig. 1). Swing, stance, and cycle durations were similar for the controlled left leg and the opposite leg; and the rapid gait did not appear to be disordered. There was no evidence for a strong competing stretch reflex near toe liftoff, when the RF muscle should have been stretched maximally. Nor did other inborn or learned behavior interfere with the controlled burst of the test muscle, whether or not the left leg was bearing body weight during different portions of the cycle.

Operant EMGs were shorter than had been typical at .45 m/sec, a characteristic that could permit contractile patterns to change rapidly at faster velocities of locomotion. It was suggested that by comparison with inborn reflex mechanisms, operant conditioning may make a substantial contribution to locomotor patterns at all forward speeds.

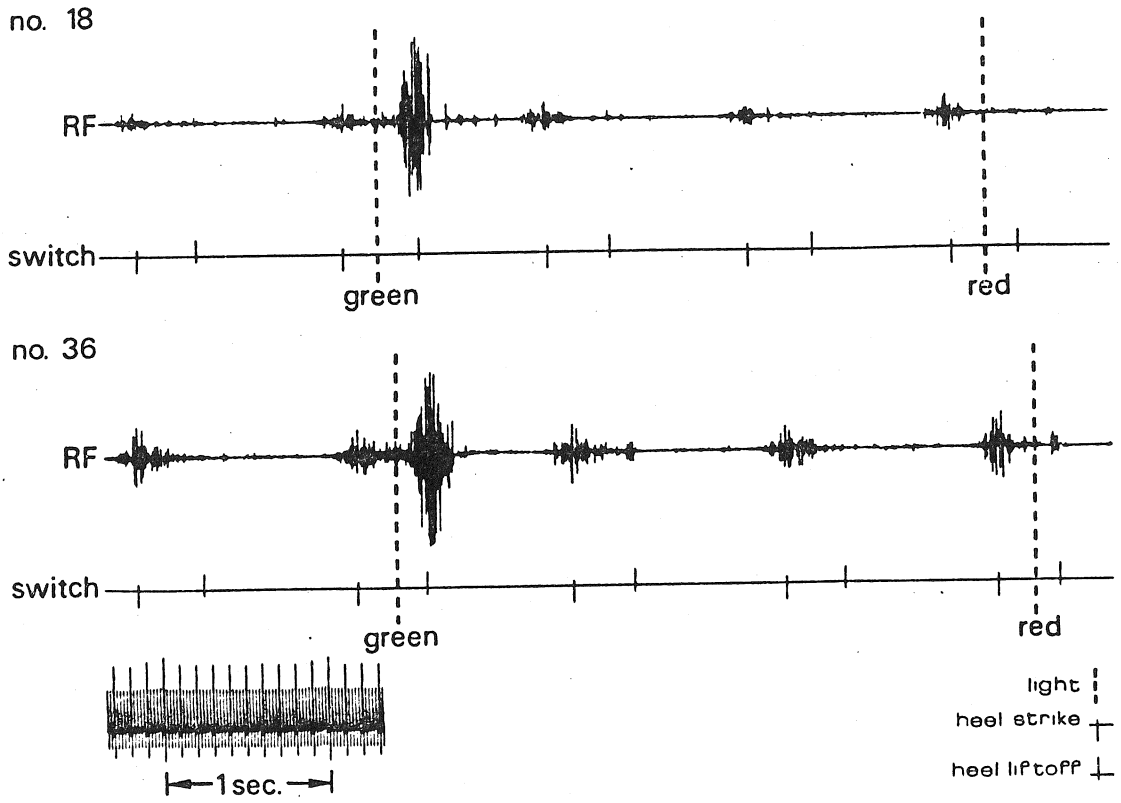

Figure 1. Five consecutive step cycles during rapid walking at .90 m/sec by two subjects, 18 and 36. Upper record for each person illustrates rectus femoris EMG at the completion of training. Downward switch marks (below EMGs) show heel strike; and upward marks, liftoff. In cycle 2, subjects successfully responded to a green light flash (first vertical dashed line) with a large, brief burst. In contrast, cycles 1, 3, and 4 had typical low-amplitude EMG activity when no colored light flashed. Similar slight activity occurred when subjects were asked not to respond after a red light flashed (second dashed line) in cycle 5.

A Computerized System for Real-Time Visualization of Ground Reaction Forces in Walking

Larry W. Lamoreux, Ph.D.
Shriners Hospital For Crippled Children
San Francisco

Force platforms have aided the study of forces and moments in ankle, knee and hip joints since the pioneering work of Bresler and Frankel (1950) at the University of California in Berkeley. They used force platforms to measure ground reaction forces, and simultaneous cine films to measure the locations of limb segments. To calculate bending moments at the joints they first multiplied the magnitude of the reaction force by the lever arm of the force about each joint, and then corrected these "raw" joint moment values for linear and angular inertia of each limb segment. For these latter calculations they had to estimate the mass and moment of inertia of each limb segment and calculate accelerations from the cine film data. With minor variations, this method has been used by numerous subsequent authors and continues to be used to this day. It is prized for its accuracy but notorious for its complexity.

For those parts of the gait cycle where accelerations of the stance limb segments are small, the corrections for limb segment inertia are also small, and the original "raw" estimates of joint moments are quite accurate. (Wells, 1981) In 1977, Cook, Cozzens and Kenoshian of the Moss Rehabilitation Hospital in Philadelphia reported a force-line visualization system that took advantage of this fact. They devised a system which superimposes a visual image of the ground reaction force vector on an image of the person stepping on the force platform, in effect making it possible for an observer to "see" the force vector as the subject walks across the force platform. No quick calculations to correct for effects of inertia are possible, because limb segment positions are not measured, but viewers of the combined image can readily observe the alignment of the force with ankle, knee and hip joints and estimate the lever arm of the force at the level of each joint. If the combined images are recorded on video tape or cine film, they can be scrutinized in more detail or even measured, but their primary appeal is the instant feedback they provide for routine assessment of knee stability, varus or valgus knee deformities, hip abductor weakness, orthosis function, prosthesis alignment and foot function, and so on.

The Moss system used a movable laser beam to draw images of the force vector, and a half-silvered mirror, or beam-splitter, to superimpose the images of the vector and the subject. In 1979, Tait and Rose of the Orthotic Rehabilitation and Locomotor Assessment Unit (ORLAU) in Oswestry, England reported a similar system which superimposed the two images by electronically injecting an image of the force vector into a video image of the subject. Since that time, a few other laboratories have developed variations of these two systems for local use. Both of these systems elected to use hard-wired analog computer circuitry to accomplish the necessary center-of-pressure and parallax calculations, because analog circuitry is fast, and the system depends on minimal time delay between application of the force to the force platform and visualization of the force on the display.

Although it is fast, such analog circuitry is lacking in versatility, stability, and accuracy when compared to a program in a digital computer.

This paper describes the design, construction and early application of a force-line visualization system built around a general purpose digital computer. The system also includes a digital display, for drawing the vectors, and a beam-splitter plus close-up lens for superimposing the vector image on the image of the subject. Major factors in the choice of a digital system were the existence of a computer in the laboratory, a desire for versatility in adding information other than force to the display, and commercial availability of a suitable digital display unit.

The primary concern in designing the force-line visualization system was overall accuracy of the displayed force vector. Six elements that can affect accuracy were considered:

1. Accuracy of joint moment estimates that ignore limb segment accelerations
2. Measurement of forces; Hysteresis, Drift, Cross-Talk
3. Viewing Projections; Right/Left and Near/Far corrections
4. Registration of the two images; Accuracy and Ease of adjustment
5. Aberrations in the optical system; Misalignment and Lens distortion
6. Response time of the calculation and display process

The present system introduces a minimum time delay of about 10 milliseconds between application of the force and appearance of the corresponding visible line on the display. Such a time delay is acceptable for studies of varus/valgus knee alignment and hip abductor function during the mid portion of the stance phase in subjects walking toward or away from the viewer. As these are the initial intended applications of the system, it meets the present need.

The limitation in speed is not caused by the required computations, which are completed in 1 millisecond, but rather by the high rates of data transfer in and out of the peripheral processor on the computer. In addition to the computations, every display cycle requires input of seven channels from the force platform, and output of 16 command words to the digital display. In our computer, there is a delay of three of these cycles from the time a force is applied until it becomes visible on the display, because the input and output operations are both double buffered by the peripheral processor. The maximum rate at which the process will run is about 300 cycles per second, which corresponds to the total delay of 3/300 second or 10 milliseconds.

The use of a dedicated single-user minicomputer could reduce the three cycle delay to one cycle, thereby speeding up the display process by a factor of three. Consequently, response times on the order of 3 or 4 milliseconds, rather than 10, appear feasible. Such rapid response would be more compatible with the performance of modern force platforms, but of no particular value for visual assessment. As one seeks to observe events that require finer time resolution, such as initial foot contact, it is important to remember that the effects of body segment accelerations, which are ignored by real-time force line visualization systems, become more significant.

REFERENCES:

Bresler, B. and Frankel, J. (1950) The forces and moments in the leg during level walking. Transactions ASME. 72:27-36

Cook, T., Cozzens, B. and Kenosian, H. (1977) Real time force line visualization. Transactions ASME. (Paper No. 77-WA/Bio-6)

Tait, J. and Rose, G. (1979) The real time video vector display of ground reaction forces during ambulation. J. Med Engg & Techn. 3:5,252-255

Wells, R. (1981) The projection of the ground reaction force as a predictor of internal joint moments. Bul Prosth Res. BPR 10-35:15-19

A MULTI-DIMENSIONAL APPROACH TO OBJECTIVE ASSESSMENT OF LOWER EXTREMITY DISABILITY

Dewaki N. Tibarewala, Ph.D.

National Institute for the Orthopaedically Handicapped

B.T. Road, Bon-Hooghly, Calcutta - 700 090, INDIA

ABSTRACT

Introduction

No process for rehabilitation of the disabled can be deemed as complete unless it is associated with suitable measures of performance evaluation. Applying the concept in the case of the lower extremity disabled - the largest single group amongst the physically disabled, determination of the success of the treatment and/or rehabilitation effectiveness assessment require the evaluation of the ability (or disability) of the involved body part with regards to locomotion and static weight-bearing which are the two independent principal functions of the human lower extremity system.

In the present approach, the assessment of the lower extremity disability has been considered as a task consisting of observations on biomechanical patterns representing the output characteristics of the involved body part and, on its inputs as supplied by the living body while engaged in performing the above-mentioned principal functions. The information obtained from such observations on input-output characteristics as well as on the interrelationships among them have been utilised to define objective measures of lower extremity functional status.

Methodology

The locomotion characteristics of the human lower extremity system have been observed by means of tachographic gait study technique based on recording the progressive component of the instantaneous velocity of the body's centre of gravity and, a set of parameters obtained by graphonumerical analysis of the recorded curves (called 'Gait Curves') have been used to represent the associated gait patterns. Along with the static weight-bearing (or, SWB - in short) patterns have been represented by the portions of the body weight transmitted to ground through a number of parafrontal zones of the foot concerned as measured by a system of strain gauge load cells. Finally, the standard technique of Indirect Calorimetery was used to measure the steady state energy expenditure rates during level walking, during standing erect and, during sitting in a chair as well. All these measurements/recordings were carried out on normal able-bodied adult males and on various types of lower extremity disabled.

Outcomes

Employing the multivariate statistical tool of discriminant analysis, the intergroup differences among various test groups as reflected in the observed parameters were found sufficient for recognising the specific patterns associated with each type of subjects whereby fresh classifications based on discriminant function scores were found to have

significant association with the original classification based on type of disability.

Representing Gait and SWB patterns belonging to different test groups in muilti-dimensional hyper spaces (gait patterns in an eight dimensional Gait Space and, SWB patterns in a six dimensional SWB space), it was observed that the points corresponding to different types of test subjects get accumulated in different zones with recognisable boundaries. This observation led the author to the definitions of 'Gait Index' and 'SWB Index' as quantitative measures of the deviations of individual patterns from the mean pattern of the control group.

Finally, application of multiple regression analysis revealed that the above-mentioned indices along with some other biomechanical variables of gait and SWB have significant correlation with corresponding energy expenditure rates. Based on these observations, criterion have been developed for objective assessment of lower extremity disability.

MAXIMAL HEIGHT JUMPING: OPTIMAL STRATEGIES BASED ON A STUDY OF THE HEEL-OFF TO LIFT-OFF PHASE OF PROPULSION

F.E. Zajac[1,2], W.S. Levine[3], Y.M. Cho[3] and M.R. Zomlefer[2]

[1]Mech. Eng. Dept.-Design
Stanford University
Stanford, CA 94305

[2]Rehab. Res. & Dev. Ct(153)
V.A. Medical Center
Palo Alto, CA 94304

[3]Elect. Eng. Dept.
University of Maryland
College Park, MD 20742

Our group has been studying vertical jumps performed by humans and cats for several years[1,2]. Reasons for studying jumping are:

- jumping may provide insight into general mechanisms of synergies and musculoskeletal interactions since the same muscles are used in locomotion and standing.
- the maximal vertical jump is commonly used as a measure of strength.
- the vertical jump is mathematically tractable because a performance criterion can be clearly defined and the dimension of the state-space model is reasonably small due to the synchrony of the two legs.
- observations of the biomechanics and muscular coordination of jumping in animals and humans are, or can be, obtained for comparison with the theoretical results.

We studied two maximal height jumps, each with a heel-off state different from the other. The subjects started both jumps from a squat with their feet flat on the ground initially in one jump and only their toes contacting the ground in the other. They were instructed to jump as high as possible from a force-plate while holding their hands above their heads. EMG activity was recorded intramuscularly from knee and ankle flexor and extensor muscles. A Selspot system was used to record trajectories of the joints. Joint angular velocities and accelerations were estimated by differentiating the joint trajectories. Ground reaction forces and center of pressure were recorded. The inverse dynamics problem was solved to estimate torques at the ankle, knee, and hip.

The computer model, composed of four parts (below), was treated as an optimal control problem and solved using differential dynamic programming.

(i) the skeletal dynamics of a 4-segment inverted pendulum;

$$\dot{\underline{\theta}}(t) = \underline{\omega}(t)$$
$$\dot{\underline{\omega}}(t) = \underline{A}^{-1}(\underline{\theta}(t))[\underline{B}(\underline{\theta}(t))\underline{\omega}^2(t) + \underline{C}(\underline{\theta}(t)) + \underline{D}\,\underline{T}(t)] \qquad (1)$$

where $\underline{\theta}(t) = [\theta_1(t)\ \theta_2(t)\ \theta_3(t)\ \theta_4(t)]'$ $\quad T_1(t)$ = ankle torque
$\underline{\omega}^2(t) = [\omega_1^2(t)\ \omega_2^2(t)\ \omega_3^2(t)\ \omega_4^2(t)]'$ $\quad T_2(t)$ = knee torque
$\underline{T}(t) = [T_1(t)\ T_2(t)\ T_3(t)]'$ $\quad T_3(t)$ = hip torque

(ii) the performance criterion, chosen as the peak height of the center of mass;

$$J(\underline{\theta}, \underline{\omega}, \underline{T}, t_f) = y_c(t_f) + \frac{1}{2g}\dot{y}_c^2(t_f) \qquad (2)$$

where t_f = the instant of lift-off
y_c = the vertical position of the center of mass
$\dot{y}_c$ = the vertical velocity of the center of mass

(iii) the torque (muscle) dynamics, so as to capture the force-length, force-velocity, and time constant properties of muscle;

$$\dot{T}_i = -\alpha_i T_i + \alpha_i [1-f_i(\tilde{\omega}_i)] T_{oi}(\tilde{\theta}_i) u_i(t) \qquad (3)$$

where T_i = torque at ith joint (i=1,2,3) $\quad \tilde{\theta}_i = \theta_{i+1} + \theta_i$ = ith joint angle

$u_i(t)$ = ith extensor muscle activation $\quad \tilde{\omega}_i = \dot{\tilde{\theta}}_i$

$1/\alpha_i$ = time constant of ith muscle

These dynamics were estimated from isometric and isokinetic records obtained when the same subjects exerted maximum voluntary contractions while strapped in a Cybex II instrument;

(iv) the initial conditions, corresponding to the state at heel-off, as estimated from experimental data.

We found that the kinematics obtained from the model are similar to the observed kinematics. Torques generated by our subjects were, however, noticeably different from torques computed from the model. We believe that series elasticity in tendon and muscle must be accounted for before these differences can possibly be resolved.

An interesting observation was that a reduction by 50% in knee strength produces, qualitatively, the same analytical result. The explanation is two-fold. First, the initial torque at heel-off is still achievable despite the halved knee strength. Second, muscle dynamics are slow relative to the duration of the heel-off to lift-off phase of the jump. Although there are questions about the accuracy of our muscle model, we believe that the basic temporal relation between the time lags in force development and the duration of rapid tasks, such as the phase of the jump studied here, is accurate. Thus, the emphasis on initial torque rather than strength is, we believe, correct and significant. Strength does limit, however, the achievable heel-off state. The point is, performance is more sensitive to heel-off state than it is to strength per se.

Finally, the optimal control, consistent with experimental observations except at the very end of propulsion, suggests that:

- extensor muscles should be maximally activated and flexor muscles inactivated between heel-off and lift-off.

- the crucial feature of the jump is the attainment of the optimal heel-off state, which requires neither maximal activation of muscles nor unique muscular coordination.

1. Levine, et al. (1983) Ankle controls that produce a maximal vertical jump when other joints are locked. IEEE Trans. on Auto. Cont., Vol. 28(11):1008-1016.

2. Zajac, et al. Dependence of jumping performance on muscle properties when humans use only calf muscles for propulsion. J. Biomechanics, (in press).

Supported by NIH grant NS17662 and the Veterans Administration. The experiments were conducted in Prof. Sten Grillner's laboratory in Stockholm.

The American Society of Biomechanics gratefully acknowledges the generous support of the following companies:

De Puy

Jim Click Ford

Kistler

Merck Sharp & Dohme

Richards Medical Company

3M/Orthopedic Products Division